Alma Mater Studiorum · Università di Bologna

**Scuola di Scienze**

**Corso di Laurea Magistrale in Fisica**

# The use of mobile single-sided NMR for the diagnosis of osteoporosis: a preliminary study

**Relatore:**

**Prof.ssa Paola Fantazzini**

**Presentata da:**

**Marco Barbieri**

**Correlatore:**

**Dott. Leonardo Brizi**

**Sessione III**

**Anno Accademico 2014/2015**

To my family

# Abstract

An original and new technique has been set-up to investigate the trabecular structure of the bone tissue through low field single-sided NMR scanners, In order to propose a new diagnostic too for osteoporosis diagnosis. Three different single-sided NMR scanners, with different advantages and disantvantages have been used to estimate the Bone Volume-to-Total Bone ratio (BV/TV), an important parameter of the trabecular structure of bone. The results have been compared with the results of micro-CT analysis. The experiments have been performed at the NMR Lab of the Department DIFA of the University of Bologna and at the NMR Lab of the School of Chemical and Physical Sciences of the Victoria University of Wellington, New Zealand, during a visit period of five months, supported by grants of the "Facoltà di Scienze" of the University of Bologna. Micro-CT analyses have been performed at the Laboratorio di Tecnologie Biomediche of the Istituto Ortopedico Rizzoli, Bologna. The research has been partially supported by the "Fondazione del Monte di Bologna e Ravenna" (project: *Tecnica innovativa per la diagnosi dell'osteoporosi mediante Risonanza Magnetica Nucleare con strumento portatile a basso campo*).

Pig bone samples have been used as model systems.
The BV/TV ratio of pig's shoulder trabecular samples has been assessed using the device NMR-MOUSE PM10. The comparison with the micro-CT data has shown a clear linear correlation between the BV/TV evaluated through NMR and those evaluated though micro-CT, the correlation coefficient $r^2$ has turned out to be 0.92. This first experiment has shown the feasibility of the proposed technique. The characterization of the tissues constituting the trabecular bone structure, and the tissues surrounding the bone (such as cartilage, muscle and fat) has been car-

ried out by two dimensional correlation maps, $T_1 - T_2$ correlation and $D - T_2$, where $T_1$ and $T_2$ are the longitudinal and transverse relaxation times, respectively, and D the self-diffusion coefficient. These experiments were performed through the NMR-MOLE, a prototype of a single-sided NMR scanner. The maps show that muscle and cartilage are characterized by longitudinal relaxation times $T_1$ much longer than transverse relaxation times $T_2$, whereas the bone marrow is characterize by $T_1$ closer to $T_2$, allowing to distinguish them in the $T_1 - T_2$ maps. The $D - T_2$ maps shows a self-diffusion coefficient of cartilage and muscle closer to the self-diffusion of the bulk water, whereas the self-diffusion coefficient of the bulk marrow has turned out to be $(6.25 \pm 0.05) \times 10^3$ $\mu$m$^2$/ms. A Diffusion-Weighted $T_1 - T_2$ pulse sequence has been developed to obtain $T_1 - T_2$ maps with different weights for the diffusion, i.e. where different times were left for the diffusion. The experiments have performed on a biological sample that contained not only the trabecular structure, but also different tissues surrounding the bone. Because of the huge difference in the self-diffusion coefficients of the tissues, it has been possible to suppress the signal of the tissues surrounding the trabecular structure (cartilage and muscle), making more realistic the scenario of *in-vivo* applications. The BV/TV ratio of a pig's femur trabecular bone sample has been evaluated with three different single-sided NMR devices, the NMR-MOLE, NMR-MOUSE PM5 and NMR-MOUSE PM10 in order to assess the differences of these device in assessing the BV/TV ratio. Also the results of this experiment have been compared with those obtained with the micro-CT analysis. By the comparison turned out that different single-sided NMR devices have advantages and disadvantages, but definitively they are able to assess the BV/TV with the advantage of being portable and low-cost devices.

The whole of the experiments performed assure that single-sided NMR scanners can be used to assess the value of BV/TV in trabecular bone, with the advantage of being portable, low-cost and non-invasive devices, so allowing to perform in an easy way wide campaigns of screening of the population at risk of osteoporosis.

# Contents

# Introduction

Osteoporosis is a systematic skeletal disease characterized by reduction of bone mass and micro-architectural deterioration of bone tissue, with a consequent increase in bone fragility and susceptibility to fracture [1]. As reported by the Italian Ministry of Health [2], and remarked by the World Health Organization (WHO), osteoporosis is a major public health problem, with a high impact on quality of life and high rates of morbidity. In the course of life, especially in the female people over 65 years old, about the 40% of population has a fracture related to a deterioration of bone tissue. Most commonly, fractures occur in the distal forearm, thoracic and lumbar vertebrate, proximal femur and wrist. The social and economic costs of this disease are important; in fact, patients with a proximal femur fracture show a mortality of 15-30% within a year from fracture. Among elderly people, the osteoporotic fractures are one of the main causes of mortality. Furthermore, among the women over 45 years old, the osteoporosis fractures require more days of health care than other common pathologies (such as myocardial infraction and diabetes). With these considerations, it is clear how the reduction of the health and the social impact of bone fragility means not only an improvement in the elderly people life quality, but also a decrease in the cost of health care.
Currently, the established modality to diagnose and monitor osteoporosis in a clinical setting is the dual-energy X-ray absorptiometry (DXA), which provides areal bone mineral density (BMD). Another technique used to assess BMD is the volumetric quantitative computed tomography (vQCT).
Both techniques provide a measure of BMD, but they do not say anything about the micro-architectural structure of the bone. Many epidemiologic evidences have shown how BMD is not clearly related to an increase of fracture risk. Laboratory data show, on average, that BMD explains the 60% of the bone strength [3]. Other

factors influence the *bone quality*, such as the bone micro-architectural structure. In order to assess the bone structure, in particular the micro-architectural structure of the trabecular bone, other techniques are necessary.
Micro-CT appears to be particularly suited to investigate the structure of calcified tissues because of the very large difference in the attenuation coefficients between bone and the surrounding soft tissues. Parameters like Bone Volume-to-Total Volume ratio ($BV/TV$), also called bone volume fraction, trabecular thickness and the number of the trabeculae are indicators of bone quality, which can be measured by micro-CT. It also is a non-dictructinve technique, as DXA and vQCT, but, on the other hand, requires a higher X-ray dose than the dose given through DXA and vQCT.
Nuclear Magnetic Resonance (NMR) seems to be a good solution for this kind of measure, because it does not use ionizing radiations. In literature there are some works about the use of NMR in assessing the bone structure, however they focus principally in the use of Magnetic Resonance Imaging (MRI) [3][4][5].

In this thesis, an original and new technique to investigate the trabecular structure of the bone through low field NMR measurement, using single-sided NMR scanners, is proposed. The instruments used int this work are the NMR-MOUSE, produced by Magritek, and the NMR-MOLE, developed by Manz et al. [6]. Both devices are open NMR sensors equipped with a permanent magnet.
The big advantage of these scanners, which belongs to the class of unilateral scanners, is that the sample can be of any size. In the usual NMR scanners, the sample must fit the limited space available in the bore of the magnet. Another relevant advantage is their low cost if compared with the NMR total body scanner. Moreover these scanners are portable, so that allowing screening of population with easy and low cost procedures.
Besides these advantages, there are some disadvantages, such as the inhomogeneity of the polarizing field $B_0$ and the RF pulse $B_1$, that degrades the sensibility of the instrument.

This thesis is divided into three parts. In the first part, the preliminary concepts regarding osteoporosis and diagnostic techniques are provided. The second part

regards materials and methods utilized in this work in order to characterize the NMR-scanners and assessing the structure of the trabecular bone of bone samples. In this part a particular attention explaining the pulse sequences is given.
In the third part, the analysis of the experiments and correspondent results are reported.

Part of this work has been performed at the NMR Lab of the Department of Physics and Astronomy of the University of Bologna. Another part has been performed at the NMR Lab of the School of Chemical and Physical Sciences of the Victoria University of Wellington (New Zealand).
The validation of the NMR results has been performed by comparison with micro-CT analysis, performed at the Istuto Ortopedico Rizzoli, Bologna, laboratorio di Tecnologie Biomediche.

This research has been partially funded by the *Fondazione del Monte di Bologna e Ravenna* (project: *Tecnica innovativa per la diagnosi dell'osteoporosi mediante Risonanza Magnetica Nucleare con strumento portatile a basso campo*).

# Part I

# Osteoporosis and Magnetic Resonance, a short background

# Chapter 1

# Preliminary concepts

In this chapter more detailed informations about the main concepts encountered in the introduction are provided. In particular, first an overview of the osteoporosis disease is given, in which the focus is on the concept of bone quality and fracture risk. Then, some main results in the field of NMR applied to the osteoporosis are reported in order to understand the current status of the research.

## 1.1 Bone and osteoporosis, an overview

Bone is a mineralized tissue that is the building tissue of human skeleton [7]. It is a living composite bio-material composed of an organic substrate, consisting largely by type I collagen (around the 40% of volume) interspersed with mineral crystals composed of hydroxyl apatite (around the 45% of volume). Water occupies the remaining volume and it either is bound to collagen or resides in the spaces of the lacuno-canalicular system.
We can classify bone in cortical bone (CB) and trabecular bone (TB). Latter is predominant in the axial skeleton and near the joints of the long bones. It consists of a network of interconnected trabeculae, which are typically 100-150 $\mu$m thick. Thickness of CB varies between 1 and 5 mm. This combination confers to the bone its unique mechanical properties in terms of tense and compressive strength. The inter-trabecular spaces are filled by marrow.

In the adult skeleton, the bone remodels itself in a process that implies a dynamic equilibrium between bone formation and bone resorption. At mid life, this process is balanced and, passed this age, the skeleton occurred in a progressive bone loss. This process is natural in the human cycle of life, and, although implies a loss of bone mass, it does not imply that an occurrence of a bone fracture is a normal process of the aging.
In some people, however, this process is more aggressive, and causes a relevant increment of the fracture risk. This disease is what is properly called Osteoporosis. The World Health Organization (WHO) defines osteoporosis how *a systematic skeletal disease characterized by low bone mass and micro-architectural deterioration of bone tissue, with a consequent increase in bone fragility and susceptibility to fracture.*
Bone mineral density (BMD) has been used by many years as a parameter for assessing bone quality, and, by inference, the fracture risk. In fact, the clinical definition of osteoporosis is based on BMD measurement. A subject having a BMD, measured at either the lumbar spine or proximal femur, less than 2.5 standard deviation below the mean of the young adult population is considered osteoporotic [1]. However, it has been remarked how *BMD only explains about 70–75% of the variance in strength, while the remaining variance is due to the cumulative and synergistic effect of other factors such as bone architecture, tissue composition and micro damage* [4]. The recognition that factors, other than BMD, determine the bone strength has given rise to the concept of *bone quality*. This concept is more related with the fracture risk, the real undesirable consequence of the osteoporosis disease.
Some of the most common parameters for the characterization of the micro-architectural structure of the bone are:

- BONE VOLUME / TOTAL VOLUME , $BV/TV(\%)$: % of bone volume in respect to the volume of total tissue analysed;
- TRABECULAR THIKNESS, Tb.Th (mm);
- TRABECULAR SEPARATION, Tb.Sp (mm);
- TRABECUALR NUMBER, Tb.N ( $mm^{-1}$).

In conclusion, the bone quality is a wide concept, that tries to take into account not only the bone mass, but also the micro-structure of the bone, in order to have a more complete view of the bone health.

### 1.1.1 Measurements of bone quality

How it has been shown previously, many parameters should be taken into account to evaluate the bone quality, and so the fracture risk. Hence, clinical measures which can help assessing the osteoporosis and monitoring its development in time, are really necessary.
At the moment, the *gold standard* technique for assessing osteoporosis is the dual-energy X-ray absorptiometry (DXA), which provides areal bone mineral density (BMD). It is a projection-imaging technique, which returns an apparent areal density, expressed as grams per centimetres squared ( $g/cm^2$), of the mineral inside the bone. In addition to DXA, volumetric quantitative computed tomography (vQCT) has been used to assess BMD. This three dimensional technique measures volumetric BMD (vBMD) and thus allows one to separate the characterization of bone geometry and bone density as elements of the fracture risk. Furthermore, vQCT can examine cortical and trabecular bone separately.
However, both techniques do not say anything about micro-architectural structure of the bone, and this leaves open the way to other clinical techniques, which can provide this information.
One of this is the micro-computed-tomography (micro-CT), that appears to be particularly suited for investigating the structure of calcified tissues, especially TB, because of the very large difference in the attenuation coefficients between bone and the surrounding soft tissues (such as the bone marrow). However, it provides great information in-vitro experiments, but in-vivo the situation is quite different. Dose limitations and point-spread function (PSF) blurring of X-ray-based tomographic methods limits the achievable resolution even at peripheral anatomic sites [3].
Besides X-rays based techniques, in the last years studies about the assessing of the bone structure through nuclear magnetic resonance (NMR), and in particular magnetic resonance imaging (MRI), have been done. Because the thesis is about

a NMR technique, a dedicate section has been reserved to the current state of this technique applied in the field of the osteoporosis.

## 1.2 NMR and osteoporosis, state of the art

A few new techniques are aimed at quantifying trabecular bone structure in addition to bone density. NMR inserts in the context of non-invasive assessment of trabecular bone architecture. Wanting to summarize the state of the art in the assessing of the osteoporosis by NMR, it can be observed that almost all of the studies are focused on the study of the TB. Moreover, almost only MRI has been used.
First, it is useful to distinguish between methods that attempt to obtain structural informations indirectly, without resolving the individual trabeculae, versus those that seek to resolve directly the TB micro-architecture.

### 1.2.1 Indirect study of trabecular bone by MRI and NMR

NMR is a technique based upon the application of a polarizing magnetic field, transmission of radiofrequency (RF) fields, and detection of RF signals from exited protons, in this case $^1H$ nuclei (called in this contest simply protons). In the study of bone structure it has to point out that the signal comes from the protons of the bone marrow and the water, whereas the bone tissue does not contribute to the signal. The presence of trabecular bone matrix, however, affects the signal intensity of bone marrow as pointed out by Majumdar and Genant in [1]:
*the magnetic properties of trabecular bone and bone marrow differ significantly. These differences produces distortions of magnetic force lines, which make the local magnetic field within the tissue inhomogeneous and alter the relaxation properties of tissue, such as the apparent transverse relaxation time $T_2*$, in gradient-echo images. Such changes in $T_2*$ should be related directly to the density of the surrounding trabecular network and its spatial geometry. Thus in a normal dense trabecular network T2* shortening should be more pronounced than in rarefied osteoporotic trabeculae.*
Qingwen Ni at al. have used low-field pulsed proton nuclear magnetic resonance

spin relaxation for characterizing the porosity and (effective) pore size distribution in-vitro in human compact bone [8]. They have used the well note relation between the relaxation time $T_2$ and the surface-to-volume ratio of the pore $\frac{1}{T_2} = \rho\left(\frac{S}{V}\right)$ where $\rho$ is the surface relaxivity.
The porosity is determined by the calibrated NMR fluid volume divided by overall bone volume, and the (effective) pore size distribution is represented by the relaxation time distribution based upon the fact that the larger pores have the longer relaxation times. Histomorphometric analysis and mercury injection porosimetry have been used to compare the results obtained with NMR. The authors conclude that *the NMR porosities are in good correlation with the results obtained from the histomorphometry measurements in eight samples from donors of different ages, and the $T_2$ relaxation distributions (or pore size distributions) are similar to the distributions obtained from the mercury porosimetry and the histomorphometry measurements* [8].

### 1.2.2 High-Resolution MRI of Trabecular Bone structure

In addition to the indirect measurements using the relaxometry, high-resolution MRI can be used to obtain images that depict the trabecular bone structure. It is a non-invasive modality and does not require ionizing radiations. Therefore, it is well suited for assessing the bone structure in a clinical setting. In conventional MRI, bone yields low signal and appears dark due to the relatively low abundance of protons and an extremely short $T_2$ relaxation time ($< 1$ ms) similar to most solid-state tissues [9].

A several number of parameters, which vary with the pulse sequence utilized, have to take into account to understand deeply the real potentialities of this technique, and, for a deeper understanding of this technique the reader can consult the work of S.Majumbar et al [1].

There are many different parameters that can be used for extracting structural information about the microstrucutre of the trabecular bone from 3D images, as pointed out in section 1.1 (BV/TV, Tb.Th, Tb.Sp, etcetera). One of the most fun-

damental parameter in MRI is related to the bone volume fraction and is denoted BV/TV (bone volume to total volume ratio). This number can be easily extracted from high-resolution images, where the intensity histogram is bimodal, by setting a single threshold and counting the number of bone pixels and total pixels within an region of interest (ROI).

With the aim to show the important of BV/TV parameter in the assess of osteoporosis we report an in-vivo study performed by S.Majumbar et al [10].
The authors have acquired high-resolution MR images or the distal radius, at $B_0 = 1.5$ T, in pre-menopausal normal (group I), post-menopausal normal (group II) and post-menopausal osteoporotic (group III) women. The classification in osteoporotic is made by BMD analysis of their distal radius. The MR images has been used to derive measures of trabecular bone structure, which include measures of trabecular bone area fraction (BV/TV), trabecular thickness, trabecular spacing and trabecular number.

Table 1.1: Results form the study by S.Majumbar et al [10].

| | pre-menopausal normal (group I) | post-menopausal normal (group II) | post-menopausal osteoporotic (group III) |
|---|---|---|---|
| Trabecular BMD ( mg/cm$^3$) | 165.31 ± 34.85 | 116.96 ± 12.62 | 101.21 ± 9.76 |
| Cortical BMC (mg) | 201.98 ± 23.46 | 186.56 ± 42.19 | 147.23 ± 60.91 |
| BV/TV (%) | 34 ± 10 | 34 ± 9 | 26 ± 8.5 |
| Tb.Th (mm) | 0.36 ± 0.08 | 0.35 ± 0.08 | 0.33 ± 0.07 |
| Tb.Sp (mm) | 0.75 ± 0.35 | 0.93 ± 0.40 | 1.34 ± 0.68 |
| Tb.N ( mm$^{-1}$) | 0.96 ± 0.20 | 0.84 ± 0.34 | 0.66 ± 0.22 |

Tab.1.1 summarize the results. The study shows how the BV/TV decreases significantly in the group III, while it remains roughly constant between group I and II.

In conclusion, this brief overview of the state of the art of the NMR applied in the field of osteoporosis, even if limited and not all-comprehensive, shows how no studies about the assessing of the structure of the trabecular bone using single-sided NMR have been done.

# Part II

# Materials and methods

In this part the materials and methods used to characterize the trabecualr bone, and to assess the microarchitectural strucutre are described. First it will be presented the NMR devices used in this thesis project. Secondly, the description and the explanation of the different pulse sequences performed in this work will be reported. This chapter has been produced using the book *Single-Sided NMR* by F. Casanova et al. [11] and the manual of the NMR-MOUSE PM10 as references. Then the attention will be focus on the nature of the utilized samples, and finally it will be described the main software used for the data analysis.

# Chapter 2

# Single sided NMR devices

As already pointed out in the introduction, the main goal of this thesis is to evaluate the feasibility of a new diagnostic technique for osteoporosis by determining the micro-architectural structure of the trabecular bone through NMR single sided devices. The main feature which differentiates this type of devices from others common NMR scanners, is the fact that they detect the signal from a sensitive volume positioned above the surface of the magnet and the RF coil. In this way the sample does not need to fit the bore of the magnet, and the sample can be of any size. In this thesis two different single sided NMR devices have been used: the NMR-MOUSE, produced by Magritek (Wellington, New Zealand), and the NMR-MOLE prototype developed by Manz et al [6] and currently present only at the NMR Lab of the School of Chemical and Physical Sciences of the Victoria University of Wellington, New Zealand.
The two devices are based on the same idea, in fact both are single sided NMR scanners, but they present a substantial difference, i.e. the shape of the designed permanent magnetic field.
The NMR-MOUSE has been designed in such a way that a constant field gradient (G) is present. On the contrary, the magnets array of the NMR-MOLE has been designed in order to create a sweet-spot in which the gradient is as less as possible, even if always present because of the single sided design.

## 2.1 NMR-MOUSE PM10 and PM5

The main feature of the profile-NMR MOUSE (MObile Universal Surface Explorer) which differentiates it from others common NMR scanners, is the fact that it detects the signal from a sensitive volume positioned over the surface of the magnet and the RF coil as shown at the point 6 in Figure 2.1(b).


(a) (b)

Figure 2.1: Profile MOSUE PM10 and KEA2 spectrometer (Magritek Ltd, NZ) 2.1(a) and schematization of NMR-MOUSE and sensitive volume position2.1(b).

In first analysis, the NMR-MOUSE is composed by a U-shaped permanent magnet, which produces a stationary magnetic field $B_0 = 0.327$ T, and a RF coil, which both produces a pulsed magnetic field $B_1$, in order to excite the spin of the protons present in the sample, and both detects the relaxation signal. With reference at Figure 2.1(b), the main components of MOUSE can be marked:

- Magnetic field lines of $B_0$, produced by the permanent magnet;
- Magnetic field lines of $B_1$, produced by the RF coil;
- U-shaped permanent magnet;
- Radio frequency (RF) coil;
- Electric circuit bounded with the coil;
- Sensitive volume, in which the $B_1$ pulsed field excites the spins of the protons present in the sample.

It could be noted that the position between permanent magnet and sensitive volume is fixed, and in the case of the NMR-MOUSE PM10 is at 11.1 mm from the surface of the magnet.
It is easy see how both $B_0$ and $B_1$ fields are, in the sensitive volume, highly inhomogeneous. This fact implies a series of problems, which have to be taken into account when one wants to perform a measure with the MOUSE.
Magritex produces four versions of profile-NMR MOUSE: PM2, PM5, PM10 and PM25. The versions differ each other by the maximum depth nominally achievable in the sample (2mm, 5mm, 10mm and 25mm). In this thesis the MOUSE PM10 and PM5 have been used.

Other three main features of the MOUSE have to be explained. First, the MOUSE have been produced in order to have a static gradient field (G) in the y direction, i.e. the direction perpendicular to the surface RF-coil. This feature is useful in order to perform many types of analysis different from relaxometry, such as diffusometry. Second, the MOUSE can be mounted on a lift that allows one to move down the permanent magnet, and so to move down the sensitive volume within the sample. That feature allows one to perform measurements at different depths inside the sample, in order to obtain a profile of the analysed parameter (i.e. spin density or $T_2$). Finally, the MOUSE-PM10 is equipped with four spacers, each of them has 2 mm of thickness. One can insert one or more of them between the permanent magnet and RF-coil, so as to reduce the distance between the coil and the sensitive volume. The smaller is the distance, the more intense is the signal. At the same time, the smaller is the distance, the smaller is the maximum depth achievable inside the sample. The MOUSE PM5 has in dotation two spacer, each of them has 2mm of thickness.

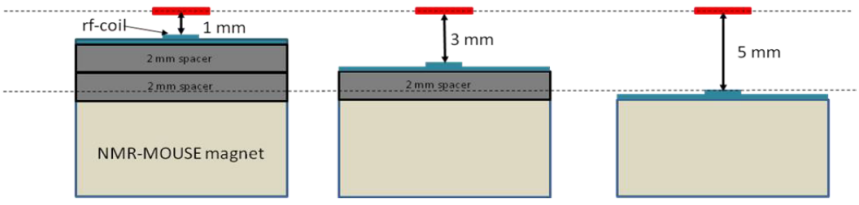


Figure 2.2: Exemple of utilization of the spacers in the MOUSE. PM5

The Figure2.2 shows different situations in which no spacers are inserted (5 mm as maximum depth achievable), one spacer is inserted (3 mm as maximum depth achievable) and two spacers are inserted (1mm as maximum depth achievable). The choice of the spacer configuration is crucial to achieve the best signal-to-noise ratio performance for the experiments. The more spacers are used, the better will be the sensitivity, and thus the shorter will be the acquisition time.
The spacers change the distance between the RF-coil and the excited sensitive volume. The closer the RF-coil is to the sensitive volume, the better will be the efficiency of the RF-pulse and the signal detection. An inaccurate selection of the spacer configuration can easily result in 10x longer measurement times.
Remarked the main characteristics of the NMR MOUSE, in Tab 2.1 the features of the MOUSE PM10 and PM5 used in the experiments are summarized.

Table 2.1: Characteristics of the profile-MOUSE PM10 and PM5

| Instrument | Larmor Frequency | B0 field | Gradient | Max. Depth | Resolution |
|---|---|---|---|---|---|
| MOUSE PM10 | 13.88 MHz | 0.327 T | 600 kHz/mm | 11.1 mm | 30 $\mu$m |
| MOUSE PM5 | 2 MHz | 0.047 T | 900 kHz/mm | 5 mm | 10 $\mu$m |

## 2.2 NMR-MOLE

The NMR-MOLE (MObile Lateral Explorer) is a single-sided scanner NMR. Differently from NMR-MOUSE, the NMR-MOLE does not have a constant magnetic field gradient, instead it presents a sweet spot in which the field is relatively homogeneous. Of course, being a single-sided device, the magnetic field generated by the permanent magnets remains highly inhomogeneous if compared with the non-single sided devices, but it is much more homogeneous in respect to the magnetic field of the NMR-MOUSE. The mean strength of the magnetic field is supposed to be 0.1175 T at 32 C$^{o}$, corresponding to 5MHz of the $1H$ Larmor frequency. In a recent paper, M. Nogueira and P.Galvosas [12] evaluated the field gradient distribution of one model of the NMR-MOLE prototype. Their results are reported in the Fig.2.3

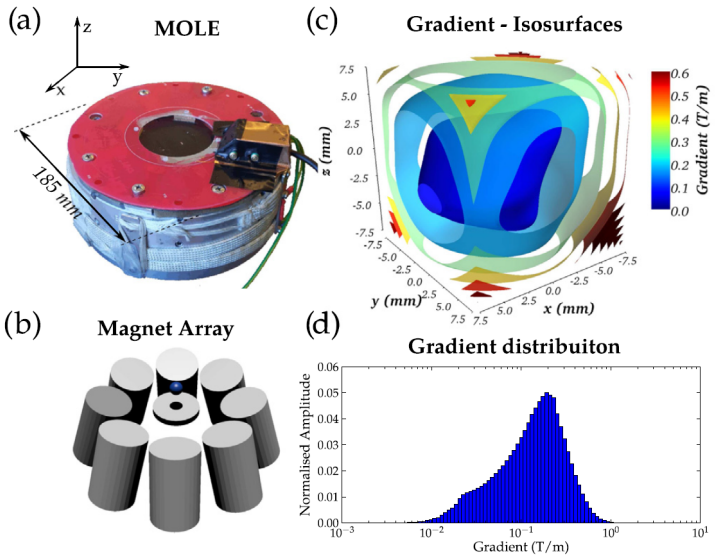


Figure 2.3: The characterization of the NMR-MOLE by M.Nougeria and P.Galvosas [12]

From the distribution of the gradient, the most present field gradient, present in the sweet spot, is 0.2 T/m, whereas the highest value is 1 T/m.

A PID system, which controls the current of a heat tape in contact with the aluminium block, is used in order to keep the temperature of the NMR-MOLE stable. The coil has been tuned at the resonance frequency of 5.07 MHz. The NMR-MOLE is connected to a KEA2 spectrometer (Magritek Ltd, NZ).
The NMR-MOLE prototype used in this thesis, is slightly different from the model used in [12], as it will be shown in section 6.2 of chapter 6. In fact it has a resonance frequency of 5.26 MHz and a field gradients distribution whit the highest value of 2 T/m, whereas the most present value is 0.6 T/m.

# Chapter 3

# NMR pulse sequences

Through the NMR-MOUSE and NMR-MOLE it is possible to perform many kind of different NMR measurements, which allow one to extract important parameters for the characterization of the analysed sample. The most common, and important, parameters extracted are:

- Spin density;
- Transverse relaxation time, $T_2$;
- Longitudinal relaxation time, $T_1$;
- Self-diffusion coefficient.

The NMR signal is due to the return of the nuclear spins to the thermodynamic equilibrium in the applied magnetic field, after the application of a radio frequency (RF) pulse at the resonance frequency. The return to equilibrium of the transverse magnetization induces in a coil the NMR signal according to the Faraday's law. In order to obtain the information about one specific parameter, a specific pulse sequence has to be performed. A pulse sequence is simply a succession of RF pules, sent in a way and with a timing useful to manipulate the nuclear magnetization.

## 3.1 Spin density and $T_2$ pulse sequences

The most simply pulse sequence is the free induction decay (FID) sequence, composed by one RF-pulse at the Larmor frequency of the protons present in the sample. This pulse excites the spins of the protons bringing the total magnetization, initially directed along the axis of the $B_0$ field (longitudinal axis z), away from the equilibrium state, creating a transverse magnetization in the transverse plane (x,y). When the RF-pulse is turned off, the magnetization relaxes coming back to the equilibrium state, and in this process the transverse magnetization decays preceding around the longitudinal axis. The signal acquired is the so called FID. An example of the sequence is given in Fig. 3.1, where a so called 90 RF-pulse is applied.

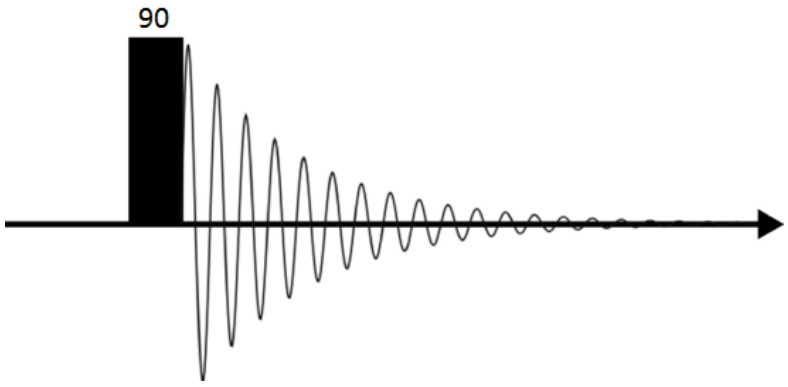


Figure 3.1: schematization of a FID pulse sequence.

The signal is given by the equation3.1.

$$S(t) = S(0) \exp\left(-\frac{t}{T_2^*}\right) \tag{3.1}$$

The intensity of the signal at zero time depends on the number of protons inside the sample. From the FID is also possible to extract the information about the $T_2^*$, that is the apparent transverse relaxation time. The term apparent is due to the fact that the the relaxation is affected by the $B_0$ field inhomogeneity.
Due to the highly in homogeneous field present in a single sided NMR device, the FID is not a good sequence with which to detect the NMR signal and extract information about the transverse relaxation time.

The most suited pulse sequence with those kind of devices is the Curr-Purcell-Melboon-Gill pulse sequence, based on the Hahn spin echo. In the next subsection those sequences are explained.

### 3.1.1 Spin-Echo pulse sequence

The equation3.2 report the spin-echo pulse sequence:

$$90_x - \tau - 180_y - \tau - Echo \quad Peak \quad acquisition \tag{3.2}$$

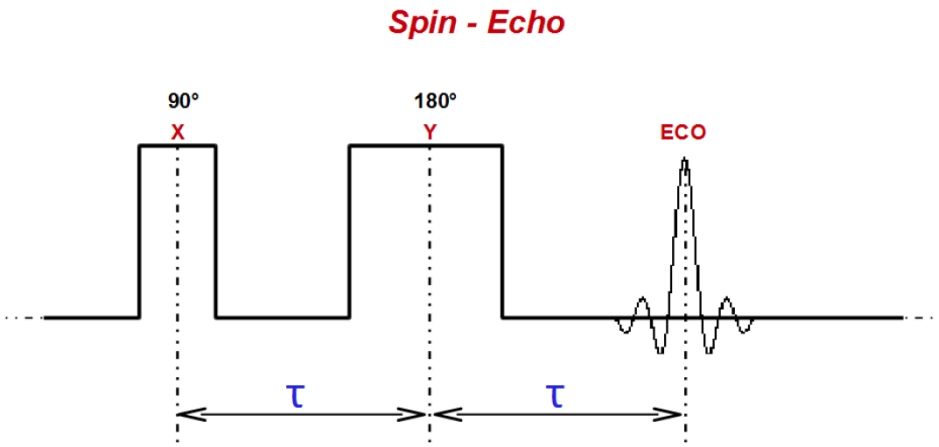


Figure 3.2: schematization of a spin echo pulse sequence.

At the thermodynamic equilibrium, the magnetization is parallel to the axis of the polarizing field $B_0$ (z-axis). A 90 pulse moves down the magnetization in the xy plane. The system, so, relaxes for a fixed time $\tau$. During this time, the transverse magnetization relaxes in accord with the equation 3.3:

$$M_{xy}(t) = M_{xy}(0) \exp\left(-\frac{t}{T_2^*}\right) \tag{3.3}$$

and, because the magnetization $M_{xy}(t)$ is proportional to detected the signal, the signal behaviour is described by the equation 3.1.
Therefore, the decay time of the transverse magnetization is an apparent transverse relaxation time $T_2^*$, which is lower of the real $T_2$. The latter is an intrinsic

characteristic of the spin system. How it is well known, the transverse relaxation is caused by a loss of coherence of the spins, which first precede with the same frequency (the Larmor frequency), because they feel the influence of the $B_0$ field. Successively, because each spin feels a local magnetic field due to the presence of neighbouring spins, each spins precedes at a different Larmor frequency, thus a loss of coherence among the spins occurs and when the coherence is completely lost there is no more transverse magnetization. It is important to note that this loss of coherence is irreversible, and it can not be recovered. Obviously, the presence of inhomogeneity in the $B_0$ field accelerates this process. In 1950, E.L. Hahn discovered a way to recover the coherence loss due to the inhomogeneities of the field $B_0$. If after a time $\tau$, a 180 pulse is given, at time $2\tau$ an echo-peak is formed. The time $2\tau$ is called echo time ($T_E$).
However, the coherence lost by the irreversible spin-spin interaction is not recovered, so that the spin-echo peak has a reduced amplitude, and so the evolution of the detected signal is described by the equation 3.4, in which the real transverse relaxation time $T_2$ is present.

$$S(2\tau) = S(0)\exp\left(-\frac{2\tau}{T_2}\right) \tag{3.4}$$

Repeating that pulse sequence for different echo-times it is possible to determinate the transverse relaxation time $T_2$ by a simple fitting of the experimental data.
A consideration has to be made now. This type of decay holds only in the absence of diffusion, when a field gradient is present.
As a result of the presence of a permanently turned on gradient in the single sided devices, the diffusion has to be taken into account. In particular the motion along the field gradient direction is significant. In the time interval $\tau$, between a 90 and 180 pulse, one spin can move in a region in which the polarizing field $B_0$ differs significant in intensity. Therefore, the Larmor frequency is different, and so the successive 180 pulse can not recover correctly the lost phase coherence of the spins system. Hence, the echo-peak will have a lower amplitude than the amplitude of the echo-peak in absence of diffusion. The equation 3.4 is then modified by adding

to the exponential a term and becomes:

$$S(2\tau) = S(0)\exp\left(-\frac{2\tau}{T_2} + \frac{2}{3}\gamma^2 g^2 D\tau^3\right) \tag{3.5}$$

the signal decays with an apparent relaxation time $T_{2app}$, where $\gamma$ is the gyromagnetic ratio, $g$ is the gradient intensity and $D$ is the diffusion coefficient.

### 3.1.2 Curr-Purcell-Melboon-Gill pulse sequence

The CPMG sequence is an extension of the spin-echo sequence. The formation of echoes can be repeated N times as discovered by Carr and Purcell. The CPMG sequence is the standard sequence for measurement of transverse relaxation decays. The equation 3.6 describes the sequence:

$$90_x - (\tau - 180_y - \tau - EchoPeak)_N \tag{3.6}$$

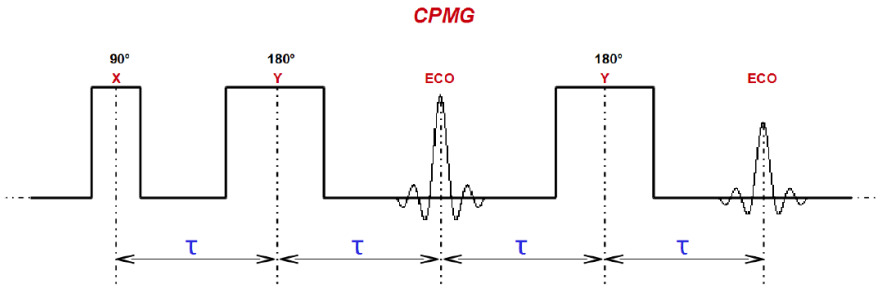


Figure 3.3: schematization of a CPMG pulse sequence.

the first two pulses are the same as in the spin-echo sequence. An echo is formed at the time t = $2\tau$. Successively, if the system is free to relax, the echo decays because of the loss of coherence of the spin system. If after another time $\tau$ a new 180 pulse is given, another echo-peak is formed at the time t = $4\tau$, and its amplitude is less than the previous echo because of the irreversible coherence loss due to the spin-spin relaxation.
Repeating this procedure for N times it is possible to acquire, in a single shot, the entire decay of the transverse magnetization, as systematized in Fig. 3.4.

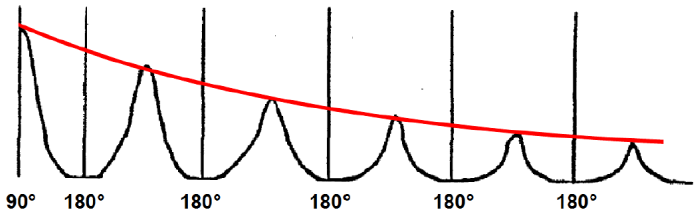


Figure 3.4: schematization of a CPMG pulse sequence.

When a CPMG echo train is generated in the strongly inhomogeneous fields, the infinite range of resonance offsets $\Omega = \omega_0 - \omega_{rf}$ leads to a wide distribution of effective RF pulse flip angles, where $\omega_0$ is the Larmor frequency and $\omega_{rf}$ is the RF-pulse frequency. The proper flip angles of 90 and 180 are only fulfilled at exact resonance for $\omega_0 = \omega_{rf}$. At some resonance offset $\Omega$ the nominal 180 pulse becomes an effective 90 pulse so that the first three pulses of a CPMG sequence generate a so called stimulated echo. In consequence, the echoes observed with a CPMG sequence in a strongly inhomogeneous magnetic field are sums of direct Hahn echoes and indirect stimulated echoes, and the echo train decays with an effective relaxation time $T_{2eff} > T_2$ [11]. Furthermore, the first echo is always a direct Hahn echo while the second one is the sum of a direct and an indirect stimulated echo, so that the first echo is smaller than the second, a fact that needs to be taken into account when evaluating CPMG echo trains by fitting model functions. Even in the CPMG sequence, the influence of the diffusion can not be neglected using the MOUSE and the MOLE as NMR scanners. The equation of the signal decay assumes, therefore, the form of the equation 3.4:

$$M_{xy}(t) = M_{xy}(0) \exp\left(-t\left(\frac{1}{T_2} + \frac{1}{3}\gamma^2 g^2 D\tau^2\right)\right) \tag{3.7}$$

This means that the sample relaxes with an apparent transverse relaxation time T2:

$$\left(\frac{1}{T2}\right)_{app} = \frac{1}{T_2} + \frac{1}{3}\gamma^2 g^2 D\tau^2 \tag{3.8}$$

However, the impact of translational diffusion can be attenuated when a short echo

time in the CPMG sequence is chosen. Due to the relevant role in the context of this thesis, below it will be explained some important parameters about CPMG sequence.

### CPMG parameters using the Prospa software

Both the NMR-MOUSE and the NMR-MOLE use the KEA2 as spectrometer. Latter uses the software Prospa (developed by Magritek for interfacing with the KEA2 spectrometer) to manage the pulse sequences.

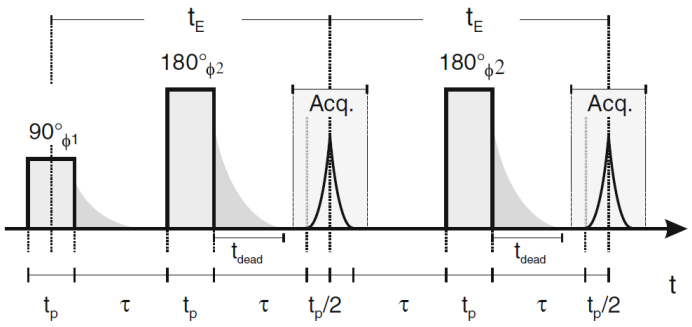


Figure 3.5: CPMG pulse sequqence with indicated some important parameters.

Fig.3.5 shows the CPMG sequence indicating some important parameters. The Most important parameters are:

- **Pulse length,** $t_p$: it is the time duration of the RF pulse. Its value is in the order of micro seconds, and it determinate the bandwith of the excited frequency, $\Delta\nu = \frac{1}{t_p}$;

- **90 and 180 attenuation**: they are the power attenuation (expressed in dB) of the transmitting coil, given a certain pulse width, to obtain respectively a 90 pulse and a 180 pulse.

- **Echo time, TE**: It is the time between two consecutive 180 pulses. The less is the echo time, the bigger has to be set the number of echoes, in order to sample all the decay of transverse magnetization, although a small echo time can limit the effect of the diffusion;

- **Number of echoes,** $N_E$: It is the number of echoes acquired in a single scan. Therefore, once set the echo time, the optimal choice of number of echoes depends on the goal of the measure. In order to acquire the entire decay of the echo signal, the optimal choice of number of echoes is $N_E = (5T_2)/t_E$; If the goal of the measure is simply estimating the signal intensity at zero time, setting high $N_E$ is not necessary.

- **Repetition time TR**: it is the waiting time between two consecutive scans, during which the longitudinal magnetization is built-up again. To fully reach the equilibrium magnetization the repetition time has to be in the order of $5 \times T_1$;

- **Number of scans,** $n_s$: it defines the number of times the experiment is repeated. The data acquired in each scan are added to improve the signal-to-noise ratio;

- **Acquisition time** $t_{acq}$: During an echo train acquisition, each echo is sampled in an acquisition window of width $t_{acq}$, which is centred at the maximum of the echo.

- **Dead time** $t_{dead}$: it is the minimum time that has to be wait between the end of the pulse transmission and the start of the signal acquisition. The presence of a dead time is because the RF-coil works both as transmitter and as receiver. It value depends on the electronic components and characteristics of the entire chain of the acquisition instrumentation.

## 3.2 $T_1$ pulse sequences

The spin-lattice relaxation time $T_1$ is the characteristic time needed by the spin system to exchange energy with its surrounding (the *lattice*). Pulse sequences designed to measure $T_1$ consist mainly of three stages:

- A preparation period, during which one or more RF pulses are used to modify the longitudinal magnetization, in order to move it away from its equilibrium state;

- A free evolution period, during which the magnetization is free to relaxes in order to return to its equilibrium state;

- A detection period, in which the longitudinal magnetization is converted, by a 90 pulse, into a transverse magnetization, in order to measure the system state achieved during the previous stage.

The measurement requires an experiment in which the duration of the free evolution period is varied to cover a time range of the order of several $T_1$s. The main sequences used are the inversion recovery and saturation recovery. Due to the high inhomogeneous filed, with the NMR-MOUSE only the saturation recovery pulse sequence is used, because of the impossibility of inverting the magnetization. With the NMR-MOLE an inversion recovery can be performed, even if the inversion is not perfect, due to the field inhomogeneity.

### 3.2.1 Saturation recovery and inversion recovery

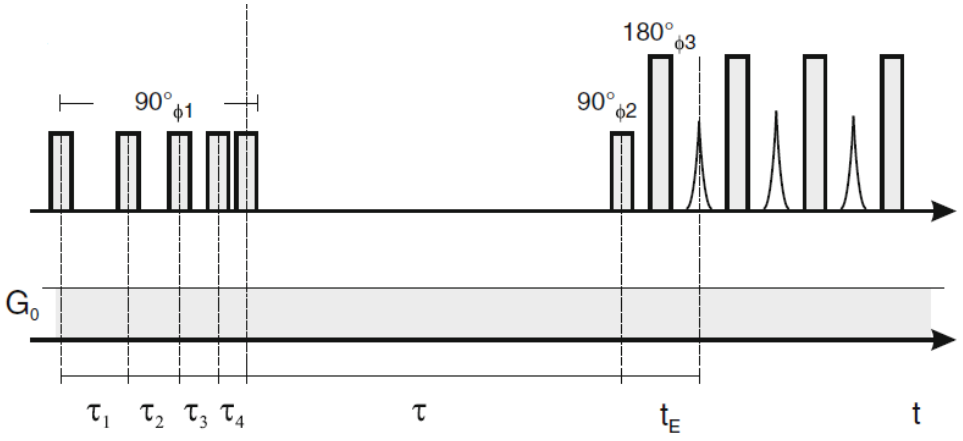


Figure 3.6: Saturation recovery pulse sequqence.

Figure3.6 shows the saturation recovery sequence. The first stage consists in an application of a train of 90 pulses, in order to saturate the transverse magnetization. In a second stage, a free evolution period $\tau$ is left. During this stage, the longitudinal magnetization grows from zero to its maximum value $M_0$ (equilibrium

state) with a time dependence shown in the equation 3.9:

$$M(\tau) = M_0 \left(1 - \exp\left(-\frac{\tau}{T_1}\right)\right) \tag{3.9}$$

A second 90 pulse moves down in xy plane the longitudinal magnetization, and a CPMG sequence is performed in order to detect the signal.
After one scan, others saturation recovery sequences are made with a different value of the free evolution period $\tau$, in order to sampling the build-up curve of the longitudinal magnetization.
Considering that the sampled function is expected to be exponential, it is convenient to vary $\tau$ logarithmically. This guarantees that the build-up curve is sampled at constant amplitude steps, setting more points at short times, where the curve varies with the largest rate, and less points at the end, where almost no variation is expected. Through an exponential fit, it is possible to extract the $T_1$ estimation of the sample, and by a Laplace transform a distribution of longitudinal relaxation times present is obtained. In conclusion the saturation recovery sequence use a saturation recovery as encoding sequence and a CPMG as a detecting sequence.

In the inversion recovery the encoding period is made by two pulse separated by an evolution period following this scheme:

$$180 - \tau - 90 - CPMG \quad detection \tag{3.10}$$

The saturation recovery has many advantages, in respect of the inversion recovery sequence.

For example, because this sequence starts nullifying the longitudinal magnetization, it does not require any recycle delay in between experiments. This not only leads to a considerable shortening of the measurement time, but it also eliminates the need to know in advance an estimation of the $T_1$ of the sample. In other words, a wrong setting of the time range for $\tau$ just leads to sample the build-up curve in a non-optimal way. Nonetheless, the characteristic time extracted from the fit is the correct one.

The NMR-MOUSE has a strong gradient, so that the presence of high inhomoge-

neous field has to be considered.
The main problem is related to the impossibility to achieve full magnetization saturation across the full sensitive volume. Saturation is only achieved for the on-resonance spins (assuming a homogeneous $B_1$ field), but just partial saturation is achieved for off-resonance ones. Consequently, some remnant magnetization stays along the z-axis after the saturation period. Hence, the $T_1$ curve at $\tau = 0$ starts from an offset value, which, for a detection bandwidth matched to the bandwidth of the pulse, is about 1/4 of the maximum signal measured for $\tau >> T_1$. In order to reduce the offset $T_1$ curve is sampled in an inverse way, starting from the longest $\tau$ value. In fact, if the first point is measured for a free evolution period $\tau >> T_1$, the value measured is close to $M_0$ and is independent by the offset left after the saturation. When $\tau$ is shortened to measure the second point, the pre-saturation achieved by the first scans reduces the longitudinal magnetization, attenuating the offset.

Below the most important parameters set utilizing the sequence with the Prospa are summarized:

- **Max. Recovery time**: it is the maximum value of free evolution period $\tau$. To obtain an optimal sampling of build-up curve it should be set equal to $5 \times T_1$. However, if a no a-priori estimate of T1 is given, even a non-correct value allows obtaining a correct value of $T_1$ by the fit;

- **Number of $T_1$ points**: Number of points (recovery times $\tau$) in the $T_1$ curve;

- **Recycle delay (repetition time)**: For a saturation recovery, in principle, the recycle decay can be set very short, since no additional recovery period is needed between different scans. However, when measuring short $T_1$ values and using a high number of echoes in the detection train, the recycle delay should be increased to avoid heating of the coil. For the inversion recovery sequence this time has to be set at least $5 \times T_1$.

## 3.3 MNR-MOUSE profile sequence

The NMR-MOUSE has the capability to perform a CPMG at different depths of the sample. This thanks to the presence of a lift, which allows one moving up or down the permanent magnet. Because the distance between the sensitive volume and the permanent magnet is fixed, moving-down the magnets means a displacement of the sensitive volume within the sample.
In this manner, it is possible to follow the variation of the signal in function of the depth within the sample.

## 3.4 Diffusion measuraments

In many systems molecular self-diffusion provides important information on molecular organization and interactions of mobile molecules with the environment. The large gradients as provided by the NMR-MOUSE simplify measurements of the diffusion coefficient in heterogeneous materials like porous materials and biological systems, since it has a always switched on gradient and there is no necessity of a gradient coil. The principle of measuring self-diffusion by NMR is to measure the mean square displacement $\langle R \rangle^2$ that magnetization components experience in a given diffusion time $\Delta$. With this aim, initial and final positions of the spins are identified by measuring their initial and final resonance frequencies $\omega_i$ and $\omega_f$, respectively, in a magnetic gradient field with field gradient $G = G_y$ (as it is the case of the NMR-MOUSE). Suitable pulse sequences, therefore, must contain at least two time intervals, one where the initial positions of the spins are tagged and one where the final positions are read out. Given that the measurement requires inhomogeneous magnetic fields, these pulse sequences are echo sequences, in particular the Hahn echo with the CPMG echo train as its extension and the stimulated Echo.

### 3.4.1 Diffusion coefficient by stimulated echo sequence

The scheme of the sequence is depicted in Fig. 3.7. In this sequence the magnetization is stored in z-direction during an evolution period $\Delta$, where the magnetization

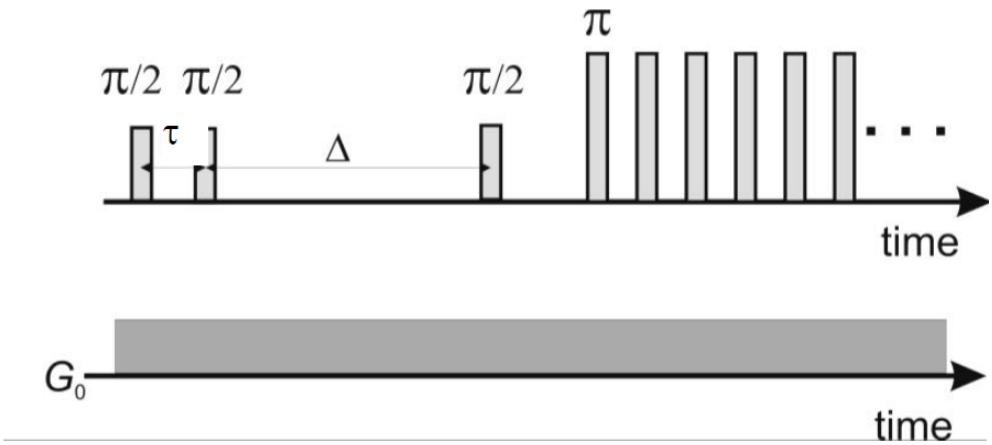


Figure 3.7: SSE + CPMG sequence for diffusion measurements.

decays due to T1. So that, compared to the Hahn-echo sequence, longer diffusion times can be realized and the measurement of D as a function of the evolution time $\Delta$ offers the possibility to probe length scales of restriction (in the case of a restricted diffusion).

By assuming a reference where z is the $B_0$ direction, a first 90 pulse is applied to move down the magnetization into the transverse plane. A single $90_x$ pulse applied after a time $\tau$ has the effect of rotating the y-component of magnetization into longitudinal polarization along the z-axis, a state in which only $T_1$ relaxation will occur. Any x-magnetization will be unaffected so that only half of the transverse magnetization can be stored in this way. After an evolution time $\Delta$, using another $90_x$ pulse, the stored longitudinal magnetization is converted into transverse magnetization. At this stage, a CPMG sequence is made in order to read out the signal, which will be attenuated by the diffusion.

The signal attenuation can be described by the equation 3.11:

$$\log\left(\frac{I}{I_0}\right) = -\gamma^2 G^2 D\tau^2 \left(\Delta - \frac{2}{3}\tau\right) \tag{3.11}$$

Where $\tau$ is the encoding time, G the field gradient, D the diffusion coefficient and $\gamma$ the gyromagnetic ratio. Self-diffusion coefficient can hence be measured by a simple linear fit.

## 3.5 2D correlation measurements

A powerful extension of the measurements of NMR relaxation and molecular self-diffusion in grossly inhomogeneous fields is the measurement of multi-dimensional distribution functions involving diffusion, transverse, and/or longitudinal relaxation [13].
The two-dimensional experiments allow one to extract inherently more information than the corrispective one-dimensional experiments, for example, in the case of multi-component systems, from the $T_1 - T_2$ map it is possible to extract the $T_1/T_2$ ratios of the single components, and from the $D - T_2$ maps it is possible distinguish components that otherwise would be undistinguishable by just performing the one-dimensional $T_2$ measurement, or one-dimensional D measurement.
In this thesis two kinds of 2D correlation measurements have been used: The $T_1 - T_2$ correlation map and the $D - T_2$ correlation map.
Because both the 2D experiments mathematically are based on the same concepts, i.e. the two-dimensional Inversion Laplace Transform (2D ILT), it is worthy to give a brief general introduction about the problem, and describe the pulse sequences used.

The measurement of 2D distribution functions of two quantities $x_1$ and $x_2$ (such as relaxation and diffusion) is based on sequences where two or more independent times are varied in such a way that the kernel of the integral reported below separates out. In that case, in fact, the measured magnetization $M(t_1, t_2)$ depends on the quantities of interest $x_1$ and $x_2$ through the equation 3.12 [13]

$$M(t_1, t_2) = \int \int f(x_1, x_2) K_1(x_1, t_1) K_2(x_2, t_2) dx_1 dx_2 \tag{3.12}$$

where $f(x_1, x_2)$ is the wanted distribution (also called *map*), and $K_1$ and $K_2$ are the kernels. Because for relaxation and diffusion NMR experiments the kernels are in the form of $\exp(-\alpha x_i t_i)$, the goal is to obtain the wanted function by a 2D ILT. The shape of the kernels depend on the specific pulse sequence, because, depending on the pulse sequence, different physical phenomena affect the spin dynamic.

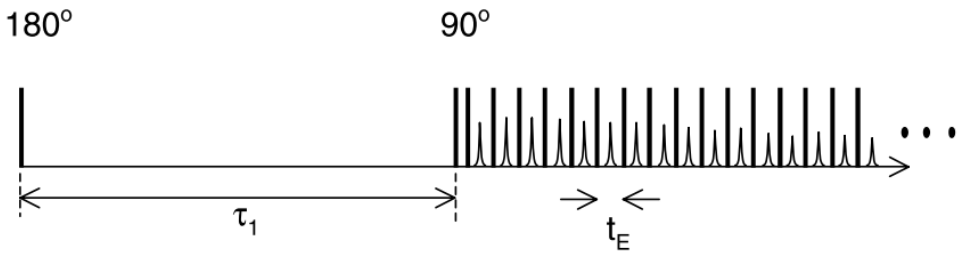


Figure 3.8: Inversion recovery + CPMG sequence.

### 3.5.1 $T_1$ Editing CPMG pulse sequence

The $T_1 - T_2$ pulse sequence can be though like a common CPMG in which the first 90 pulse is replaced by an *editing* sequence that allow one to make the system sensitive to the longitudinal relaxation. This can be easily made by adding to an inversion recovery a CPMG sequence like sketched in Fig.3.8.

The time$\tau_1$ is varied during the experiment, whereas $t_E$ is kept constant, and as short as possible to avoid the effect of the diffusion during the CPMG decay.
In this case the equation 3.12 becomes:

$$M(\tau_1, kt_E) = \int\int f(T_1, T_2) \left(1 - 2\exp\left(-\frac{\tau_1}{T_1}\right)\right) \exp\left(-\frac{kt_E}{T_2}\right) \tag{3.13}$$

and $f(T_1, T_2)$ is the 2D density distribution of the relaxation times, computable by the 2D ILT.

### 3.5.2 Diffusion Editing CPMG pulse sequence

In this case the sequence is a stimulated spin echo (SSE) followed by a CPMG, where the SSE is the editing sequence in which the effect of the diffusion is encoded . The sequence is sketched in the Fig. 3.9. It is the same sequence described in section 3.4.1. the only change is the way in which the data are saved. In this case the CPMG echo train decay is acquired, whereas in the simply SSE the CPMG echo train is summed, implying a loss of information about the transverse relaxation.

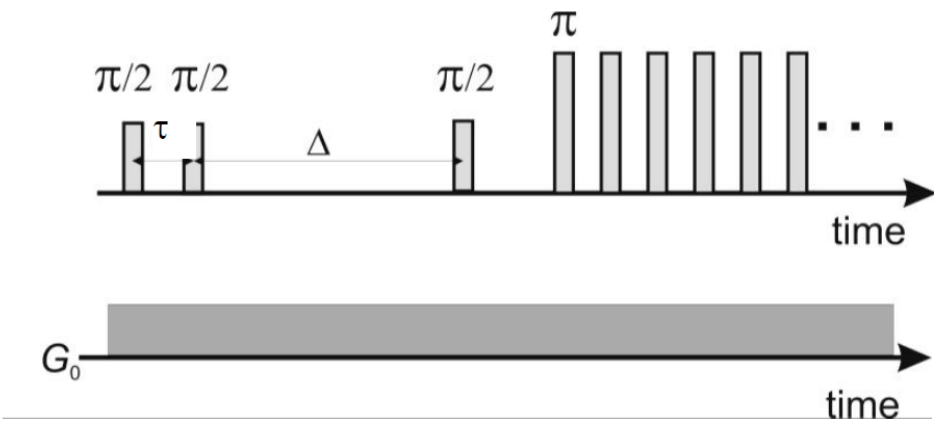


Figure 3.9: SSE + CPMG sequence for diffusion measurements.

In this case the equation 3.12 becomes:

$$M(\tau, kt_E) = \int\int f(D, T_2) \exp\left(-\gamma^2 G^2 D\tau^2 \left(\Delta - \frac{2}{3}\tau\right)\right) \exp\left(-\frac{kt_E}{T_2}\right) dD dT_2 \tag{3.14}$$

and $f(D, T_2)$ is the 2D density distribution of the diffusion coefficients and $T_2$ times, computable by the 2D ILT.

# Chapter 4

# Materials

In this chapter the compounds and the samples used in this work, and their role in the context of the research, are presented.

## 4.1 Distilled Water

Water is an important substance to analyse. For example, the human body is for more than 70% composed by water [14].
In the field of NMR, water is a great source of signal because of his abundance of $^1H$ nuclei. To characterize the instruments, in this project water has been used as reference sample, because of its well-known properties.

## 4.2 Cu(II)-EDTA

EthyleneDiamineTetraacetic Acid (EDTA), is an aminopolycarboxylic acid, water-soluble solid. The main features of EDTA is its role as a hexadentate ligand and chelating agent, i.e., its ability to "sequester" metal ions such as $Ca^{2+}$ and $Fe^{3+}$. In the specific case EDTA is bounded with $Cu^{++}$ ions, as it is show in Fig.4.1
EDTA have application in many fields, such as industry, medicine and cosmetics. In NMR Cu(II)-EDTA is important because of the presence of the copper, it gives to the solvent, in which this salt is dissolved, a paramagnetic properties. Hence, it decreases the relaxation time of the solvent. In this research, EDTA has been

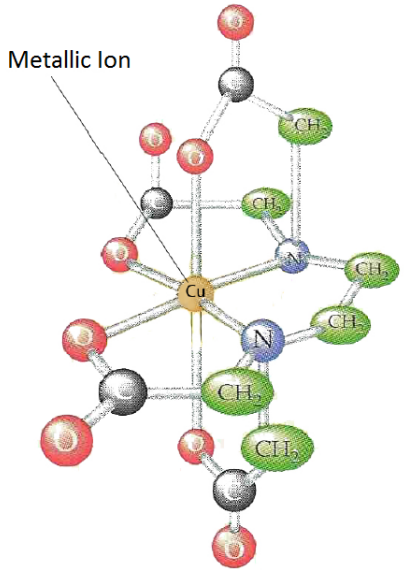


Figure 4.1: Picture of CuEDTA molecule. Figure taken from Wikipedia.

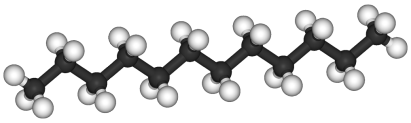

Figure 4.2: Molecule of soltrol 170

used in solution with distilled water.

## 4.3 Soltrol 170

The Soltrol 170 (Fig. 4.2) is a liquid alkane hydrocarbon, with the chemical formula $CH_3(CH_2)_{10}CH_3$, an oily liquid of the paraffin series. It has 355 isomers [15]. It is used as a solvent, distillation chaser, and scintillator component. It is used as a diluent for tributyl phosphate (TBP) in reprocessing plants.

In this work, the Soltrol 170 has been used to test the diffusion measurement and to verify that the technique gives a reliable result, because its diffusion coefficient is well known in literature.

## 4.4 Bone Marrow

Bone marrow is the soft tissue in the interior of the bones. In humans, red blood cells are produced by the bone marrow in the heads of long bones in a process known as hematopoiesis. On average, bone marrow constitutes the 4% of the total body mass of humans.
The hematopoietic component of bone marrow produces approximately 500 billion blood cells per day, which use the bone marrow vasculature as a conduit to the body's systemic circulation [16]. Bone marrow is also a component of the lymphatic system, producing the lymphocytes that support the body's immune system.
The two types of bone marrow are *red marrow*, which consists mainly of hematopoietic tissue, and *yellow marrow*, which is mainly made up of fat cells. Red blood cells, platelets, and most white blood cells arise in red marrow. Both types of bone marrow contain numerous blood vessels and capillaries.
Red marrow is found mainly in the flat bones, such as the pelvis, sternum, cranium, ribs, vertebrae and scapulae, and in the spongy material at the epiphyseal ends of long bones such as the femur and humerus. Yellow marrow is mostly found in the medullary cavity, the hollow interior of the middle portion of long bones.
In this work only pig bone marrow has been used. Its role in the aim of the research is of great importance, because of the assumption that in the analysed trabecular bone samples, mainly the bone marrow gives the NMR signal.
Because the bone marrow is an organic sample, after few hours from the preparation of a sample, a new one was prepared, so a few samples of bone marrow have been used.

## 4.5 Trabecular bone samples

In this thesis the attention is focused on the micro-structure of the trabecular bone (TB). In particular, as already pointed out, the goal is to evaluate the BV/TV ratio using an NMR technique.
The TB samples can be divided in two main sets according to the type of measurement performed.

TB samples used to perform the BV/TV ratio measurements belong to the first set. TB samples utilized to perform the relaxometry characterization belong to the second set.

### 4.5.1 TB samples to assess BV/TV ratio

Nine samples of pig bone have been used in order to test the feasibility of a NMR-based technique to assess the BV/TV ratio using single-sided devices.
They belong to three different subsets:

1 One bone sample, labelled *Bone I*, from the pig's shoulder: it is the first trabecular bone sample analysed with the NMR-MOUSE PM10. Many measurements have been performed, in order to characterize the sample and to set-up the optimal experimental conditions. It is important to observe that in this case the micro-CT measurements have been performed before performing the NMR measurements.
The sample, represented in Fig.4.3, is cylindrical shaped with a diameter of 1 cm and height of 3 cm. The sample has been prepared by the Istituto Ortopedico Rizzoli.

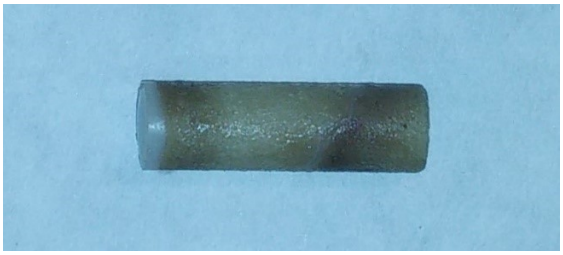

Figure 4.3: Bone I.

2 A set of six trabecular bone samples from different sites of the pig's shoulder. The samples are showed in Fig.4.4, and they are labelled as:

- Condilo IB;
- Condilo IIB;
- Testa IIA;

– Testa IIB;

– SC I SX;

– SC IIS X

Each sample represented in Fig.4.4 has cylindrical shape with diameter of 1 cm and height of 1.5 cm.

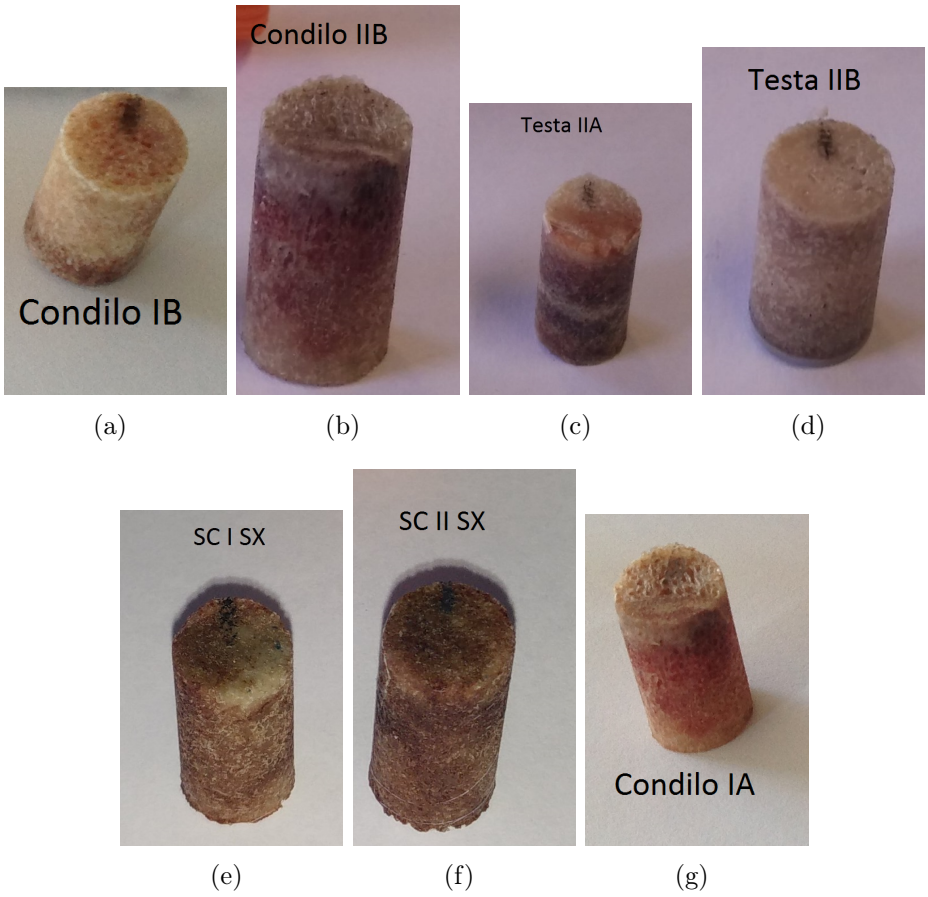


Figure 4.4: Second set of trabecular bone samples to assess the BV/TV ratio.

These samples have different levels of porosity, because of the different structure of the trabecular matri. The BV/TV values obtained by NMR has been compared with the values evaluated by micro-CT analysis. For these samples, the NMR measurements have been performed before micro-CT measurements. The samples have been prepared at the Istituto Ortopedico Riz-

zoli.

3 A TB sample coming from the pig's femur, labelled *Bone III*, used for comparing the performances of the NMR-MOUSE and NMR-MOLE in assessing the BV/TV ratio. The sample has cylindrical shape with diameter of 2.5 cm and height of 1.5 cm. The sample is shown in Fig.4.5.

Figure 4.5: Bone III.

### 4.5.2 TB samples to study the bone composition using the NMR-MOLE

This second set of biological samples has been used to perform a study to characterize the trabecular bone using relaxometry, and to characterize the tissues that surround the trabecular bone, like cartilage, fat and muscles. These samples, extracted from the pig's shoulder, contains not only the trabecular structure, but also the different tissues that surround the bone.
Three sample, labelled *biological samples*, have been used and are listed below:

- *Biological sampleI*;
- *Biological sample II*;
- *Biological sample III*.

The pictures of the samples will be shown in the part III, inside the chapter where the experiments performed over them will be described.

# Chapter 5

# Software

This chapter gives a brief presentation of algorithms and software utilized to analyse the experimental data. Just the algorithm utilized to make the inversion Laplace transform (ILT) will be analysed in detail, because of its importance in the field of NMR relaxometry measurements. On the contrary, the others will be just listed.
The list of the software is given below:

- UpenWin, the software that manages UPEN, which is the algorithm that makes the ILT;
- PSI-Plot, a software to create graph and performing data interpolation;
- Igor Pro, a software to create graph and performing data interpolation;
- Excel;
- Matlab.

## 5.1 UPEN - UniformPENalty ILT

UPEN and UpenWin have been developed at the University of Bologna to elaborate the NMR relaxation data [17]. A brief introduction of UPEN is here given.
Usually, observing the relaxation of complex systems, there is the presence of multi-exponential relaxation curves.

In the presence of multi-exponential relaxation it is always possible to identify a discrete distribution of the relaxation times, where each components has an amplitude that weighs the contribution to the signal, able to fit the experimental data. This relationship is described by the equation 5.1

$$S(t_i) = \sum_{k=1}^{m} a_k \exp\left(\frac{t_i}{T_{(1,2)k}}\right) \tag{5.1}$$

Where $i = 1, \ldots, n$ , $t_i$ represents the i-th sampling time of the signal, and $m$ is the number of components of the analysed system. $\chi^2$ parameter has to be minimized in order to extract the parameters of interest of each components, such as the equilibrium magnetization and relaxation times $T_1$ and $T_2$, from the sampled signal.

As a matter of fact, the computed distribution could represent only a good way to represent the data, but could have nothing to do with the real composition of the analysed system.

Increasing the number of components, a more realistic description of the behaviour of the system is reached, and hence, supposing a continuous distribution of the relaxation times, the equation 5.1 becomes:

$$S(t) = \int_0^\infty f(T_{1,2}) \exp\left(-\left(\frac{t}{T_{(1,2)}}\right)\right) dT_{1,2} \tag{5.2}$$

Because S(t) is the interpolation function of the experimental points, which are affected by error, the parameter $\epsilon$ has to be introduced in the equation5.2, which becomes:

$$S(t) = \int_0^\infty f(T_{1,2}) \exp\left(-\left(\frac{t}{T_{(1,2)}}\right)\right) dT_{1,2} + \epsilon \tag{5.3}$$

For this equation infinite solutions exist. The Upen software resolves the problem minimizing a function, in which, in addition to the sum of squared residuals, penalty terms that produce a smoothing of the distribution are present, in order to cut-off the excess of variations:

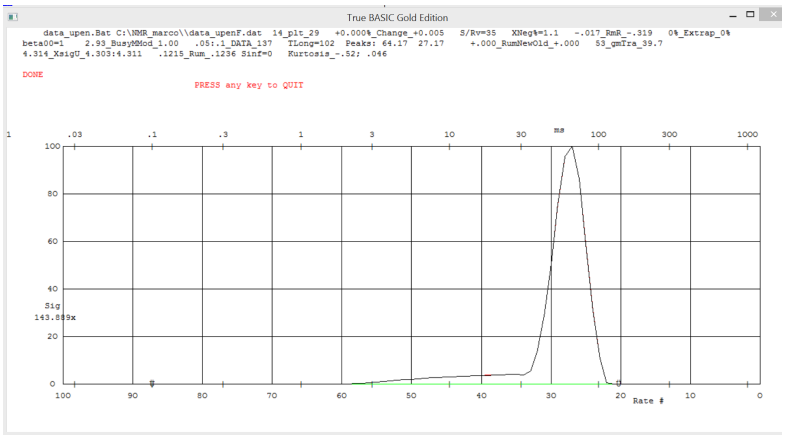


Figure 5.1: Frame of an elaboration of CPMG data by UpenWin

$$\underbrace{\sum_{i=1}^{N}\left(g_0+\sum_{k=1}^{M}g_k\exp\left(-\frac{t_1}{T_k}\right)-s_i\right)^2}_{\text{Sum of squared error of fit}}+\underbrace{\sum_{k=2}^{M-1}C_k(g_{k-1}-2g_k+g_{k+1})^2}_{\text{Penalty term}} \tag{5.4}$$

Upen introduces the coefficient $C_k$ that varies over the entire distribution in such a way to maintain almost constant the penalty at each R-point of the distribution (from that the name *Uniform Penalty*). The introduction of this regularization coefficient reduces the creation of artefacts inside the distribution. In fact, the programs with constant regularization coefficients often produce distributions, in which the tails are dived into peaks, (inducing an error due to the individuation of different non existing populations of $^1H$) even if a more simple distribution is justifiable, as the distribution that usually UPEN gives. In order to show an example of the Upen elaboration, the Fig.5.1 shows a distribution computed by Upen from CPMG relaxation data.
Below a short explanation of the main quantitative parameters is given:

- *Xsig*, is the extrapolation to zero time of the signal;
- *Peaks*, is the time of the peaks of the distribution;
- *gmT*, is the geometric-mean relaxation time of the computed distribution of relaxation times;

- *S/Rv*, is the SNR (signal-to-noise ratio). It can be used as a measure of data quality.

# Part III

# Experiments and results

In this part, the experiments performed, and the obtained results, are showed.
It is worthy to point out in more detail the idea behind the research project devoted to assess the micro-structure of the trabecular bone through single-sided NMR. In this way it will be more clear to follow the description of the experiments performed.

As remarked many times in this work, assessing the micro-architectural structure of the trabecular bone is important to estimate correctly the fracture risk of bones. It has been also shown that many parameters can be measured to characterize the micro-architectural bone structure (see section 1.1 in chapter 1.2.2), and high resolution MRI can allow to assess them.
However, high resolution MRI is expensive, and so it is worthy trying to find new ways that allow one to measure these kind of parameters and, at the same time, reducing the related costs.
A way to reduce the cost is to switch from high-field NMR to low-field NMR.
However it is possible to transfer techniques and knowledges from different NMR fields to solve this problem, in particular the field of NMR applied to the study of porous media. In this field, NMR is used to assess the porous structure using different kinds of techniques, and many of them are suitable for low-field NMR.
For example, a simple way to estimate the porosity of a rock sample is by computing a ratio of signal intensities. First, the rock sample is saturated of distilled water, and the signal of the water inside the pore of the rock sample is acquired by a FID or a CPMG. Then, the same measurement is made over a sample of bulk water of the same volume. The ratio of this two signals is the percent of water inside the rock sample, that is the porosity of the sample. This parameter gives an information about the internal structure of the rock sample.
Now, because the trabecular bone is a porous media, why do not apply the same concept to assess its structure? In a simplified view, the trabecular bone is composed by bone traeculae and in the inter-trabecular space there is the bone marrow, as sketched in Fig.5.2.
In this scenario it seems possible to extract the information about the porosity of the TB, that is equal to the bone marrow percent, using this technique, where the water is substituted by the bone marrow. In particular the bone quality

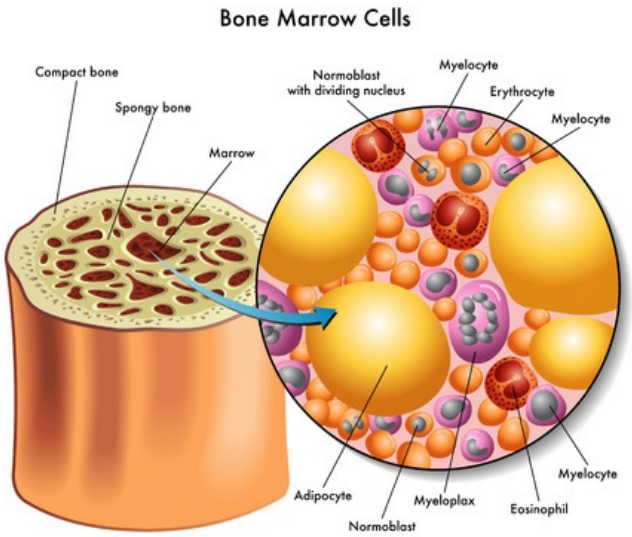


Figure 5.2: Representation of bone marrow inside trabecular bone, picture from Wikipedia.

parameter that in that way is possible to assess is the BV/TV ratio, because is just the complementer to one hundred of the porosity, according to the following equations:

$$Porosity(\%) = 100 \times \frac{S_{TBsample}}{S_{Msample}} \tag{5.5}$$

where $S_{TBsample}$ is the signal of a trabecular bone sample, and $S_{Msample}$ is the signal of a sample of marrow of same dimensions of the trabecular bone sample. And so,

$$\frac{BV}{TV}(\%) = 100 - Prosity(\%) \tag{5.6}$$

Of course the TB, being a biological sample, is a complex system. Thus a feasibility study has to be performed in order to verify the correctness of that approach, that even if it seems to work in theory may not be feasible in practise.
What makes that study worthy is the prospective to be able to assess a parameter as the BV/TV without the necessity of a imaging technique, and so switch to low-field NMR, with also the possibility to use single-sided NMR with their advantages. This procedure could open the way to a low-cost screening of the

population at risk of osteoporosis.

The experiments and results are presented following the spatio-temporal development of the work. In fact, the research has been started in Bologna, using the NMR-MOUSE PM10 in order to study the feasibility of the procedure able to assess the BV/TV ratio of the trabecular bone. The goodness of the technique has been evaluated by the comparison with the results obtained by the micro-CT. This topic is presented in chapter 7.
Once verified the feasibility of such a technique, the research has been developed in order to test the performance of a different single-sided device, the NMR-MOLE, performing the BV/TV assessing, and in order to solve some open questions appeared during the developments of the first part of the research, which will be more clearly pointed out in the following chapters.
This second part has been developed at the NMR group of the Victoria University of Wellington, and it is the topic of chapter 8.3.
In chapter 6 the experiments and results performed in order to characterize the single-sided NMR devices, the NMR-MOUSE PM10 and the NMR-MOLE, are presented.

# Chapter 6

# Instruments characterization

In this chapter the experiments and results performed in order to characterize the NMR-MOUSE PM10 and the NMR-MOLE are reported.

## 6.1 Characterization of the NMR-MOUSE PM10

To characterize the NMR-MOUSE PM10 is an important task because it allows one to have an idea of the performance of the instrumentation when analysing samples of unknown properties. With this aim, reference samples, such as distilled water and Soltorl 170 have been used due to their well-known properties.
In particular two kinds of characterizations have been made:

1 To control if all the instrumentation chain was working correctly and, at the same time, improving the knowledge of how the different settable parameters can affect the performance of the MOUSE. This goal has been pursued by performing relaxometry and diffusometry measurements on samples of well known properties;

2 To obtain an estimation of the dimensions of the available sensitive volume.

### 6.1.1 Relaxometry measurements

The evaluation of distilled water relaxation time $T_1$ and $T_2$ have been made by, respectively, a saturation recovery and a CPMG pulse sequence.

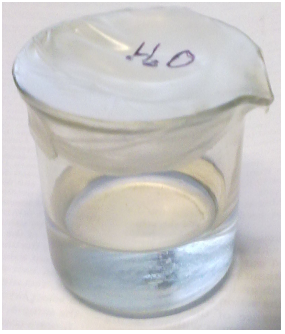

Figure 6.1: Distilled water sample utilized.

The liquid is contained into a backer as represented in Fig. 6.1. The measurements have been performed in two configurations.
First, with all four spacers inserted between the permanent magnet and the RF-coil (labelled 8 mm configuration). In this way the SNR ratio, fixed the number of scans, is the maximum achievable.
Second, with none spacers inserted (labelled 0 mm configuration), in order to assess the degradation of the SNR varying the distance between the RF-coil and the sensitive volume. The measurements have been performed at room temperature.

In Tab. 6.1 and Tab. 6.2 the main parameters of the utilized sequences are reported.

| | $t_p$ | 90 Att. | 180 Att. | $T_E$ | $N_s$ | TR | Max. Rec. Time | $T_I$ points |
|---|---|---|---|---|---|---|---|---|
| 8 mm | 5$\mu$s | -10 dB | -4 dB | 50 $\mu$s | 4 | 16 s | 15 s | 32 |
| 0 mm | 15 $\mu$s | -7 dB | -1 dB | 60 $\mu$ | 4 | 16 s | 15 s | 32 |

Table 6.1: Saturatio recovery parameters.

| | $t_p$ | 90 Att. | 180 Att. | $T_E$ | $N_s$ |
|---|---|---|---|---|---|
| 8 mm | 5$\mu$s | -10 dB | -4 dB | 50 $\mu$s | 8 |
| 0 mm | 15 $\mu$s | -7 dB | -1 dB | 60 $\mu$ | 128 |

Table 6.2: CPMG parameters

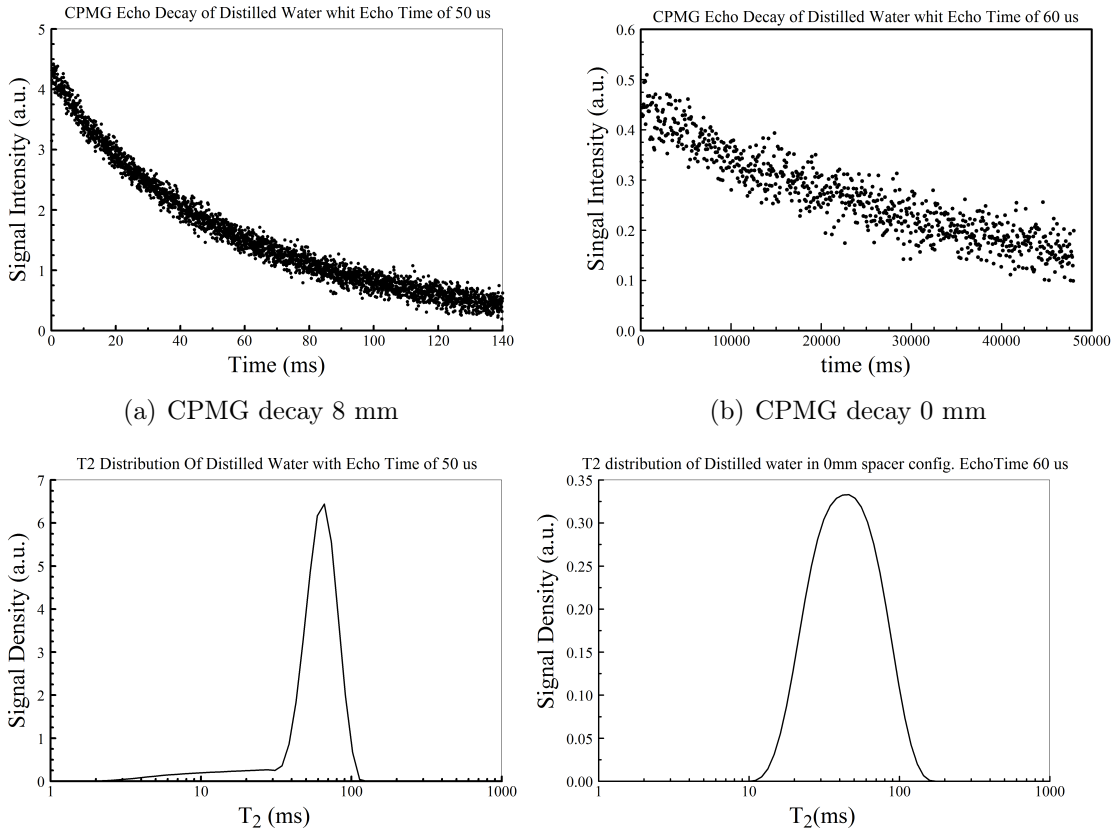


(a) CPMG decay 8 mm

(b) CPMG decay 0 mm

(c) $T_2$ distribution 8 mm

(d) $T_2$ distribution 0 mm

Figure 6.2: Results of the CPMGs perofrmed ovdr distilled water in different configurations with the NMR-MOUSE PM10.

The results of the CPMG measurements are reported in Fig. 6.2. Few main features can be extracted from them: the computed $T_2$ distribution, show a very short relaxation time with a peak around 70 ms, and this is due to the diffusion; moreover, the SNR in the 0 mm configuration is equal to 9, whereas in the 8 mm configuration the SNR is equal to 35.

In order to see the effect of the diffusion depending on the echo time two CPMG with longer echo times have been performed. The results are reported in Fig. 6.3. As expected, because of the diffusion, setting longer the echo time produces a shortening of the $T_2$ value.
The result of the saturation recovery measurements are reported in Fig. 6.4

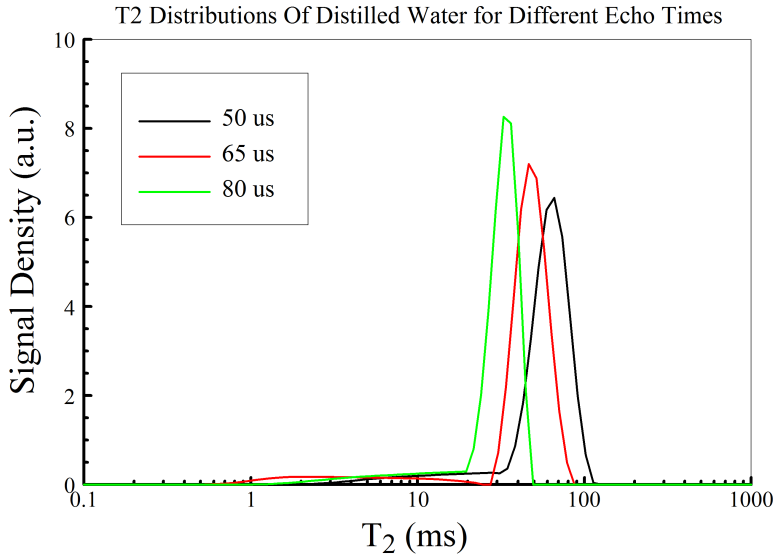


Figure 6.3: $T_2$ distirbutions for different echo times in 8 mm configurations.

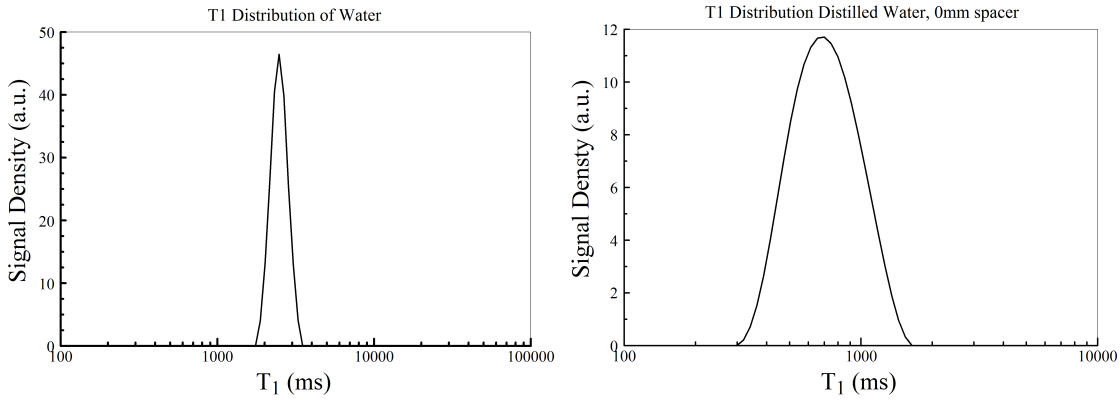


(a) $T_1$ distribution 8 mm

(b) $T_1$ distribution 0 mm

Figure 6.4: $T_1$ distributions of distilled water in different configurations with the NMR-MOUSE PM10.

The computed $T_1$ in much higher than the $T_2$ and this is because the $T_1$ relaxation time is not affected by the diffusion. Moreover the saturation performed at 0 mm configuration shows a $T_1$ peak shifted toward longer $T_1$ times in respect to the experiment performed in the 8 mm configuration. This is due to the higher room temperature in the case of the 0 mm configuration.

### 6.1.2 Self-diffusion coefficient Measurement

The self-diffusion coefficient of bulk Soltrol 170 has been assessed through a stimulated echo sequence in a 8 mm configuration, the parameters of the pulse sequence have been reported in Tab. 6.3. Because the value is well-known from the literature, the aim of the experiment is testing the capability of the NMR-MOUSE PM10 to reproduce a correct value of the self-diffusion coefficient. The sample is represented in Fig. 6.5


Figure 6.5: Soltrol 170 sample utilized.

| TR | $\tau_{min}$ | $\tau_{max}$ | $\Delta$ | Number of $\tau$ inc. |
|---|---|---|---|---|
| 400 ms | 0.025 ms | 0.36 ms | 1 ms | 15 |

Table 6.3: Stimulated Spin Echo parameters

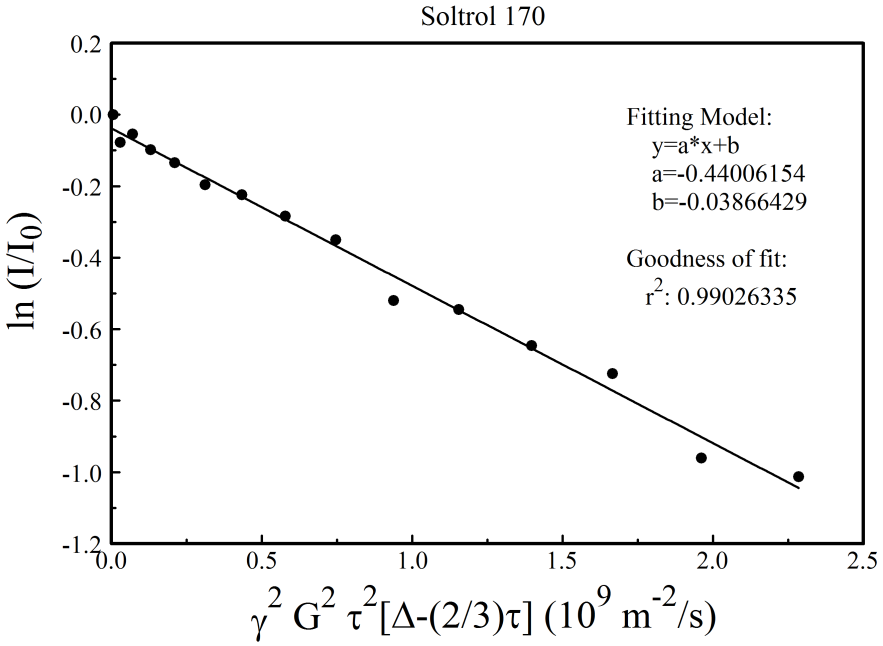


Figure 6.6: Experimental data and PSI plot fit.

In Fig. 6.6 the result of the experiment is reported. Using PSI-plot to make a linear fit of the experimental data it is possible to compute the self-diffusion coefficient of the Soltrol 170 according to the equation 3.11.
PSI-plot gives also the standard errors over the fit parameters.
The $D_{Soltrol170} = (0.44 \pm 0.01)\,\frac{\mu m^2}{ms}$, which is consistent with that presents in literature.

### 6.1.3 Sensitive volume

The term sensitive volume for a single-sided NMR scanner means the volumetric region, above the magnet and the surface coil, that can be excited from a RF-pulse. It is an important feature to know, because knowing which fraction of the sample is really analysed with the NMR-MOUSE makes possible to do a more significant comparison with the micro-CT data.

The size and the shape of this sensitive volume mainly depend on two factors.
First of all, it depends on the shape of the polarizing field $B_0$. In fact, $B_0$ de-

termines what will be the Larmor frequency of the protons in a region. It also depends on the duration of the RF-pulse (pulse length). In fact, the reciprocal of the pulse length gives the frequency bandwidth (eq. 6.1).

$$\frac{1}{t_p} = \Delta\nu \tag{6.1}$$

The shorter is the pulse, the bigger is the bandwidth, and hence the size of the sensitive volume. In an inhomogeneous field scenario, in which is always present a magnetic field gradient, this argument is even more important than in the high field NMR.
Of course, if the gradient has a well-shaped profile, like in the case of the NMR-MOUSE (linear gradient along the y-axis), the pulse length gives a direct information about the thickness of the sensitive volume.
In the case of the NMR-MOUSE PM10 the gradient is 600 KHz/mm, so we can directly compute the thickness of the slice both in the 8 mm configuration ($t_p = 5$ $\mu$s) and in the 0 mm configuration ($t_p = 5$ $\mu$s):

$$\frac{1}{5\mu s} = 0.2MHz \rightarrow \Delta y \simeq 300\mu m \tag{6.2}$$

$$\frac{1}{15\mu s} = 0.06MHz \rightarrow \Delta y \simeq 100\mu m \tag{6.3}$$

Under the assumption that the $B_1$ field is almost homogeneous in such a tick slice, the sensitive volume is a parallelepiped with a thickness indicates by equation 6.2 or 6.3, depending on the spacers configuration.
Also the dimensions of the base surface of this slice have to be determined. The RF-coil has an area of $(2.5 \times 2.5)$ $cm^2$, and of course the area of the sensitive volume in the zx plane has to be less or equal to this area. However, because of the $B_1$ and $B_0$ inhomogeneities, it is expected to be smaller.
In order to obtain this information, distilled water doped with Cu-EDTA has been used. It has been poured into a cylindrical container made of plastic, as shown in Fig. 6.7.
The container has the following dimensions:

- *Inner diameter*: 2 mm;

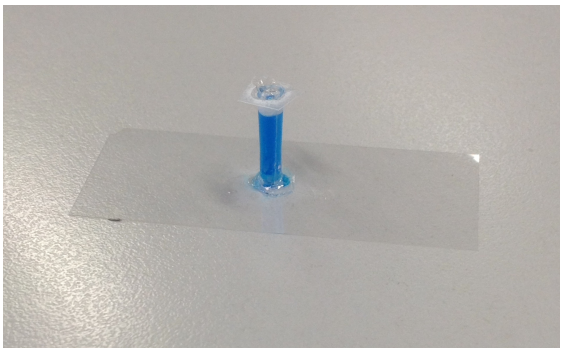

Figure 6.7: Cu-EDTA sample utilized.

- *Outer diameter*: 4 mm;

The singal has been acquired as shown in Fig. 6.8. A graph paper has been placed above the surface of the NMR-MOUSE PM10, as shown in Fig. 6.9, in order to be able to know the position of the sample within the RF-coil area.
The idea is to acquire the signal coming from the sample in different positions within the RF-coil area. A CPMG sequence in a 8 mm configuration has been used to assess the signal.
If the sample is outside the sensitive volume there is no signal detected. On the contrary, if the sample is inside, a non-zero signal is detected.
Two main considerations have to be made:

1 In order to sample the signal in a reasonable number of points within the RF-coil area, the sample has to have a relative small size, and for this reason the plastic container described above has been used. However, a sample with a great spin density is necessary to provide a sufficient signal. Distilled water was the sample whit the biggest spin density within the set of available samples in the laboratory. Although all the spacers have been inserted, the signal coming from a sample of such dimensions is still quite low and a high number of scans are necessary to achieve a reasonable good SNR. In our case 2048 scans have been acquired.
Because the $T_1$ of distilled water is about 2 s, the time needed to perform one CPMG on distilled water, with 2048 scans, is roughly one hour.
A good way to decrease the measurement time, maintaining a high number of scans, is to use the Cu-EDTA to dope the distilled water. It, thanks to

its paramagnetic properties, can reduce the $T_1$ of the water, and the higher is EDTA concentration, the shorter is the relaxation time.
In this experiment the concentration of Cu-EDTA has been set in a way to produce a $T_1 = 200$ ms. Therefore, the time needed to perform a measure is roughly 7 minutes. A more reasonable measurement time.

2 A CPMG of the plastic container without the doped water inside, and a CPMG of the container filled with doped water have been performed. A comparison of the signals are reported in Fig. 6.8.
It can be observed that the signal of the plastic container decays more rapidly in respect to the signal of the container filled with doped water, but the signal intensity is not negligible, and the resolution in the displacement would be 4 mm, not 2 mm.
In order to reach a sample of just 2 mm of diameter the first 1 ms of the echo decay has been cut from the elaboration, cutting off the contribution of the plastic container. Therefore the sample can be considered as a cylinder with a diameter of 2 mm.

The sample, represented by a blue circle in Fif. 6.10, has been moved over the grid, with steps of 2 mm, in order to acquire the signal in different position within the RF-coil area.
In this way a grid of 11 $\times$ 11 points has been obtained, and using MATLAB to interpolate the data it has been possible to obtain a 2D normalized function f(x,y), which expresses how much signal, in percent, is present in a voxel in function of the position inside the RF-coil surface.

The result of the MATLAB elaboration is reported in Fig. 6.11, and it shows an area in which the signal is different to zero in a circle of radius around 8 mm, but a region in which the signal is above the 80% of around 5 mm. Moreover, inside that region it is clearly evident a column in which the signal is lower than the signal coming from the neighbour voxels, meaning a discontinuity of the polarizing field $B_0$.

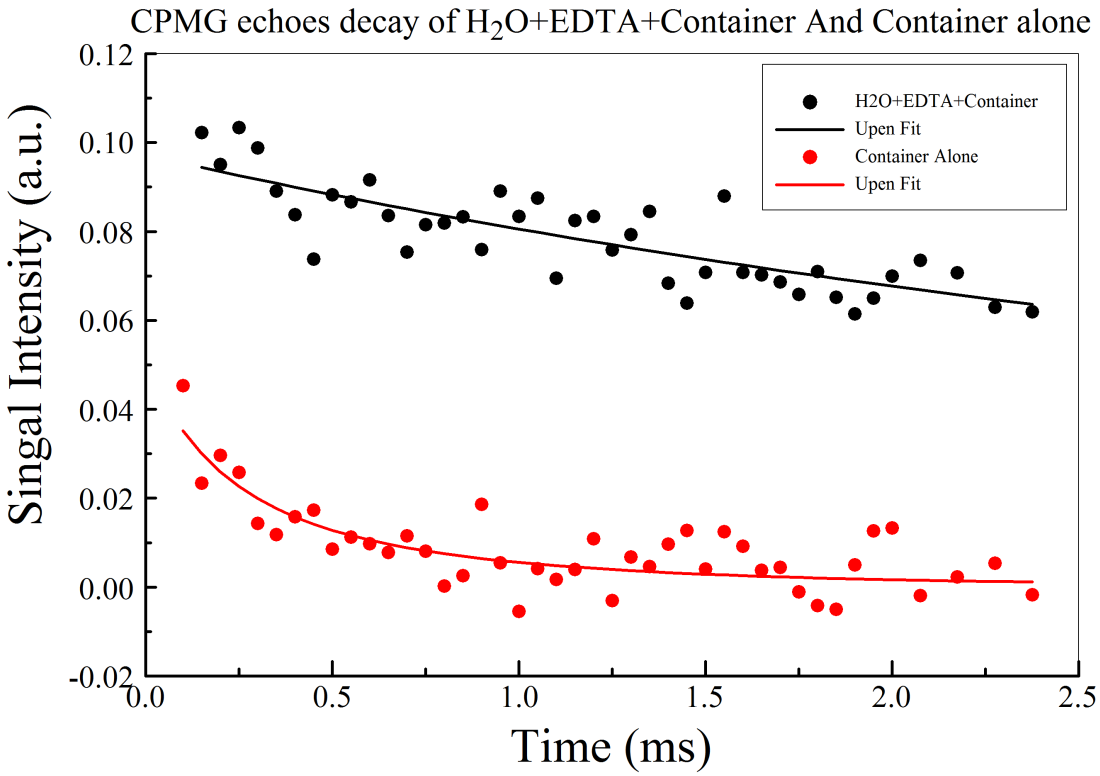


Figure 6.8: Signal Intensity Vs time of doped ditilled water+container and container alone.

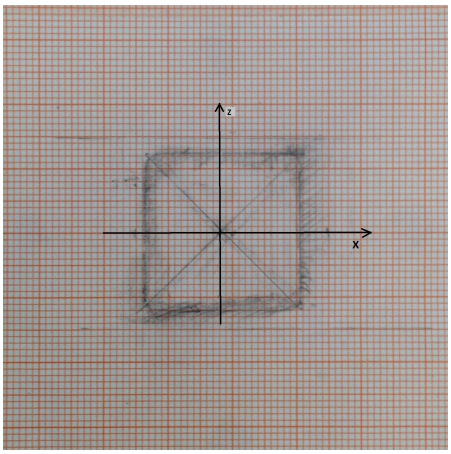

Figure 6.9: Picture of the graph paper placed over the surface coil.

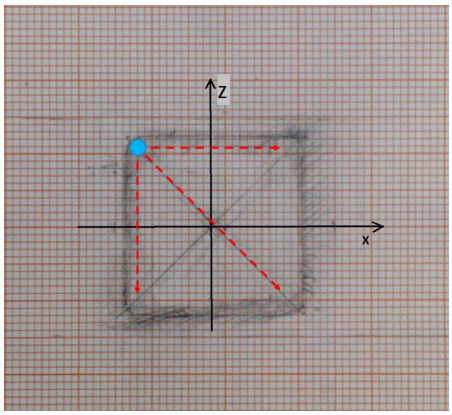


Figure 6.10: Picture the graph paper placed over the surface coil, with indicate the performed experiment.

## 6.2 Characterization of the NMR-MOLE

The characterization of the NMR-MOLE follows the same idea that has drove the NMR-MOUSE PM10 characterization.
The NMR-MOLE is a prototype, and so that it has been necessary to set-up and checking the instrument components such as the probe circuit and the polarizing field in order to find the correct Larmor frequency.
The results of preliminary experiments indicated a degradation of the performance respect to the previous experiments. Many analysis have been made, and so just a summary of what it has been done it is described.

A new probe circuit has been built, but the substitution of the probe circuit did not solve the problem, in particular the signal intensity was still considerably lower than the intensity that a same amount of water used to give in the past.
In order to find the cause of this behaviour, several checks have been performed over the KEA2 and the external amplifier, a new coil has been built and the cable and connections have been modified in order to reduce the noise.
A field map of the NMR-MOLE has been made using the Gaussmeter LakeShore MNT-4E04-VH. The probe has been used to measure the magnetic field strength at different positions.
In order to generate a volumetric field map, the field strength has been sampled

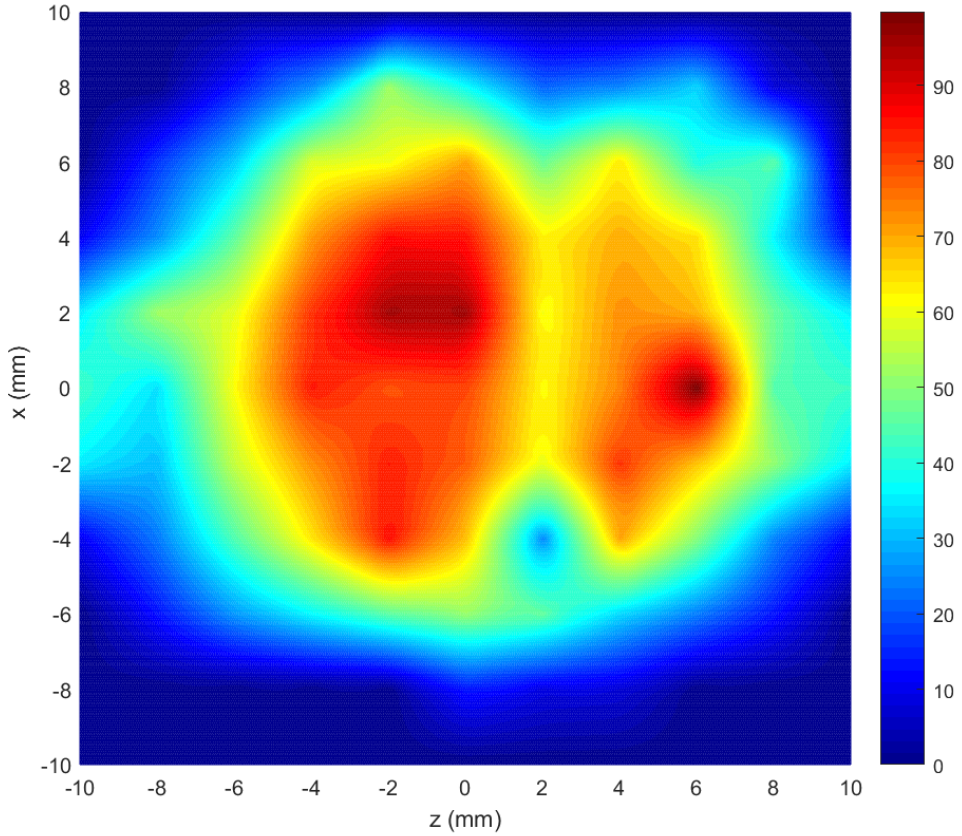


Figure 6.11: Signal intenisty in function of the position within the RF-coil area, 2D Matlab extrapolation.

in 819 points. A lift has been built by using a 3D-printed flat support and 3M screws (i.e. the diameter of the screws is equal to 3 mm) as it showed in Fig. 6.12 The screws allow one to lift up the support of 0.5 mm per each turn. Using this set-up it has been possible mapping the field strength in a three dimensional way. For each height, the field has been measured starting from the centre of the polar grid and following a circular sampling. The support has been lifted up 8 times with steps of 1.5 mm. A picture of the measuring procedure is shown in Fig. 6.13.

The acquired data have been analysed with MATLAB, and a iso-surface plot is reported in Fig 6.14. The z-axis represents the distance from the surface coil, and

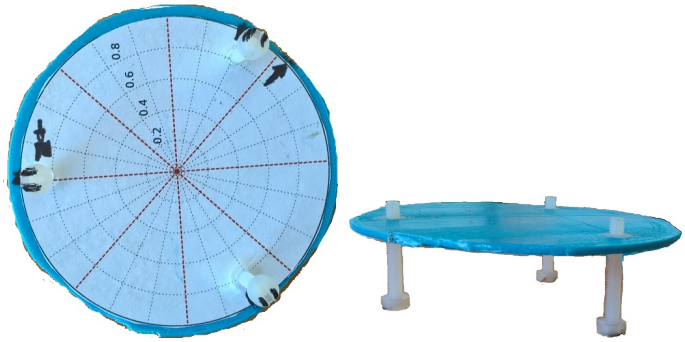


(a) Top view of the used lift (b) View of the upside-down lift

Figure 6.12: Lift used to measure the field at different hight in the NMR-MOLE.

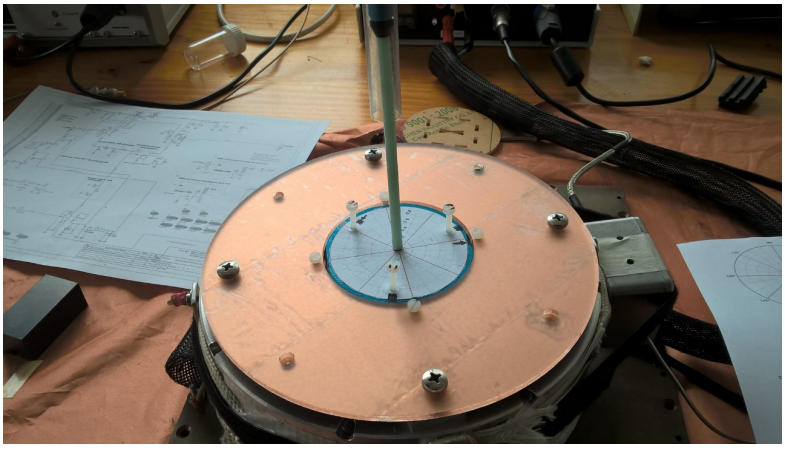

Figure 6.13: Frame of a measuring procedure.

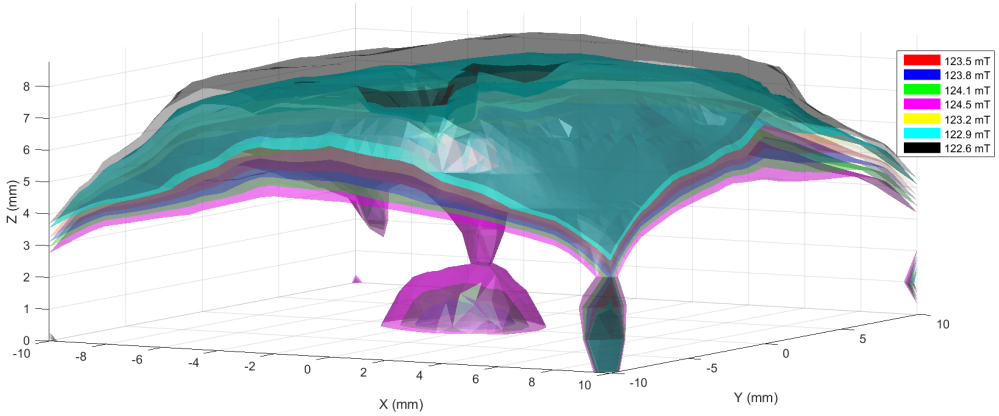


Figure 6.14: Iso-surface plot of field strengths computed with MATLAB.

it is also the direction of the polarizing field $B_0$.

Observing this field map it is clear what was the problem. The NMR-MOLE was supposed to be a 5 MHz NMR scanner, but from the field map the magnetic filed strength makes the Larmor frequency equal to 5.26 MHz. All the preliminary measurements have been performed assuming a 5 MHz Larmor frequency, so the RF-coil has been always tuned to that frequency.

Tuning and matching the RF-coil at the right frequency has made possible to acquire good data.

At this point it has been possible to proceed with the characterization and calibration, because the device was correctly working.

All the calibration and characterization measurements have been performed using doped water instead of distilled water in order to make the measurements faster. First of all, a pulse amplitude calibration has been performed in order to determinate the correct amplitude attenuation to give the correct 90 pulse. The pulse length has been fixed to 12 $\mu$s, in this way the RF excitation bandwidth is $\Delta\nu = \frac{1}{12}\mu s = 0.083$ MHz.

From the calibration the correct 90 pulse attenuation has been fixed equal to -10 dB.

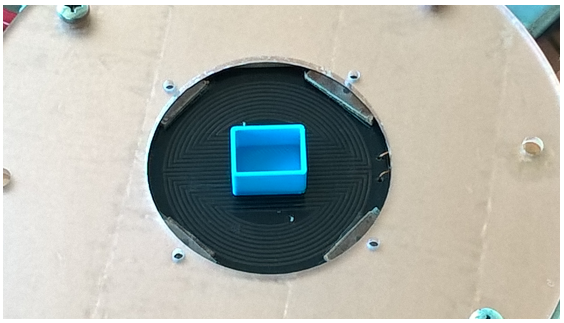

Figure 6.15: bulk doped water used to perform the diffusion editing measurement.

Once calibrated correctly the pulse attenuation, the next step is to characterize the sensitive volume. In particular the gradient distribution and the dimensions of the sensitive volume had to be estimate.

### 6.2.1 Gradient distribution of the NMR-MOLE

The procedure utilized to determine the gradient distribution is the same described in the article [12] by M. Nogueira and P.Galvosas.

The idea is performing a $D-T_2$ map on a reference sample, in this case bulk doped water, as shown in Fig. 6.15. If just one gradient value is present, the resulting map shows a well defined single component (a circle) in the map. However, if different gradient values are present, a broadening along the D axis will be observed. This can be considered as a signature of the device and using a customize kernel it is possible to compute the gradients distribution present in the volume occupied by the reference sample.

The result of the experiment is given in Fig. 6.16.

As it can be obtained from the distribution, the most present gradient value is 0.6 T/m, and the highest value is around 2 T/m. These values are much more low in respect to the gradients values of the NMR-MOUSE scanners, and so the diffusion affects less the measurements.

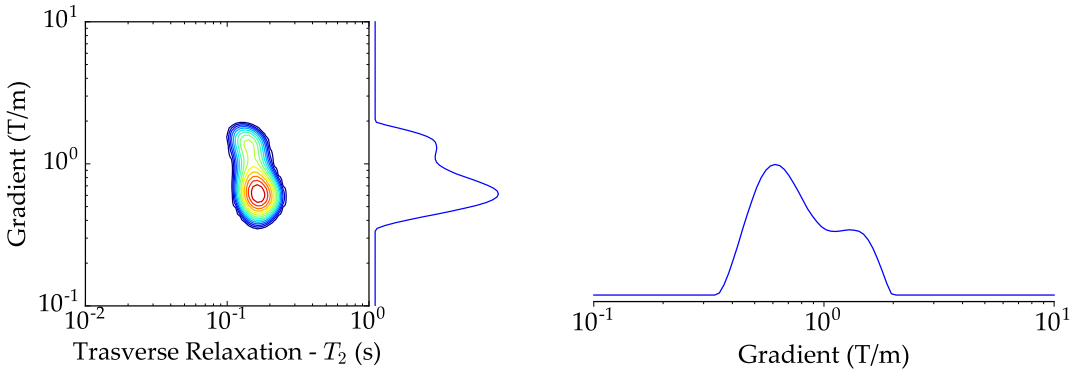


(a) $D - T_2$ map

(b) Gradient distribution

Figure 6.16: Determination of the gradient distribution of the MOLE via a Diffusion Editing CPMG pulse sequence.

### 6.2.2 Sensitive volume of the NMR-MOLE

Because of its design, the NMR-MOLE has a distribution of magnetic field gradients, and this means that, fixed the pulse length of the RF-pulse, all the three dimensions of the sensitive volume have to be assessed, because there is no trivial relation between pulse length and thickness as in the case of the NMR-MOUSE.

In order to determinate the thickness and the area of the sensitive volume, and its distance from the surface coil, four cylindrical glass bottles have been used as container for doped water.
Each bottle differs from the others by the diameter:

- Bottle 1 = 1.5 cm of diameter;
- Bottle 2 = 2 cm of diameter;
- Bottle 3 = 2.5 cm of diameter;
- Bottle 4 = 4.5 cm of diameter;

For each bottle, the volume of doped water inside has been systematically increased starting from a layer 1 mm thick up to 2 cm thick, adding 1 mm of water each step. A Spin Echo sequence has been used to detect the signal.

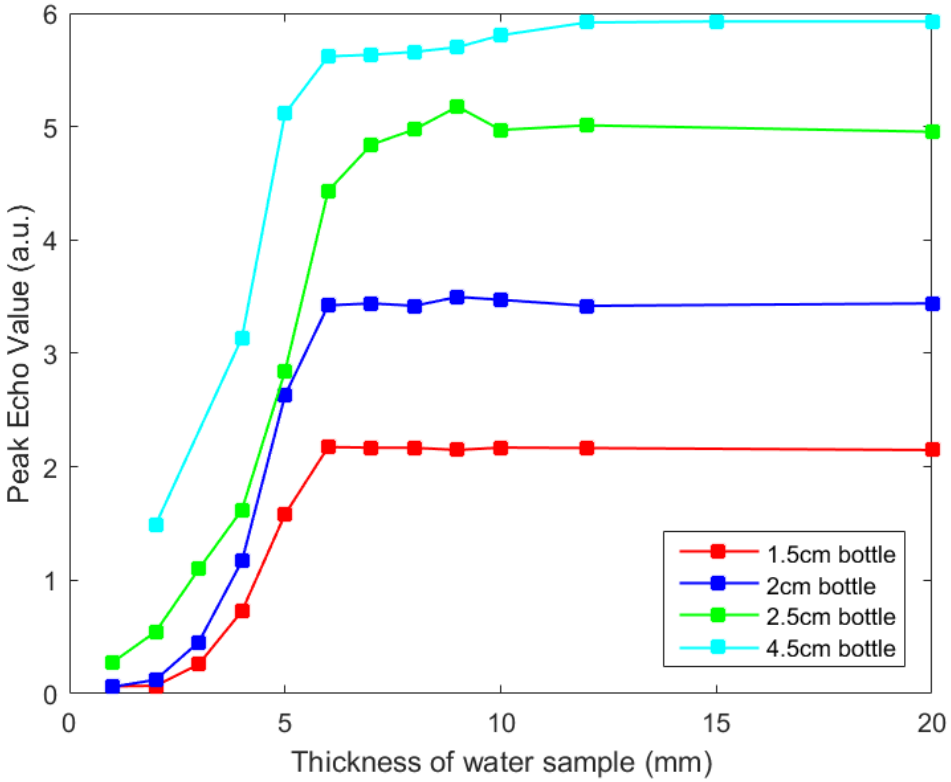


Figure 6.17: Result of the sensitive volume experiment.

The $T_2$ of the prepared doped water, measured with a CPMG, is equal to 10 ms. That gives a rough idea even of the $T_1$, indicating that a short repetition time can be done. In this way it has been possible to acquire 2048 scans for each Spin Echo experiment. The SE parameters are reported in Tab. 6.4

| $t_p$ | 90 Att. | 180 Att. | $T_E$ |
|---|---|---|---|
| 12 $\mu$ s | -9 dB | -3 dB | 800 $\mu$s |

Table 6.4: SE parameters used in the sensitive volume experiment.

Fig. 6.17 shows the result of the experiment. From the graph it is clear that the sensitive volume has a thickness around 6 mm, starting from the surface of the coil, and a diameter of at least 4.5 cm.

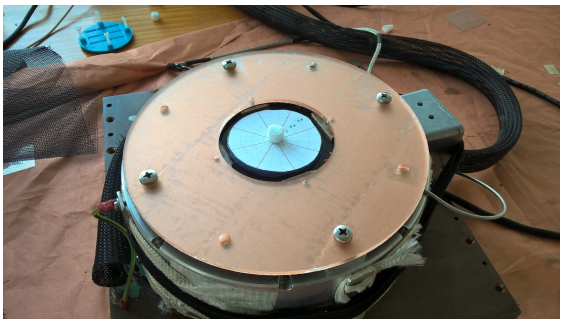

Figure 6.18: Picture of the utilized measuring procedure to perform the experiment.

It is also possible to characterize the sensitive volume in the xy plane acquiring the signal in different positions within the plane parallel to the surface coil, at a fixed height from the RF-coil. The height has been fixed at 3 mm. A cylinder of Teflon has been used as container in which doped water has been put inside. The properties of the doped water are the same as described in the previous experiment, and so even the SE parameters has been set equal to the previous experiment. The dimension of the sample are:

- *Inner diameter*: 5 mm;
- *Height*: 7 mm;

The Teflon does not give NMR signal, so that just the inner diameter is relevant.

The sample has been moved in the plane, following the idea described in section 6.1.3, sampling 41 points. A picture of the measuring procedure is given in Fig. 6.18 The data have been analysed with MATLAB and the results are showed in Fig. 6.19.
The result is similar to that obtained for the NMR-MOUSE PM10, even if the area in which the signal is not to zero is bigger. It is useful to explain that even if the area of the slice marked in by the elaboration is lower than the estimation made analysing the result of the previous experiment, the two results are not in disagreement. In fact, as already remarked many times, the $B_0$ profile is not trivial, and at different height this experiment can give different sensitive area size.

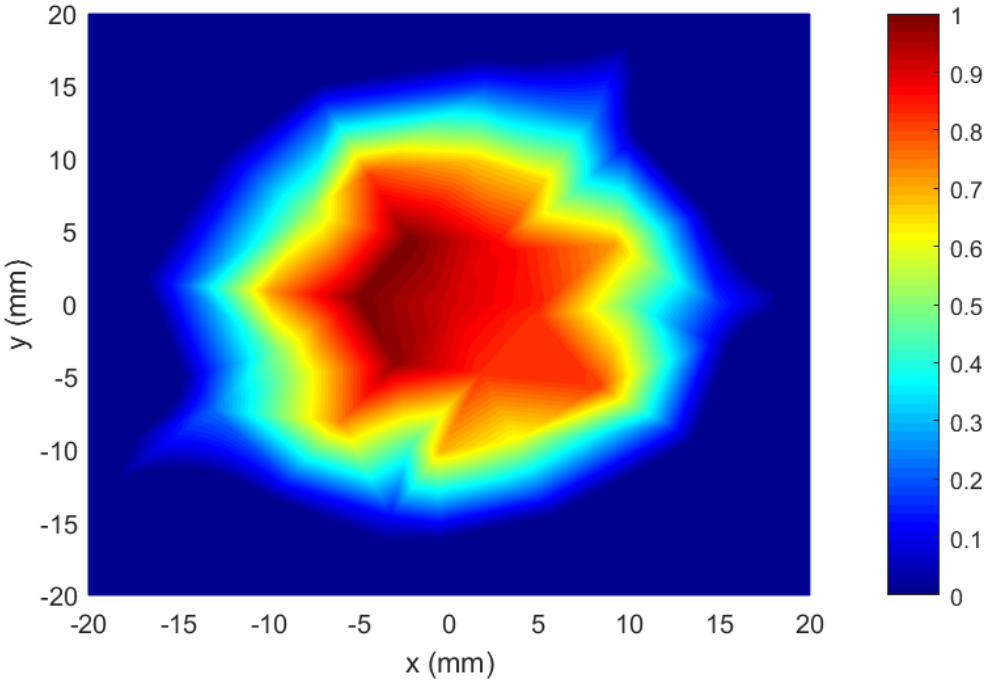


Figure 6.19: Matlab elaboration of the acquired data for a slice of the sensitive volume of the NMR-MOLE.

# Chapter 7

# Feasibility study, assessing the BV/TV ratio with the NMR-MOUSE PM10

In this chapter, the experiments and results of the feasibility study about the possibility to assess the BV/TV ratio of trabecular bone through single-sided NMR are presented.
The NMR-MOUSE PM10 has been used to perform all the experiments presented in this chapter.
The chapter is dived in two sections. In the first section, the relaxometry and diffusometry study of the marrow is presented. In the second section, the assessing of the BV/TV ratio by NMR and the comparison with the results obtained by the micro-CT are presented.

## 7.1 Relaxometry and diffusometry study of the Bulk Marrow with the NMR-MOUSE PM10

Bone marrow is the compound that mainly contributes to the NMR signal in the experiments performed on bone samples. Therefore, it is important to characterize it, even because it has been used as reference to evaluate the BV/TV ratio.
The bulk marrow samples have been prepared by drilling the medullary cavity of

a tibia of pig with a glass tube of 0.8 cm of diameter. Two kind of studies have been performed over them:

- Relaxometry study, performing saturation recovery and CPMG experiments, in order to know the $T_1$ and $T_2$ distributions;
- Diffusometry study, performing a stimulated spin echo, in order to assess the self-diffusion coefficient of the bulk marrow.

The configuration with all the spacers inserted has been used, because in this way the SNR, fixed the number of scan, is the maximum achievable.

### 7.1.1 Relaxometry study

The parameters utilized for the saturation recovery are reported in Tab 7.1.

| $t_p$ | 90 Att. | 180 Att. | $T_E$ | $N_s$ | TR | Max. Rec. Time | $T_I$ points |
|---|---|---|---|---|---|---|---|
| 5$\mu$s | -10 dB | -4 dB | 60 $\mu$s | 64 | 2000 ms | 2000 ms | 40 |

Table 7.1: Saturatio recovery parameters.

The results are reported in fig. 7.1
The peak of the distribution is at 75 ms, and there is a tail toward longer $T_1$ times up to 1 s, even if the area under the curve for $T_1$ longer than 400 ms is almost neglecting in respect to the total area. This consideration is worthy because the longest $T_1$ component drives the choice of the repetition time, and in this case it would not be worthy choosing 1s as longest component because the contribution to the signal of that component is negligible.

The CPMG parameters are reported in Tab. 7.2

[hbtp]

| $t_p$ | 90 Att. | 180 Att. | TR | $T_E$ | $N_s$ |
|---|---|---|---|---|---|
| 5$\mu$s | -10 dB | -4 dB | 2000 ms | 50 $\mu$s | 1024 |

Table 7.2: CPMG parameters.

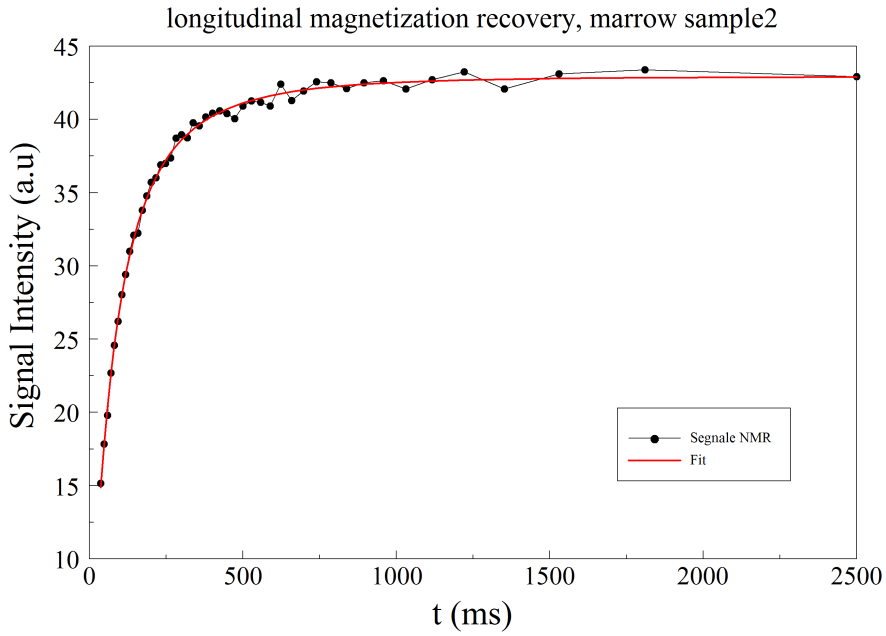


(a) Build-up magnetization curve

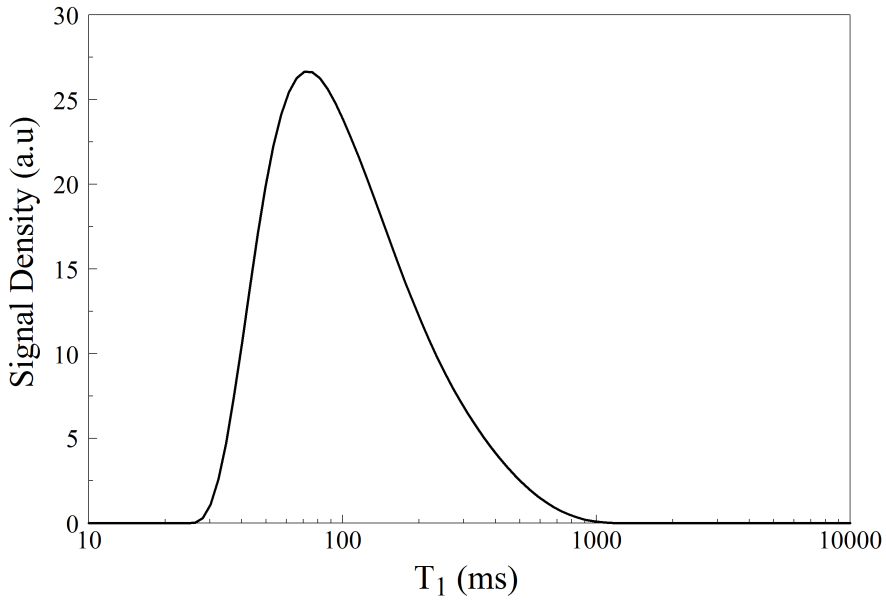


(b) $T_1$ distribution of the bulk marrow

Figure 7.1: Saturation recovery of bulk marrow.

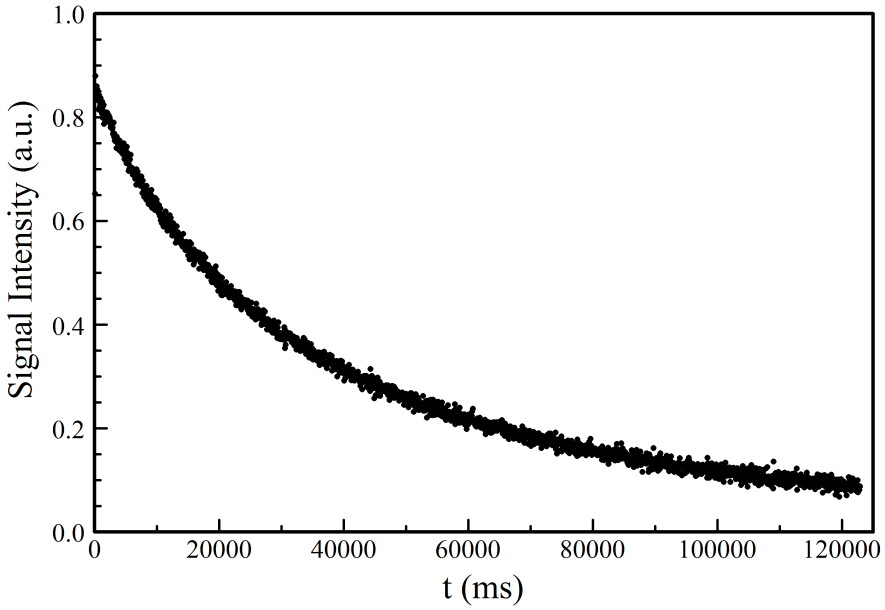


(a) CPMG echo train decay

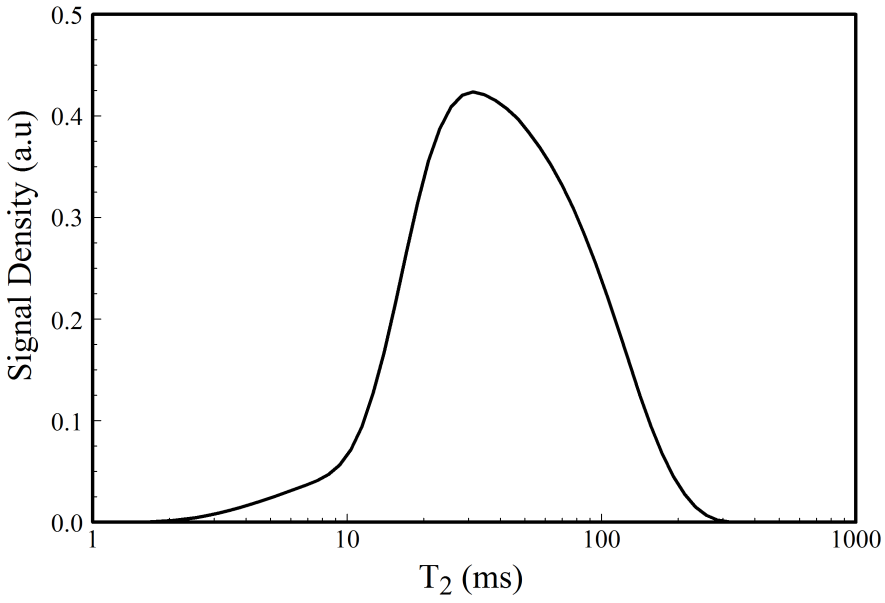


(b) $T_2$ distribution of the bulk marrow

Figure 7.2: CPMG of bulk marrow.

The results are reported in fig. 7.2.
The peak of the $T_2$ distribution is around 30 ms, and so it is similar to the $T_1$ distribution even if, as expected, shorter.

### 7.1.2 Diffusometry study

Because the marrow fills the inter-trabecular space, experiments based on the diffusion phenomenon could be useful to assess the micro-structure of the trabecular bone. For example, using the fact that the molecules of the marrow are embedded in the trabecular matrix, the self-diffusion coefficient, leaving enough time to diffuse, appears lower than in the bulk regime. In the porous media field of research this regime is called *restricted diffusion regime*, and it can be useful to extract information about the geometry of the porous media itself. However, in order to be able to extract this kind of information, the molecules have to feel the restriction during the experiment time. To be able to feel this restriction the self-diffusion coefficient of the marrow has to be *sufficiently high*, where this *sufficiently high* is related to the experimental conditions.
In fact, to assess the diffusion coefficient with the NMR-MOUSE PM10 the stimulated echo pulse sequence is used. In order to allow the molecules to feel the effect of the restriction, the evolution time $\Delta$ has to be increased .
Now, during the evolution time, the transverse magnetization is stored in the longitudinal axis and so its decay rate depends on $T_1$. Therefore, $\Delta$ has to be short enough to not produce a significant decay of the longitudinal magnetization, otherwise, the echo attenuation would be due to the relaxation more than the diffusion.

Whit these preliminary considerations, a stimulated echo has been performed on a bulk marrow sample in order to evaluate its self-diffusion coefficient D.
The utilized parameters of the sequence are reported in Tab. 7.3.

| TR | $\tau_{min}$ | $\tau_{max}$ | $\Delta$ | Number of $\tau$ inc. |
|---|---|---|---|---|
| 5000 ms | 0.05 ms | 1.35 ms | 10 ms | 48 |

Table 7.3: Stimulated Spin Echo parameters

The result of the experiment is reported in Fig. 7.3

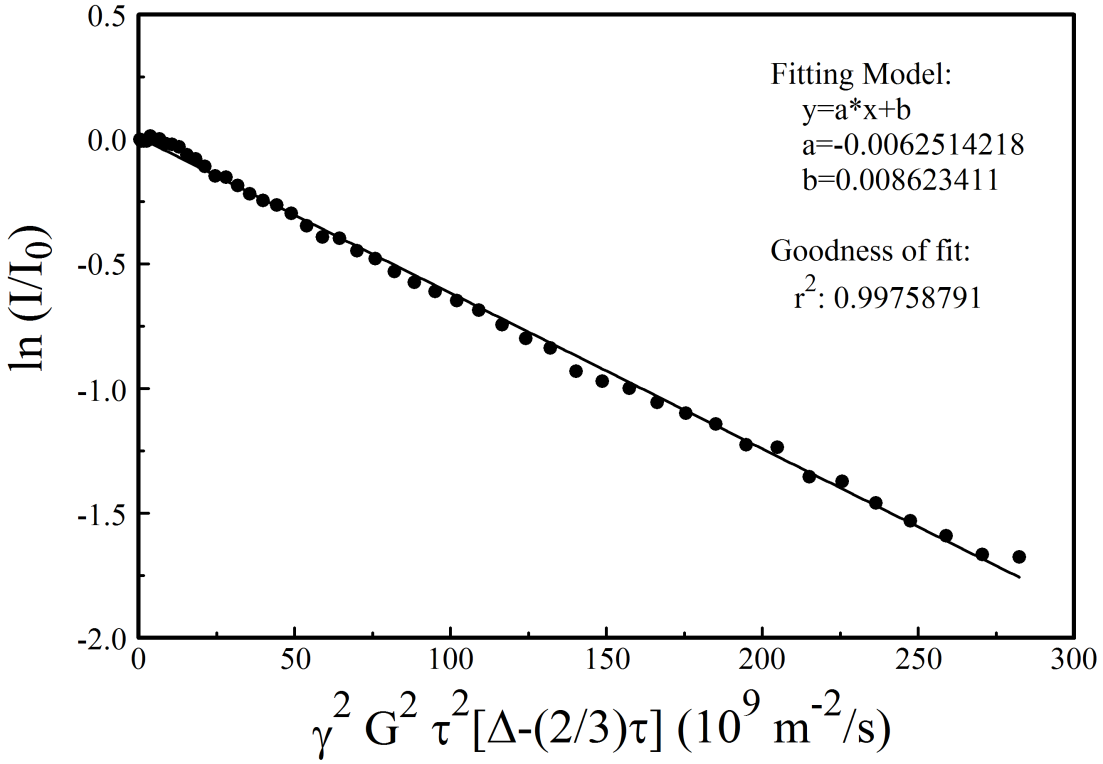


Figure 7.3: SSE experimental data and PSI-plot fit for bulk marrow.

From the PSI plot fit, the self-diffusion coefficient is
$D_{BM} = (6.25 \pm 0.05) \times 10^{-3} \frac{\mu m^2}{ms}$.
This value is too low to allow one to see the restriction regime of the marrow molecules embedded in the trabecular bone matrix. In fact, the mean value of the diffusion length for free diffusion is given by the equation 7.1:

$$\langle R \rangle^2 = 2Dt \tag{7.1}$$

where t is the time leaved to the molecule to diffuse (the evolution time $\Delta$ in this case), and D is the self-diffusion coefficient. The peak of the $T_1$ distribution of the bulk marrow is around 75 ms, hence the maximum evolution time $\Delta$ that can be leaved to the molecule to diffuse, which has to be smaller than $T_1/5$, is 15 ms.

Allowing this time to diffuse, the mean displacement is 0.433 $\mu$m. The inter-trabecular space is in the order of one hundred micron, and so this simple consideration shows the impossibility to assess the micro-structure of the trabecular bone using the diffusion.
As last bur very important consideration one can observe that due to its small self-diffusion coefficient the effect of the diffusion performing measurements with the NMR-MOUSE PM10 on marrow can be neglected.

## 7.2 Assessing the BV/TV ratio by single-sided NMR, a comparison with the micro-CT

In this section the experiments, and the correspondent results, performed on the bone samples presented in section 4.5.1 are reported. The goal of the measurements is to characterize the samples and to assess the BV/TV ratio of them, which have to be compared with those evaluated by the micro-CT analysis performed on the same samples.

### 7.2.1 Bone I

Bone I is the first trabecular bone sample analysed. The goal of the measurements on this sample is to characterize the sample by a relaxometry study and verify the possibility to assess the target parameter and to make a first comparison with the micro-CT data.

#### Relaxometry study of Bone I

A saturation recovery and a CPMG sequence, in a 0 mm configuration, have been performed to assess the $T_1$ and $T_2$ distributions of Bone I. The sample has been placed above the coil with its cylindrical axis perpendicular to the surface and the RF-coil, and with the cartilage base facing the RF-coil. The parameters of the pulse sequences are reported in Tab. 7.4 and Tab. 7.5.

| $t_p$ | 90 Att. | 180 Att. | $T_E$ | $N_s$ | TR | Max. Rec. Time | $T_I$ points |
|---|---|---|---|---|---|---|---|
| 15$\mu$s | -7 dB | -1 dB | 60 $\mu$s | 24 | 3000 ms | 3000 ms | 48 |

Table 7.4: Saturatio recovery parameters.

| $t_p$ | 90 Att. | 180 Att. | TR | $T_E$ | $N_s$ |
|---|---|---|---|---|---|
| 15$\mu$s | -7 dB | -1 dB | 2000 ms | 60 $\mu$s | 256 |

Table 7.5: CPMG parameters.

The results of the study are shown in Fig. 7.4.
It can be observed that the relaxation time distributions are quite similar to the distributions of the marrow, and this similarity is marked in Fig. 7.4(a), where the two normalized distribution are compared. This result confirms the a priori assumption that the mainly compound present in the inter trabecular space is marrow.

**Bone porosity with profile NMR**

The aim of these measurements is to characterize the sample by determining the porosity at different depths, and comparing these results with those obtained with the micro-CT analysis.
Two profiles have been performed, one with the sample placed in the same position of the previous study, and one with the principal axis parallel to the surface of the RF-coil. The spacers configuration chose is a 0 mm spacers configuration. In this way the available penetration depth is the maximum achievable (11 mm).
The results are summarized in Fig. 7.5
The vertical profile clearly shows the presence of the cartilage at the base of the sample, whereas the horizontal profile shows that the maximum of the signal (in that configuration) is achieved around 5-6 mm of depth. This behaviour is not due to the particular composition of the sample, but it simply explainable by geometrical factors. The sample is a cylinder, hence in the middle of its height there is the maximum intersection between the sensitive volume and the sample.

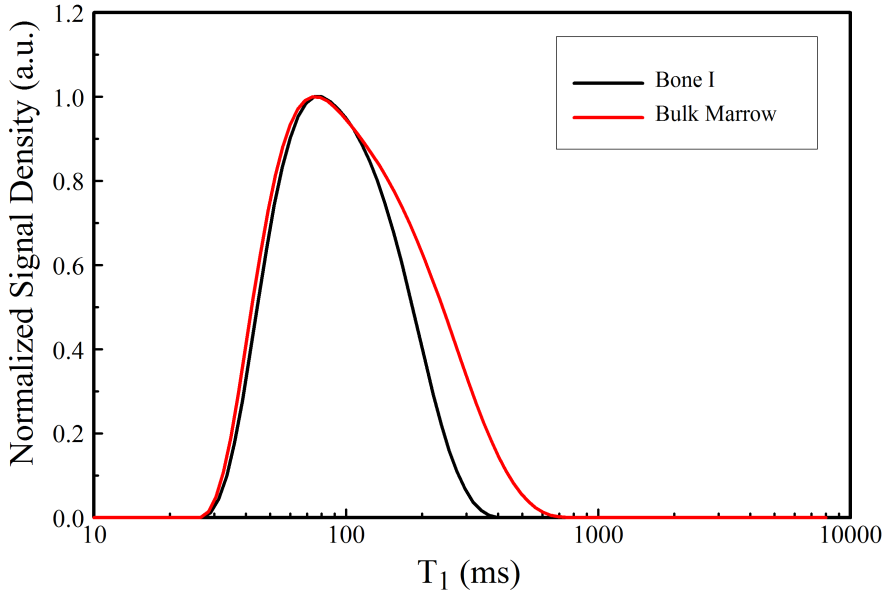


(a) Normalized $T_1$ distribution of Bone I and bulk Marrow

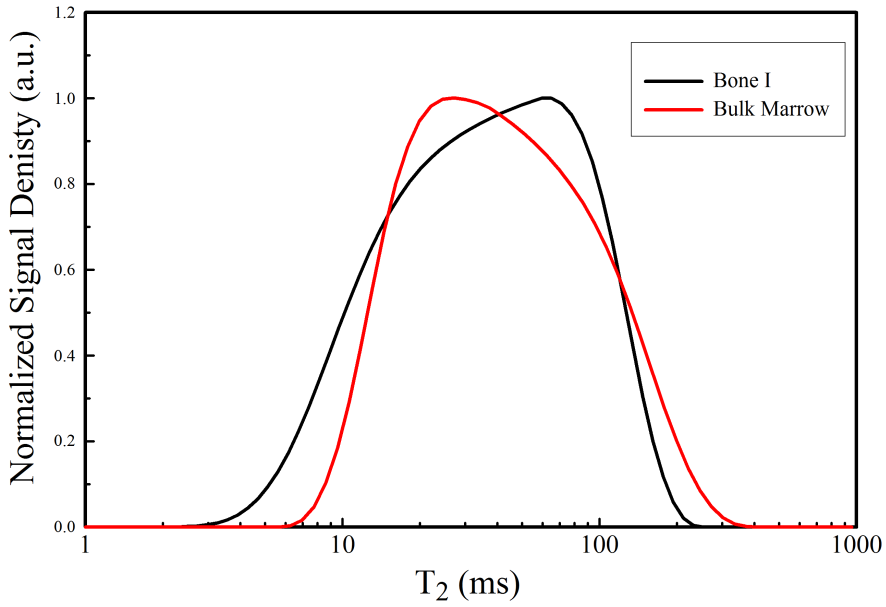


(b) Normalized $T_2$ distribution of Bone I and bulk Marrow

Figure 7.4: Relaxometry study of Bone I.

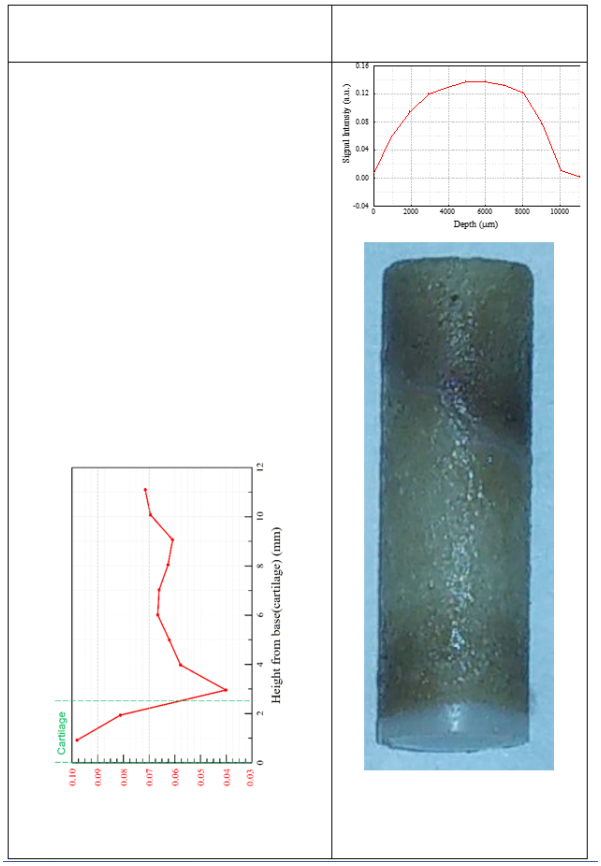


Figure 7.5: Profiles study of Bone I performed with the NMR-MOUSE PM10 along two perpendicular directions.

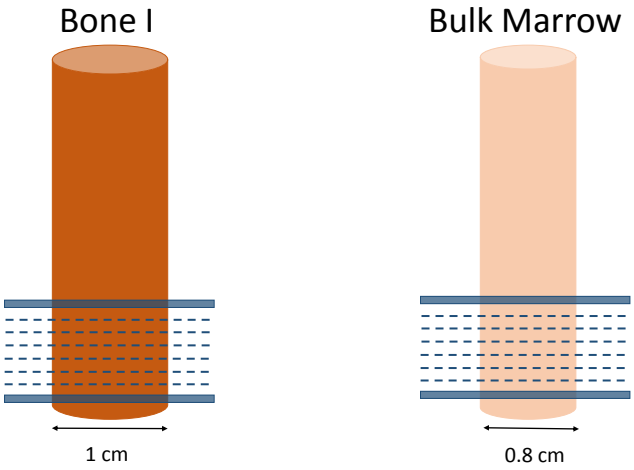


Figure 7.6: Sketch of the evaluation of the bone porosity by profile-NMR.

From the profile data, it is possible to obtain the porosity of the bone sample at different depths by performing another profile, with the same parameters, on a sample of bulk marrow, having the same size, and making the ratio of the signal intensities. The idea it is sketched in Fig. 7.6

If the samples have the same size, the porosity is evaluated by equation 7.2:

$$Porosity(\%) = \frac{Bone \quad Sample \quad Signal}{Bulk \quad Marrow \quad Sample \quad Signal} \tag{7.2}$$

Therefore, a bulk marrow sample has been prepared using a glass test-tube with diameter of 0.8 cm. It has been placed whit its principal axis perpendicular to the surface of the RF-coil and a profile has been performed on it. The parameters of the profile measurement have been set the same used to acquire the profile of Bone I.
However, in order to obtain a correct result, a preliminary operation has to be made. Both the samples (Bone I and the marrow sample) are cylinders, but they have different diameters (1 cm for Bone I, 0.8 cm for the marrow sample). Hence, a correction of the signal has to be made in order to avoid errors. The correction follows simple geometrical considerations.
Let us remember that, for a given homogeneous sample, the signal (S) is propor-

tional to the volume of that sample (V):

$$S \propto V \tag{7.3}$$

and assuming a cylindrical shape

$$V = r_{Bone}^2 \pi h \tag{7.4}$$

$$V' = r_{Marrow}'^2 \pi h \tag{7.5}$$

so, that imply

$$\frac{S'_{Marrow}}{S_{Bone}} = \frac{V'}{V} = \frac{64}{100} \tag{7.6}$$

So, the correction to the signal of the marrow follows the relationship expresses by the following equation:

$$S_{corrected} = \frac{100}{64} \times S_{measured} \tag{7.7}$$

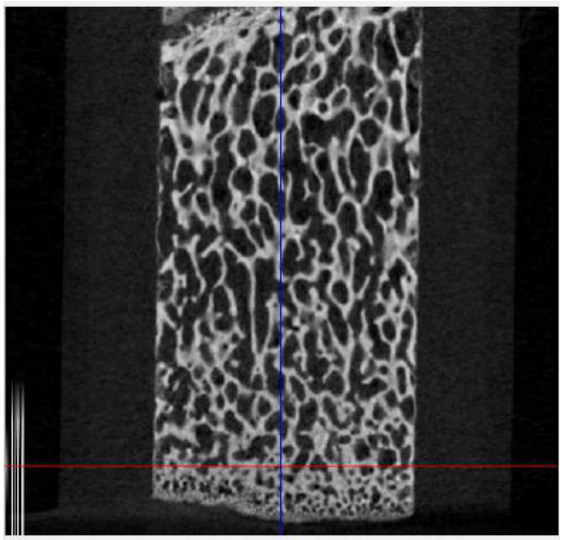

Figure 7.7: micro-CT image of a slice of Bone I.

Now, the porosity at different depths obtained by the NMR profile and the same parameter obtained by the micro-CT analysis are reported in Fig. 7.8, and a

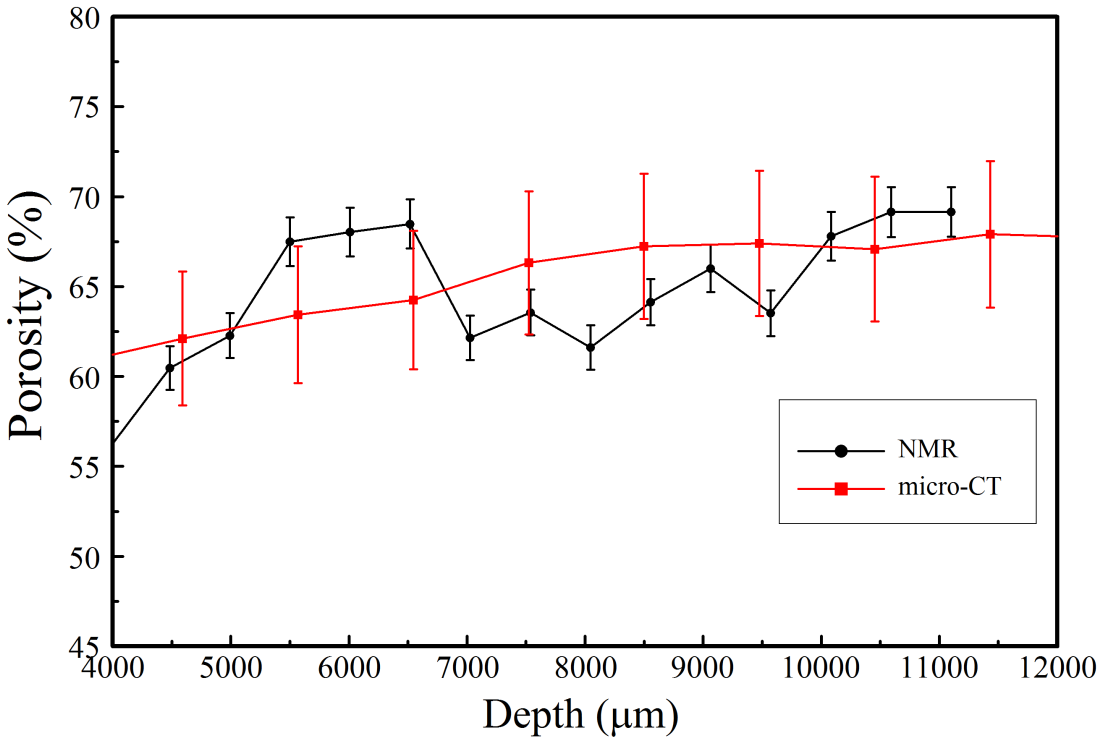


Figure 7.8: Bone Porosity at different depths evaluated by NMR and micro-CT.

micro-CT image of the sample is reported as example in Fig. 7.7.

The error bars for the NMR profile have been evaluated by acquiring the signal coming from a certain slice ten times and evaluating the standard deviation, and so the error bar is equal to two standard deviations. It is worthy to remark that the slice thickness is around 100 $\mu$m. For the micro-CT profile, each point is evaluated as the average of 50 adjacent slices, each around 20 $\mu$m tick, and the error bar is equal to two standard deviations.
The graph shows a quite good agreement of the values, leaving open the way for a deeper study. It is important to observe that the micro-CT values vary less than the NMR values because of the averaging operation done for the micro-CT values.

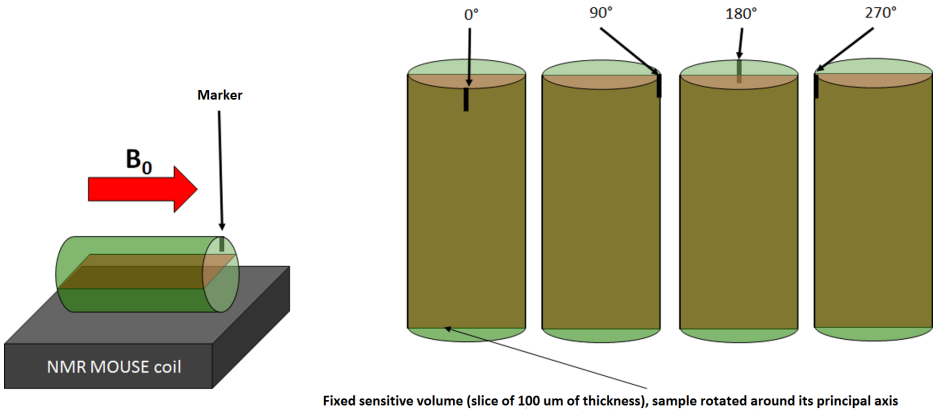


Figure 7.9: Sketch of the four CPMG experiment.

### 7.2.2 Second subset of traecular bone samples, assessing the BV/TV ratio

This subset of trabecular bone samples is the main set utilized to evaluate the feasibility of a technique capable to assess the BV/TV. As pointed out in section 4.5.1, the six samples utilized have different BV/TV ratios because they have been cut from different sites of a pig's shoulder. A good comparison with the micro-CT analysis would confirm the goodness of the technique.

Because the final aim of this research is a clinic application of this new technique, the following experiment, preformed over each sample, has been design in such a way to simulate a possible diagnostic test.

For each sample four CPMG (in the 0 mm configuration) have been performed with the sample placed with its principal axis parallel to the surface RF-coil, as shown in Fig. 7.9. After each CPMG the sample has been rotated of $90^o$, $180^0$ and $270^0$ around its principal axis, in order to assess the signal in different slices inside the sample.
The CPMG is performed at a depth of 5400 $\mu$m inside the sample. In this way, there is the maximum overlapping between the sensitive volume of the NMR-MOUSE PM10 and the sample, how it has been shown by the characterization of

Bone I and summarized in Fig. 7.5.
Because the final application of this research is a clinical application, a special attention about the measurement duration is necessary and a good compromise between SNR and acquisition time has to be found. In fact, in a clinical scenario a relatively short test time is desirable.
Hence, the CPMG parameters have been set in such a way to obtain a total measurement time of 12 minutes.
The parameters of the CPMG are reported in Tab. 7.6

| $t_p$ | 90 Att. | 180 Att. | TR | $T_E$ | $N_s$ |
|---|---|---|---|---|---|
| 15$\mu$s | -7 dB | -1 dB | 2000 ms | 60 $\mu$s | 100 |

Table 7.6: CPMG parameters for the four CPMG experiments.

The data have been analysed with UpenWin, and the signal intensity has been evaluated by the extrapolation of the echo train decay to zero time using the UPEN parameter Xsig.
Because four CPMG for each sample have been taken, the signal intensity is the average of the four CPMG signal intensities, and the standard deviation is the error associated to it.
As it is already explained, this signal is strictly bound to the presence of the inter-trabecular marrow. Hence, the higher is the signal intensity, the higher is the porosity.
The signal intensity, for each sample, is reported in the graph of Fig. 7.10.
By the graph a significant different signal intensities among the samples, having the same shape and volume, can be observed, that is an indication of the different trabecular structures.
However, nor porosity, nor BV/TV has been obtained yet. To reach this information it is necessary to normalize these values by the signal coming from a sample, of the same dimensions, of bulk marrow, performing the four CPMG experiment.
A sample of bulk marrow has been prepared with the same operations described in the previous sections, and the four CPMG experiments have been performed.
A picture of the experimental set-up is shown in Fig. 7.11.

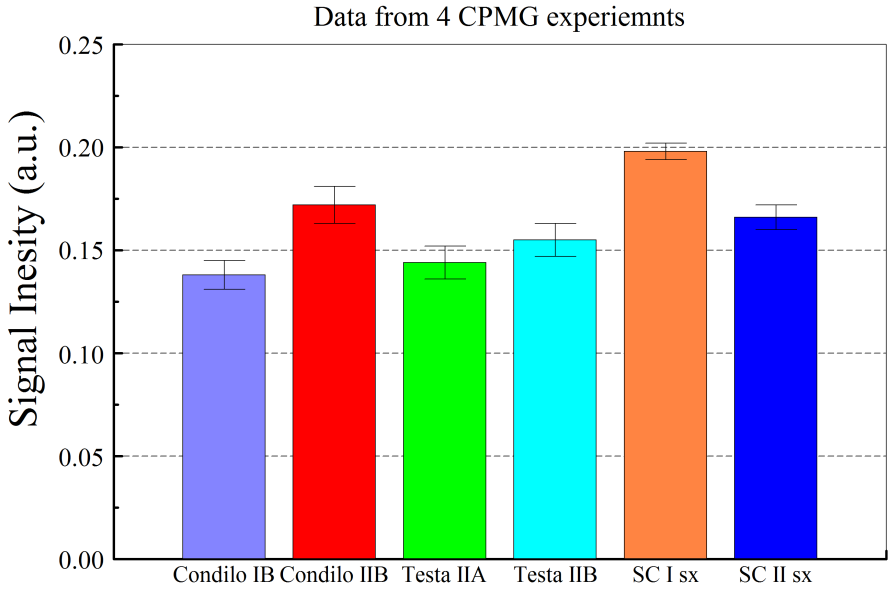


Figure 7.10: Signal intensity, for each TB sample, extracted by the 4 CPMG experiments.

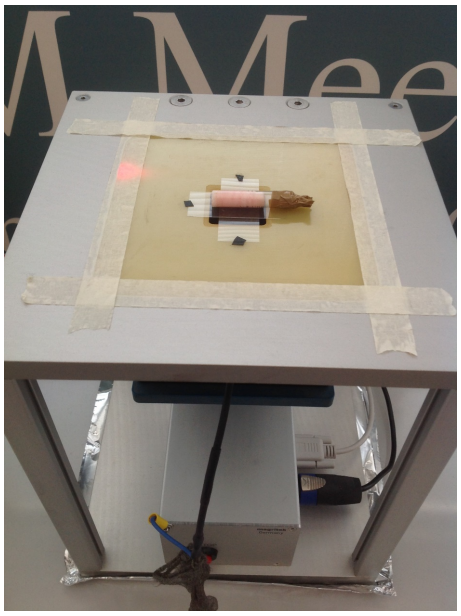

Figure 7.11: Picture of the experimental set-up for the four CPMG experiments on a sample of bone marrow.

Elaborating the data in the same manner of the trabecular bone samples, the resulting average signal is:

$$S_M = (0.21 \pm 0.01)\, a.u. \tag{7.8}$$

Because the diameter of the glass test-tube is 0.8 cm, whereas the diameter of the bone samples is 1 cm, a correction is necessary to make consistent the two data:

$$S_{corrected} = \frac{1}{0.8} \times S_{measured} = (0.26 \pm 0.01)\, a.u. \tag{7.9}$$

It is possible to obtain the porosities and the BV/TV ratios of the samples simply performing a ratio according to the following equation:

$$BV/TV \quad (\%) = 100 - \frac{S_M}{S_B}(\%) \tag{7.10}$$

The results are reported in Tab. 7.7.

| Sample | Porosity (%) | BV/TV (%) |
|---|---|---|
| Condilo IB | 53 ± 4 | 47 ± 4 |
| Condilo II B | 66 ± 6 | 34 ± 6 |
| Testa II A | 55 ± 5 | 45 ± 5 |
| Testa II B | 60 ± 5 | 40 ± 5 |
| SC I SX | 76 ± 4 | 24 ± 4 |
| SC II SX | 64 ± 5 | 36 ± 5 |

Table 7.7: Porosity and BV/TV ratio of trabecular bone samples by NMR.

These results have to be compared with those obtained by micro-CT.
Using the reference markers present in each sample, and knowing that the NMR signal comes from a 100 $\mu$m thick slice placed at 5400 $\mu$m of depth inside the sample, for each sample it has been tried to perform the micro-CT analysis roughly over the same four slices analysed with the NMR-MOUSE PM10, even if the correspondence is only approximate.
An expample of a micro-CT image for each sample is reported in Fig. 7.12.

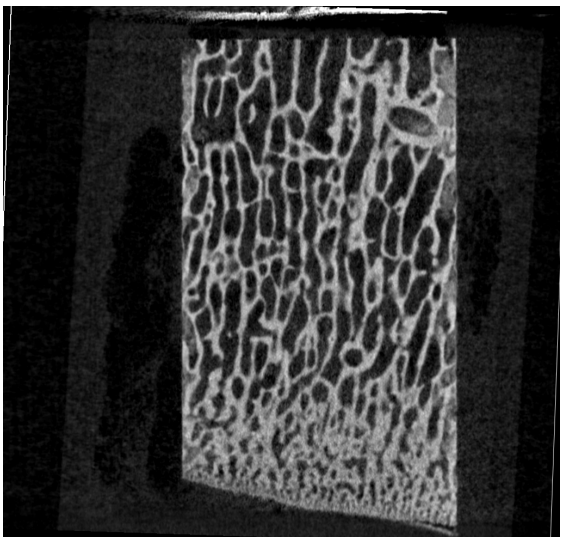

(a) Condilo IB

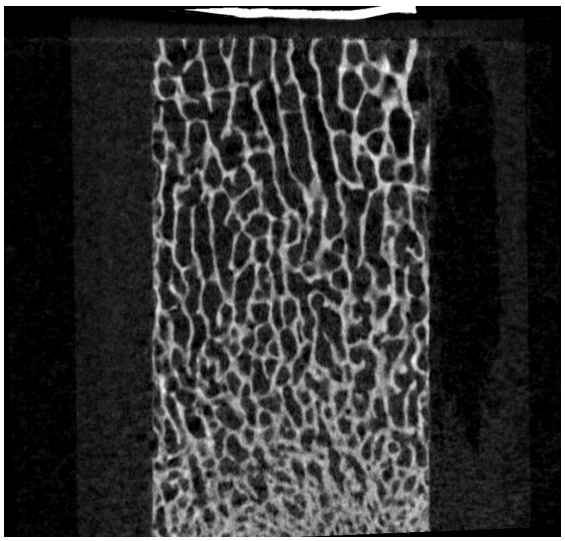

(b) Condilo II B

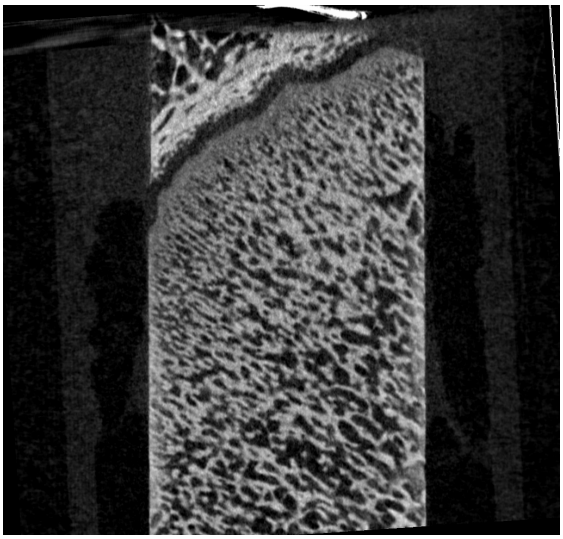

(c) Testa II A

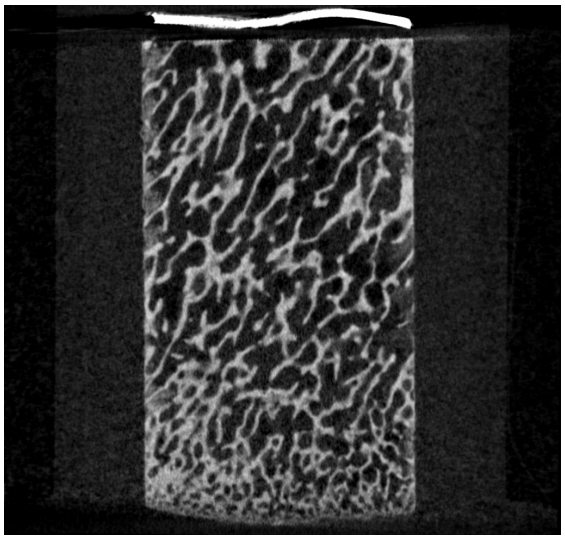

(d) Testa II B

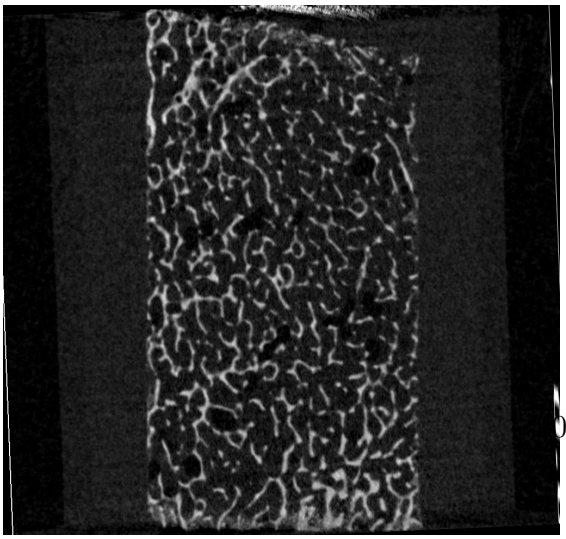

(e) SC I SX

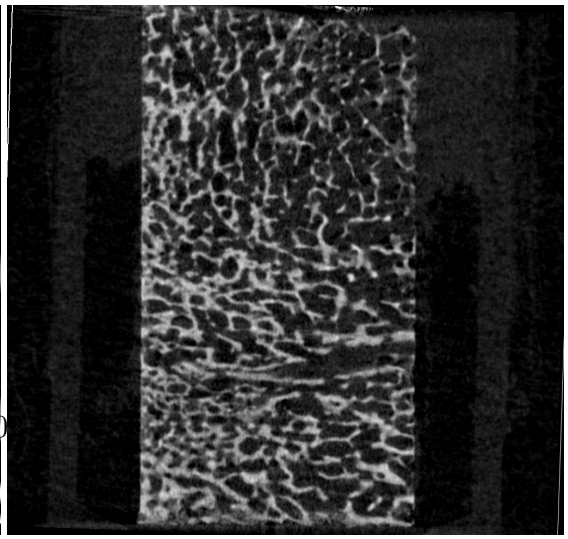

(f) SC II SX

Figure 7.12: Examples of micro-CT images of the six samples.

It is important to mark how four samples contain not only bone tissue and marrow, but even growth cartilage. Micro-CT can separate the two tissues, and it is possible assess the micro-architectural structure of the trabecular bone matrix alone and of the growth cartilage alone, by selecting a correct threshold value.
The water inside the cartilage contribute to the NMR singal, however it has not been possible to separate the contribution of the cartilage because the $T_2$ distribution of a sample shows just one broad peak. This means that it is not possible to separate the two contributions. Moreover, the growth cartilage, according to the considerations made by the Istuto Ortopedico Rizzoli, presents a porous structure with marrow inside, even if this porosity is much lower than the trabecular bone porosity.

| Sample | $\frac{BV}{TV}$(%) (bone) | $\frac{BV}{TV}$(%) (cartilage) | % cartilage | $\frac{BV}{TV}$(%) (bone + cartilage) |
|---|---|---|---|---|
| Condilo IB | 38 ± 1 | 73.2 ± 0.2 | 19 | 47 ± 1 |
| Condilo II B | 30 ± 1 | 65.2 ± 0.4 | 10 | 36 ± 1 |
| Testa II A | 39 ± 1 | 64 ± 1 | 40 | 55 ± 3 |
| Testa II B | 28.7 ± 0.4 | 47.4 ± 0.1 | 8 | 32.2 ± 0.4 |
| SC I SX | 20 ± 1 | 0 | 0 | 20 ± 1 |
| SC II SX | 35 ± 1 | 0 | 0 | 35 ± 1 |

Table 7.8: BV/TV ratio of trabecular bone samples by micro-CT.

Tab. 7.8 shows the results of the micro-CT analysis over the samples, where: $\frac{BV}{TV}$(bone) is the ratio of the volume of the bone tissue to the total volume (bone tissue + bone marrow) computed in a region in which no cartilage is present; in the same manner $\frac{BV}{TV}$(cartilage) is the ratio of the volume of the cartilage tissue and the total volume (cartilage + bone marrow) computed in a region in which no bone tissue is present; finally, $\frac{BV}{TV}$(bone + cartilage) is the ratio of the volume of the cartilage plus the bone tissue, to the total volume (cartilage + bone + bone marrow).
It is this parameter that has to be compared with the parameter obtained by the NMR analysis. Tab. 7.9 summarize the results.

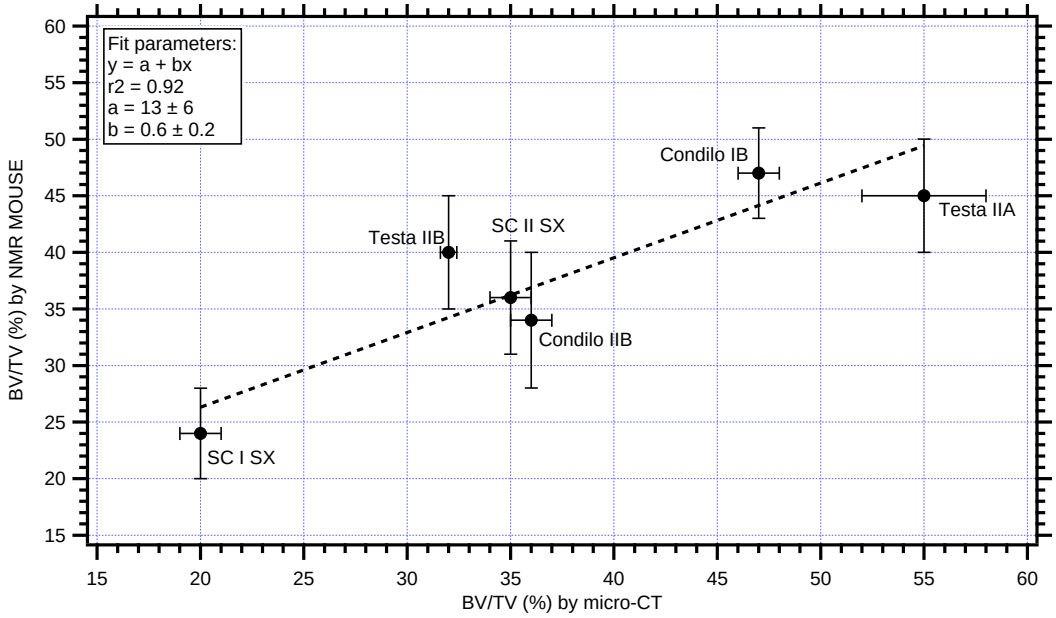


Figure 7.13: BV/TV measured by the NMR-MOUSE PM10 Vs the BV/TV measured by micro-CT.

| Sample | BV/TV (%) micro-CT | BV/TV (%) NMR |
|---|---|---|
| Condilo IB | 47 ± 1 | 47 ± 4 |
| Condilo II B | 36 ± 1 | 34 ± 6 |
| Testa II A | 55 ± 3 | 45 ± 5 |
| Testa II B | 32.2 ± 0.4 | 40 ± 5 |
| SC I SX | 20 ± 1 | 24 ± 4 |
| SC II SX | 35 ± 1 | 36 ± 5 |

Table 7.9: BV/TV ratio of trabecular bone samples evaluated by micro-CT and NMR.

In Fig. 7.13 the BV/TV ratios obtained by NMR is plotted versus those obtained by micro-CT. If the agreement would be perfect, the points should be distribute in such a way that, interpolating the data with a linear fit, the resulting interpolation function should be in the form $y = x$.

The parameter fit $a$, which should be ideally zero, turns out to be 13 ± 6. It is

easy to see that Testa IIB and Testa IIA are the samples for which the evaluation of the BV/TV differs, between the NMR and micro-CT, by more than ten percent points.
Even if it can be observe a quite good agreement between the two set of parameters, the correlation coefficient $r^2$ is 0.92, and even if, from a statistic point of view, the best way to proceed, in order to try to solve the problem, would be increasing the number of samples, it would be worthy try to explain the origin or the deviations of these two samples. However, many causes can contribute to these deviations, and to figure out the most probable ones some considerations can be made:

- The two samples have been extracted from the same site, i.e. the head of a pig's shoulder.
- In these two samples cartilage is present. Moreover, Testa IIA presents the highest percent of cartilage among the samples, while Testa IIB presents the lowest percent of cartilage among the samples. Hence there is not a clear correlation between the amount of percent of cartilage and the amount of the deviation.
- There is the possibility of a mismatching between the analysed slices. Because of the small thickness of them, it is hard to exclude this possibility.
- Some degradation could ave affected the samples in-between NMR and micro-CT.

The result of the comparison between NMR and micro-CT results shows a general good agreement, proving the goodness of the new technique proposed in this thesis work, even if more investigations are needed in order to understand the origin of some deviations between NMR and micro-CT analyses. The presence of different tissues that can contribute to the NMR signal beyond the marrow, such as the cartilage, can affect both the comparison with the micro-CT and even the accuracy of the NMR technique itself.

# Chapter 8

# Analysis of Bone strucutre by NMR-MOLE

In the previous chapter, a feasibility study of a novel low-field single-sided NMR technique has been presented. The results show a good agreement of the BV/TV values by NMR and micro-CT analysis, but some developments are possible, and some of them are summarized below.

- To use a different single-sided NMR device, with a lower intensity of the field gradient and a larger sensitive volume, to assess the BV/TV ratio, and to compare its performance with that of the NMR-MOUSE;
- Wanting for the extension of the measurements in an *in-vivo* scenario, a deeper study is needed about the procedures to discriminate the signal coming from the marrow contained in the inter-trabecular space and the others tissues surrounding the bone, such as muscle, cartilage and fat.

The NMR-MOLE is the chosen device to perform these developments, because it has a sensitive volume in which the polarizing field $B_0$ is more homogeneous as compared to that of the NMR-MOUSE. Moreover, the sensitive volume of the NMR-MOLE is larger and, as a first result, an increase of the SNR is expected.

This chapter is divided into three sections. The first section shows the study on the characterization of the trabecular bone and surrounding tissues using $T_1 - T_2$ and $D - T_2$ correlation maps. In the second section, a customize pulse sequence, diffusion weighted $T_1 - T_2$ sequence (DW $T_1 - T_2$), is presented. It has been used to perform a study on a biological sample, and the results show a way to suppress the signal coming from the surrounding tissues.
In the last section, the evaluation of the BV/TV ratio of the sample Bone III (see section 4.5.1) through NMR-MOLE, NMR-MOUSE PM5 and NMR-MOUSE PM10, in order to compare the performance, is presented.

## 8.1 Characterization of trabecular bone and surrounding tissues through two-dimensional correlation maps

### 8.1.1 $T_1 - T_2$ correlation map of biological samples

A $T_1 - T_2$ correlation map has been performed on the pig sample (*Biological sample I*), shown in Fig. 8.1 , using the NMR-MOLE. The sample contains not only the trabecular structure, but also different tissues surrounding the bone.
The parameters of the pulse sequence are reported in Tab. 8.1.

Table 8.1: $T_1 - T_2$ correlation map parameters.

| $t_p$ | 90 Att. | 180 Att. | min $\tau_1$ | max $\tau_1$ | TR | $T_E$ | $N_s$ |
|---|---|---|---|---|---|---|---|
| 12 $\mu$s | -10 dB | -4 dB | 1 ms | 1000 ms | 2 s | 150 $\mu$s | 8 |

The two-dimensional ILT and the graphical elaboration have been computed by a customize program wrote in Python. The resulting correlation map is reported in Fig. 8.2
The three dashed lines represent, starting from the diagonal, $T_1 = T_2$, $T_1 = 2 \times T_2$ and $T_1 = 10 \times T_2$.
The resulting map shows components in which $T_1$ is close to $T_2$, but also components in which $T_1$ is much longer than $T_2$. It is also worthy pointing out that each

Figure 8.1: *Biological sample I.*

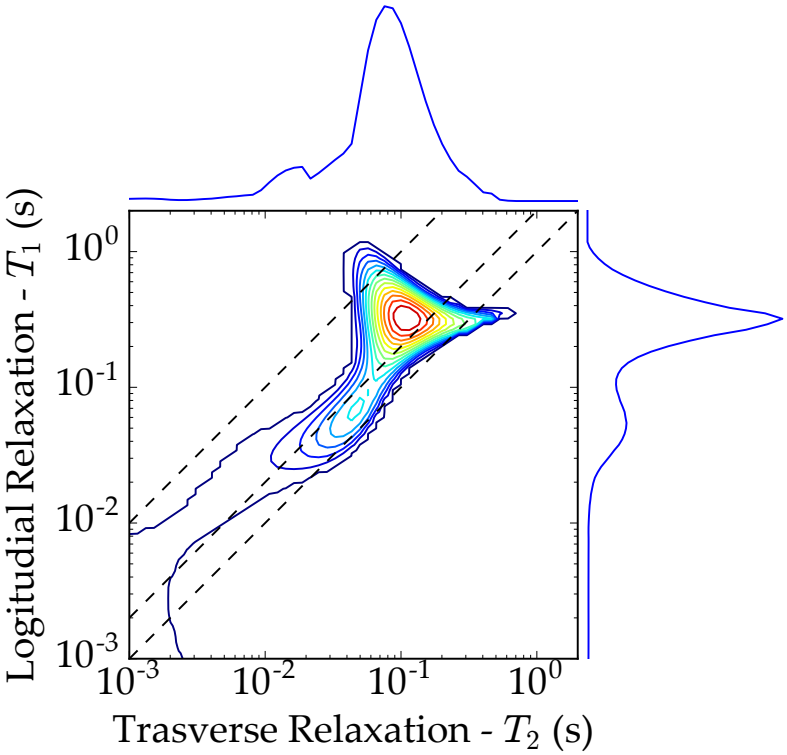


Figure 8.2: $T_1$-$T_2$ correlation map of *Biological sample I.* obtained by NMR-MOLE.

Figure 8.3: *Biological sample II.*

component below the diagonal has to be considered as an artefact of the 2D ILT, in fact such a scenario is not physically possible.
However, the map showed quite significant features, and the next step was to figure out the relationships between the tissues and the different components present in the map.

Whit this aim, a second pig sample has been prepared, labelled *Biological sample II.* The sample is shown in Fig. 8.3.

In this sample, beyond the trabecular bone structure, three more tissues were clearly recognizable: cartilage, fat and muscle.
A $T_1 - T_2$ map has been performed on this sample using the same parameters of the previous experiment. Then, the sample has been cut trying to have samples made just by one type of tissue as showed in Fig. 8.4. Moreover, a sample of bulk marrow and muscle have been prepared. $T_1 - T_2$ maps have been performed on

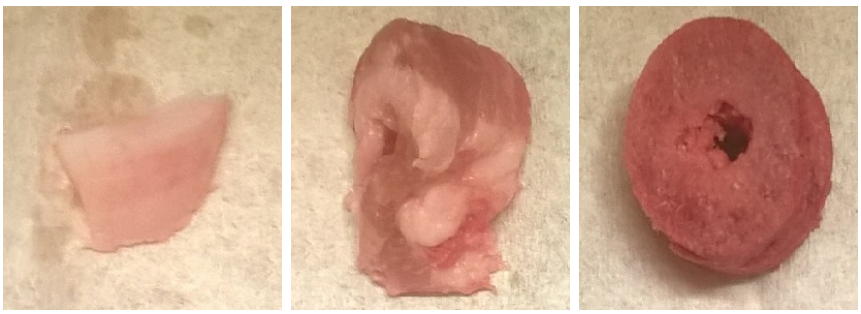

(a) Cartilage (b) Muscle and Fat (c) Trabecular Bone

Figure 8.4: *Biological sample II after being cut.*

these samples.

The maps are reported in Fig. 8.5. It can be seen that marrow and fat (Fig. 8.5(f) and 8.5(c)) are characterized by distributions in which $T_1$ is relatively close to $T_2$, on the contrary, cartilage and muscle (Fig. 8.5(e) and 8.5(d)) are characterized by distributions in which $T_1$ is much longer than $T_2$.

In the cartilage, the signal comes from the water inside the collagen and this can explain why $T_2$ is shorter than $T_1$. The water is embedded into pores, and this restriction makes the relaxation times $T_1$ and $T_2$ shorter, according to the well-known relation 8.1:

$$\frac{1}{T^*_{1,2}} = \left(\frac{1}{T_{1,2}}\right)_{bulk} + \rho\frac{S}{V} \tag{8.1}$$

where $\rho$ is the surface relaxivity, $S$ is the surface of the pore and $V$ is its volume. However, at the same time, there is an exchange of magnetization between collagen and water. Therefore, $T_2$ decreases because the water diffusion is restricted, but $T_1$ remains longer due to the magnetization exchange of water ${}_1H$ with collagen ${}^1H$ nuclei [18].

In the muscle, the signal comes from blood and the behaviour shown in the $T_1 - T_2$ map could be due to the presence of iron that, due to its paramagnetic properties, decreases the $T_2$ without necessarily decreasing the $T_1$.

It is interesting to analyse in more detail the map performed on only trabecular bone (Fig. 8.5(b)). It is clearly visible the distribution of the marrow, and that is the main component, but it is definitely present also a fluid component, that could be blood and/or cartilage present inside the trabecular matrix.

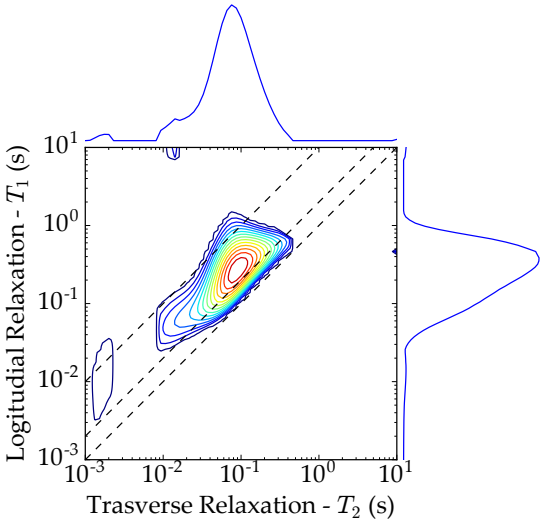


(a) $T_1$-$T_2$ map of *Biological sample II*

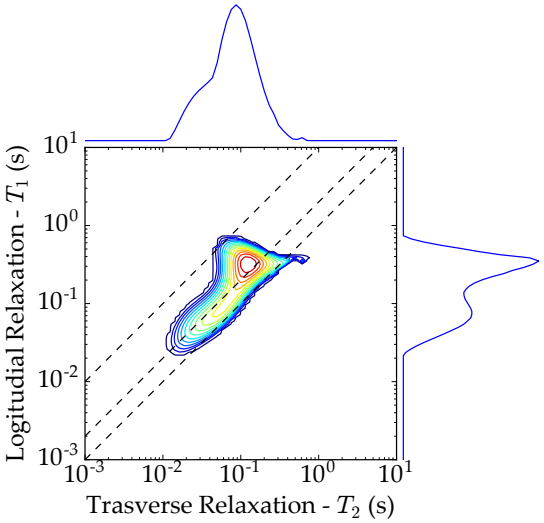


(b) $T_1$-$T_2$ map of trabecular bone

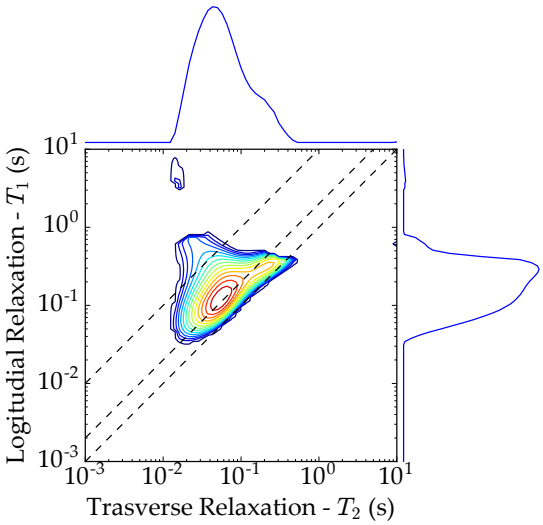


(c) $T_1$-$T_2$ map of muscle and fat

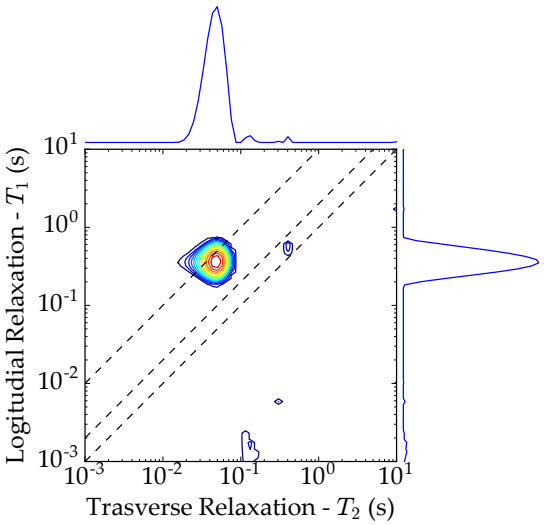


(d) $T_1$-$T_2$ map of muscle

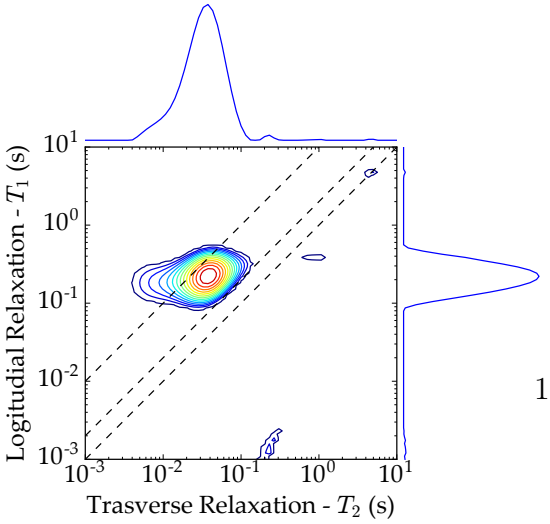


(e) $T_1$-$T_2$ map of cartilage

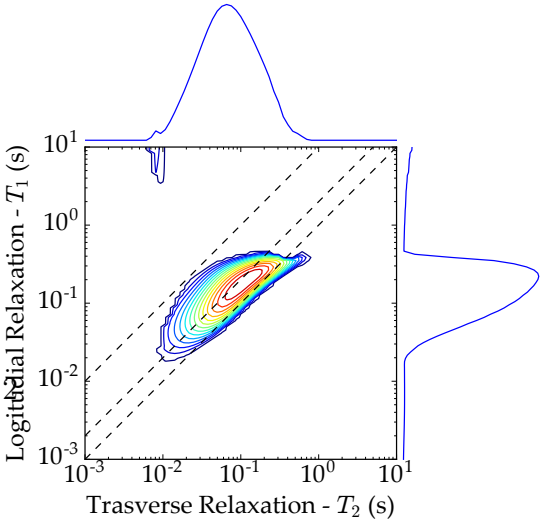


(f) $T_1$-$T_2$ map of marrow

Figure 8.5: $T_1$-$T_2$ maps of trabecular bone and surrounding tissues.

### 8.1.2 D-$T_2$ maps

The next step was to assess the self-diffusion coefficient of those components. Theoretically, cartilage and muscle should have a self-diffusion coefficient higher than the marrow.
$D-T_2$ maps have been performed on samples of bulk marrow, cartilage and muscle. The $D-T_2$ experiment of the marrow has been performed using the NMR-MOUSE PM10 in Bologna, whereas the $D-T_2$ experiments of the cartilage and the muscle have been performed using the NMR-MOUSE PM5 in Wellington. The parameters of the sequences are reported in Tab. 8.2

Table 8.2: D-$T_2$ parameters.

| Sample | $t_p$ | 90 Att. | 180 Att. | $\tau_{min}$ | $\tau_{max}$ | $\Delta$ | $T_E$ | $N_s$ |
|---|---|---|---|---|---|---|---|---|
| Cartilage | 6.25 $\mu$s | -8 dB | -2 dB | 0.02 ms | 0.15 ms | 1 ms | 100 $\mu$s | 16 |
| Muscle | 6.25 $\mu$s | -8 dB | -2 dB | 0.02 ms | 0.15 ms | 1 ms | 100 $\mu$s | 16 |
| Marrow | 15 $\mu$s | -10 dB | -4 dB | 0.05 ms | 1.35 ms | 10 ms | 60 $\mu$s | 128 |

The data have been analysed with MATLAB and the resulting maps are reported in Fig. 8.6. Comparing the map of the marrow (see 8.6(c)) whit those of the cartilage and the muscle (see 8.6(a) and 8.6(b)), it is possible to see that the self-diffusion coefficient of the marrow is much lower than that of the cartilage and the muscle. In fact, for these tissues D is more close to the self-diffusion coefficient of the bulk water, even if it is, as expected, lower due to the restriction of the water molecules inside those tissues.

## 8.2 Diffusion Weighted $T_1 - T_2$ correlation map

The results presented in the previous section have shown the huge difference of the diffusion coefficients between the fluid components of muscle and cartilage and the marrow. This suggests a way to suppress the signal coming from those tissues using a single-sided NMR scanner. The key idea is to use the always switched-on field gradient of these NMR devices.
In more detail, if a period in which the diffusion can act is leaved before to detect

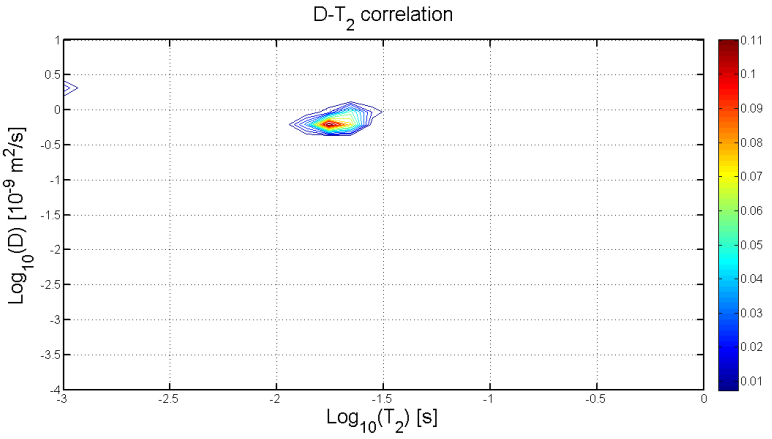


(a) Cartilage

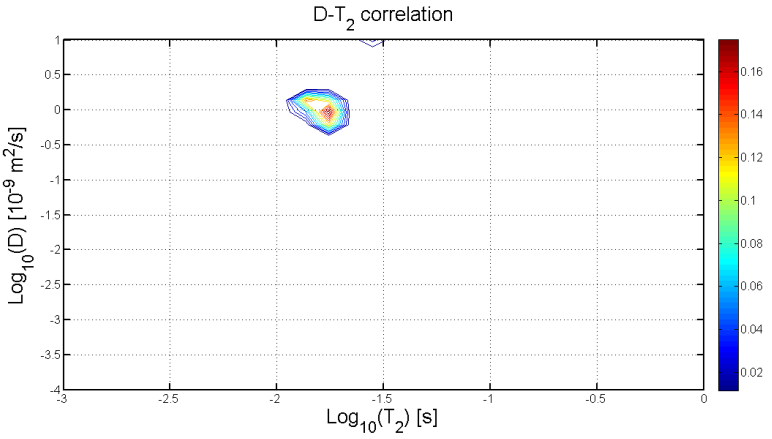


(b) Muscle

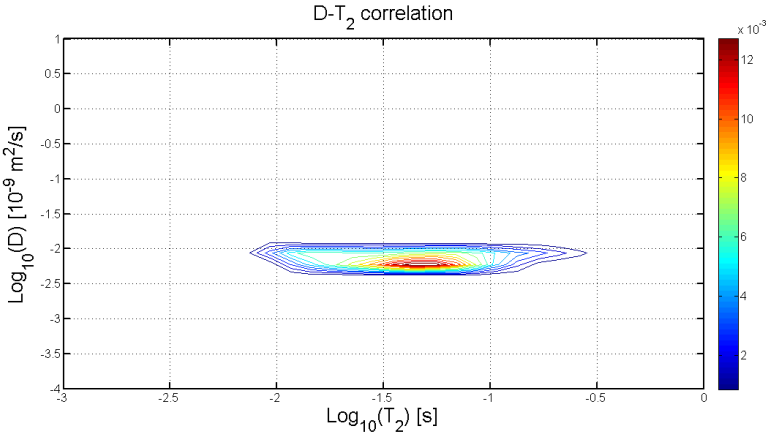


(c) Marrow

Figure 8.6: D-$T_2$ maps of cartilage, muscle and marrow.

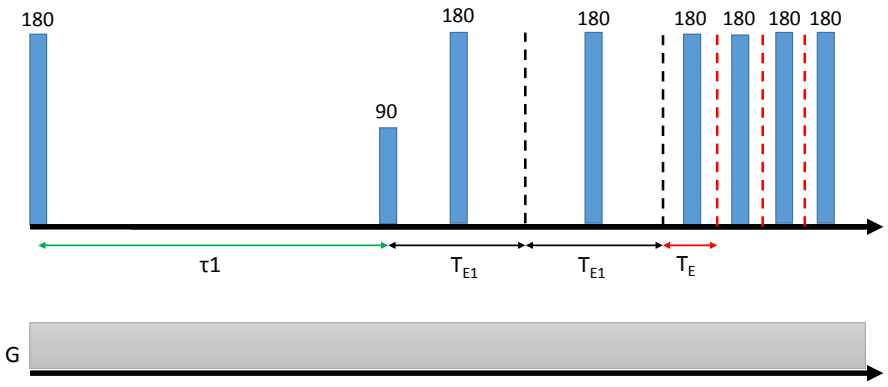


Figure 8.7: DW $T_1 - T_2$ pulse sequence.

the signal with a CPMG , it would be possible decrease the signal coming from the more diffusive components due to the faster decay in respect to the less diffusive components.
In the case of the trabecular bone, the marrow would be affected by the diffusion much less than cartilage and muscle, producing a suppression of the signal coming from these tissues. The intensity of the suppression is related to the time leaved to the diffusion.

A Diffusion-Weighted $T_1$-$T_2$ (DW $T_1 - T_2$) correlation map has been set to verify this idea. To do that, the $T_1 - T_2$ pulse sequence has been modified producing a DW $T_1 - T_2$ pulse sequence. The sequence is represented in Fig. 8.7.

It is a classical inversion recovery followed by a CPMG where the first two echoes of the CPMG are created using an echo time (named *First Echo Time*, $T_{E1}$) longer than the echo time ($T_E$) of the following 180 train. Provided that $T_E$ is sufficiently short, $T_{E1}$ is the period in which the diffusion mainly acts. By setting different values for this first echo time the diffusion weights more or less the correlation

$T_1 - T_2$ correlation map.
It is worthy to note the fact that during the first echo time $T_{E1}$ there is a decay due to both the diffusion and the transverse relaxation. Therefore, $T_{E1}$ has to be short enough to not produce a significant decay of the transverse magnetization, otherwise, the echo attenuation would be due to the relaxation more than to the diffusion. Because in this case shortest $T_2$s are in the order of few ten milliseconds, $T_{E1} = 10$ ms is the maximum first echo time value that can be set. Finally, the choice of producing two echoes using $T_{E1}$ is bond to this consideration, because in this way the diffusion can act twice.

Performing different $DW - T_1 - T_2$ maps on a biological sample using different first echo times allows one to assess if, leaving sufficient time to the molecules to diffuse, the components related to the cartilage and the muscle disappear from the map.
Three $DW - T_1 - T_2$ maps have been performed on *Biological sample III* whit $T_{E1}$ equals to 150 $\mu$s, 5000 $\mu$s and 10000 $\mu$s whit $T_E = 150$ $\mu$s. In this way the first map is not weighted by the diffusion. The resulting maps are presented in Fig. 8.8

The map 8.8(a) presents all the components and is similar to the map 8.5(a). The map 8.8(b) shows a distribution in which the signal densities of the components with $T_1$ much longer than $T_2$ are much lower than in the first map, looking really similar to the $T_1 - T_2$ map of the marrow (see Fig. 8.5(f)), and in the third map 8.8(c) those components are completely disappeared, and only the fat component is present.

That result demonstrates the possibility, with this composite pulse sequence, to suppress the signal coming from cartilage, muscle and blood vessels in a *in-vivo* experiment.

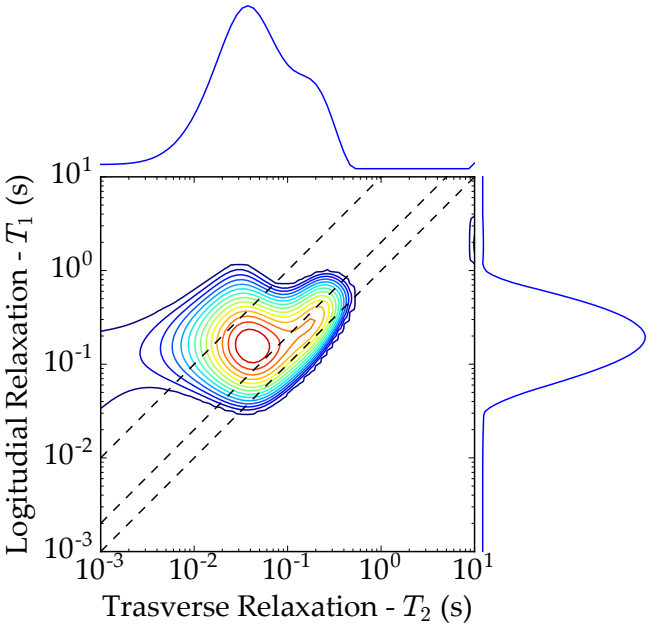


(a) $T_{E1} = 150$ $\mu$s

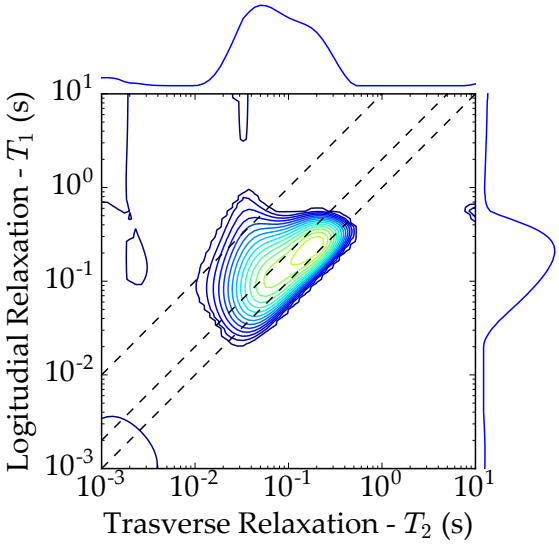


(b) $T_{E1} = 5000$ $\mu$s

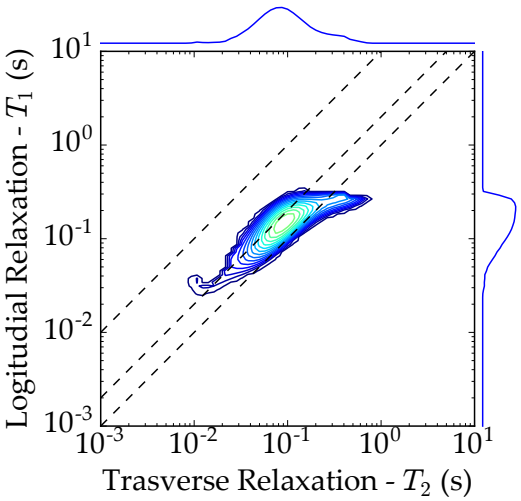


(c) $T_{E1} = 10000$ $\mu$s

Figure 8.8: DW $T_1$-$T_2$ maps of trabecular bone and surrounding tissues for different $T_{E1}$ times.

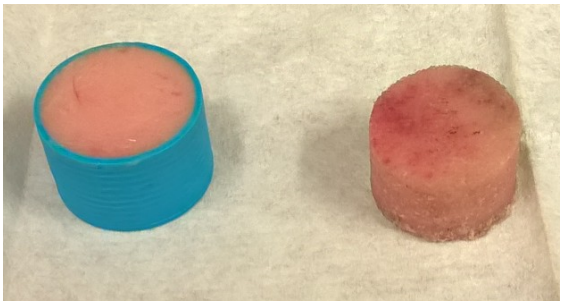

Figure 8.9: Bone III *and bulk marrow samples used to assess the BV/TV ratio whit the NMR-MOUSE PM5, NMR-MOUSE PM10 and NMR-MOLE.*

## 8.3 BV/TV ratio: a comparison between the NMR-MOLE and NMR-MOUSE

The final step was to evaluate the performance of the NMR-MOLE in assessing the BV/TV ratio of a trabecular bone sample, and comparing it whit the NMR-MOUSE.
For this comparison a new sample has been prepared (Bone III) and measured by NMR-MOLE, NMR-MOUSE PM5 and NMR-MOUSE PM10.

The BV/TV has been assessed using a CPMG sequence, and performing the same experiment on a sample of bulk marrow of same sizes. The samples are cylinders with diameter of 2.5 cm and height of 1.5 cm. A picture of the samples is presented in Fig. 8.9. The BV/TV ratio has been computed as explained in the previous chapter, and the parameters of the CPMG sequences are reported in Tab. 8.3

| Instrument | $t_p$ | 90 Att. | 180 Att. | TR | $T_E$ | $N_s$ |
|---|---|---|---|---|---|---|
| MOLE | 12$\mu$s | -10 dB | -4 dB | 5000 ms | 150 $\mu$s | 32 |
| MOUSE PM5 | 6.25$\mu$s | -8 dB | -2 dB | 5000 ms | 100 $\mu$s | 32 |
| MOUSE PM10 (0 mm) | 15$\mu$s | -7 dB | -1 dB | 5000 ms | 60 $\mu$s | 32 |
| MOUSE PM10 (8 mm) | 15$\mu$s | -10 dB | -4 dB | 5000 ms | 50 $\mu$s | 32 |

Table 8.3: CPMG parameters utilized to assess the BV/TV ratio of *Bone III.*

For each sample, four CPMG experiments have been performed on the same slice.

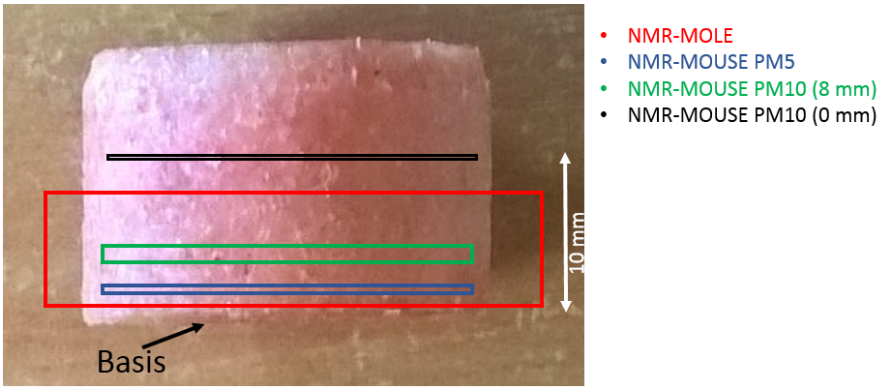


Figure 8.10: Sketch of the sample's slices assessed using different NMR scanners.

In the case of the NMR-MOUSE PM5 all the spacers have been inserted (4 mm) so that the penetration depth was 1 mm. at this depth the SNR is the maximum achievable by that instrument. For the NMR-MOUSE PM10 the measurements have been performed both in 0 mm configuration (10 mm of penetration depth) and 8 mm configuration (3 mm of penetration depth).
Because the three devices have different sensitive volumes, each device detects the signal from a different slice inside the sample, as sketched in Fig. 8.10.

Tab. 8.4 summarizes the slices assessed with the three NMR devices.

| Instrument | Slice colour in Fig. 8.10 | Slice Position from the basis | Thickness |
|---|---|---|---|
| NMR-MOLE | Red | 0 mm | 6 mm |
| NMR-MOUSE PM5 | Blue | 1 mm | 160 $\mu$m |
| NMR-MOUSE PM10 (0 mm) | Black | 10 mm | 100 $\mu$m |
| NMR-MOUSE PM10 (8 mm) | Green | 3 mm | 300 $\mu$m |

Table 8.4: Assessed slices for the three NMR devices.

The BV/TV ratio of the four slices has been also assessed by micro-CT analysis. The results are reported in Tab. 8.5

| Slice | $\frac{BV}{TV}$ (%) by micro-CT | $\frac{BV}{TV}$ (%) by NMR | SNR (NMR) |
|---|---|---|---|
| Red | 25 ± 2 | 20.0 ± 0.3 | 50 |
| Blue | 26 ± 2 | 19 ± 1 | 15 |
| Green | 25 ± 2 | 18 ± 1 | 46 |
| Black | 26 ± 2 | 20 ± 2 | 8 |

Table 8.5: BV/TV ratio comparison between NMR and micro-CT.

The error associated to the values in Tab. 8.5 has been computed as follows. Regarding the NMR measurements, in the case of the NRM-MOLE and NMR-MOUSE PM5 (slices red and blue) the error has been evaluated computing the standard deviation, from repeated measurements of the same slice, for both the trabecular bone sample and the bulk marrow sample, and computing the final error using the theory of the error propagation.
For the NMR-MOUSE PM10 (slice green and black), in addition to the standard deviation of repeated measurements as just discussed, a profile of the bulk marrow sample has been used. The signal coming from 5 slices above and below the detected slice, when performing a CPMG experiment in 0 mm and 8 mm configuration, have been detected. Than, the average value and the standard deviation have been evaluated. In fact, although the bulk marrow should be quite homogeneous, small changes in the composition are possible, and the resulting NMR signal can be slightly different. Whit the NMR-MOUSE the slice thickness is in the order of a few hundred of micrometers, and so acquiring the signal in one slice or another can give different results. This operation allows one to estimate how the variation in the signal, coming from adjacent slices of the bulk marrow sample, affects the computation of the BV/TV. Then, the two source of uncertainty has been added in quadrature.
It is also worthy to note that the bulk marrow sample used with the NMR-MOUSE PM10 is different from the one used to perform the measurements with the NMR-MOLE and NMR-MOUSE PM5.
Regarding the micro-CT analysis, the main source of uncertainty is the choice of the threshold value for the segmentation of the image. Hence, the BV/TV ratio of

a micro-CT image of the sample Bone III has been evaluated for different threshold values, in particular in the interval $Threshold = 126 \pm 5$, where 126 is the value chosen as "optimal" threshold value to make the thresholding operation.
In Fig. 8.11 the micro-CT image utilized for computing the error, and three examples of thresholded images are reported.

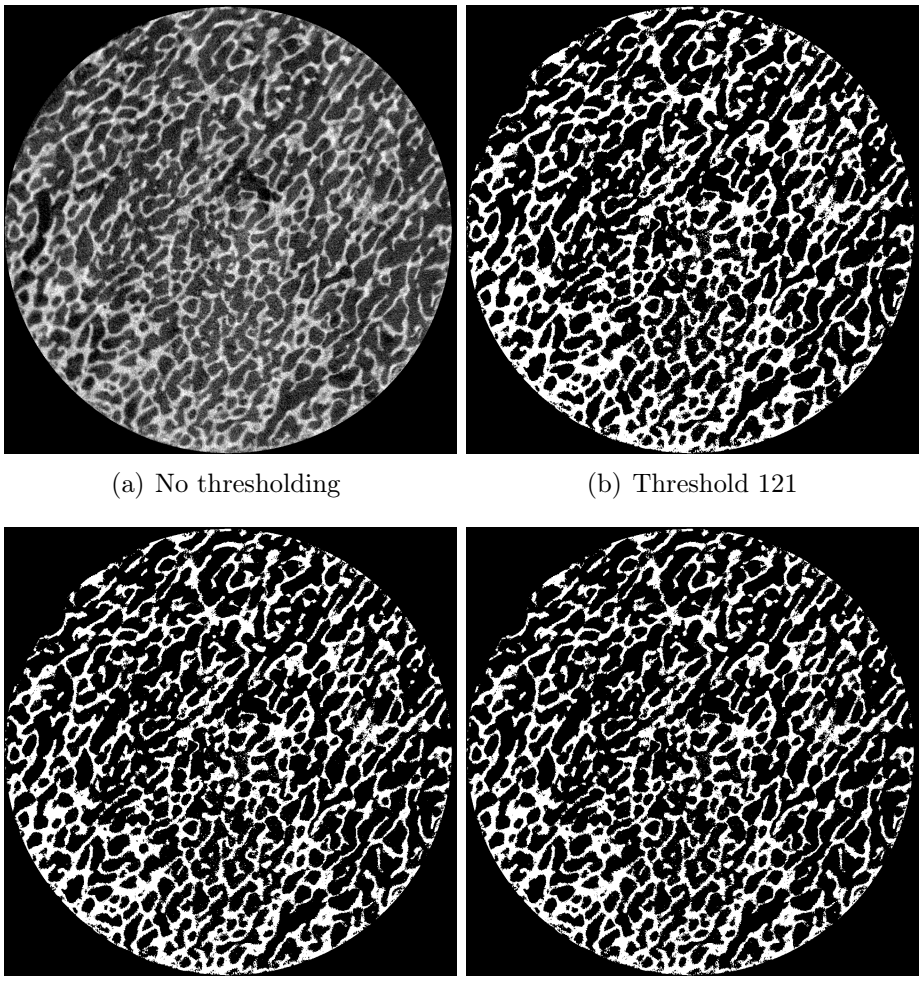

(a) No thresholding (b) Threshold 121

(c) Threshold 126 (d) Threshold 131

Figure 8.11: Micro-CT image of Bone III without thresholding operation and for different values of threshold.

The resulting standard deviation is the 7% of the average value. This is the error associated to the values reported in Tab. 8.5.

Although there is a bias between the micro-CT values and those obtained by NMR, the two data set are consistent. The BV/TV of this sample, evaluated in different slices, is constant along the sample. In fact, micro-CT and NMR data obtained on the different slices do not show variations and are contain within two standard deviations. The fact that the values are biased could be due to different factors, such as the choice of the threshold value in the micro-CT analysis and/or the presence of compounds, different from the marrow, that gives NMR signal in the bone (for example water or blood).
The important thing is that the NMR technique performed thought different single-sided NMR scanners, each with specific limits and advantages allows one to draw the same conclusions of the micro-CT analysis.
By looking at the NMR data set, it is also possible to make some considerations about the performance of the NMR-MOLE and the NMR-MOUSE in assessing the BV/TV. The NMR-MOLE has the largest sensitive volume, and this not only assures the maximum SNR, but makes the measure less sensitive to the changes in the BV/TV along the sample. The NMR-MOUSE, on the contrary, assures the possibility to select the depth of the slice inside the sample, and also the slice thickness, but the SNR can be very small.

As final consideration it can be worthy to show that the BV/TV can be evaluated by high-resolution MRI. An MRI analysis has been performed on *Bone III* with a Bruker Avance 400 Systems ($^1H$ frequency of 400 MHz) at the NMR Lab of the University of Wellington. In Fig. 8.12 an image of approximatively the same slice of the sample acquired by MRI and micro-CT is presented. The slice thicknessfor MRI is 100 $\mu$m, whereas the slice thickness for micro-CT is 18 $\mu$m.
In the MRI image the marrow gives signal, so the trabeculae are dark in that image, whereas the marrow is bright. In the micro-CT image the bone tissue has a linear attenuation coefficient higher than the marrow, so that the trabecualae appear bright, whereas the marrow is darker (even if not dark as the background). Of course one could estimate BV/TV on those images, but the use of such a high magnetic field (9.4 T) is not advisable for osteoporosis diagnosis.

In summary, in this chapter it has been shown that the BV/TV, a such important

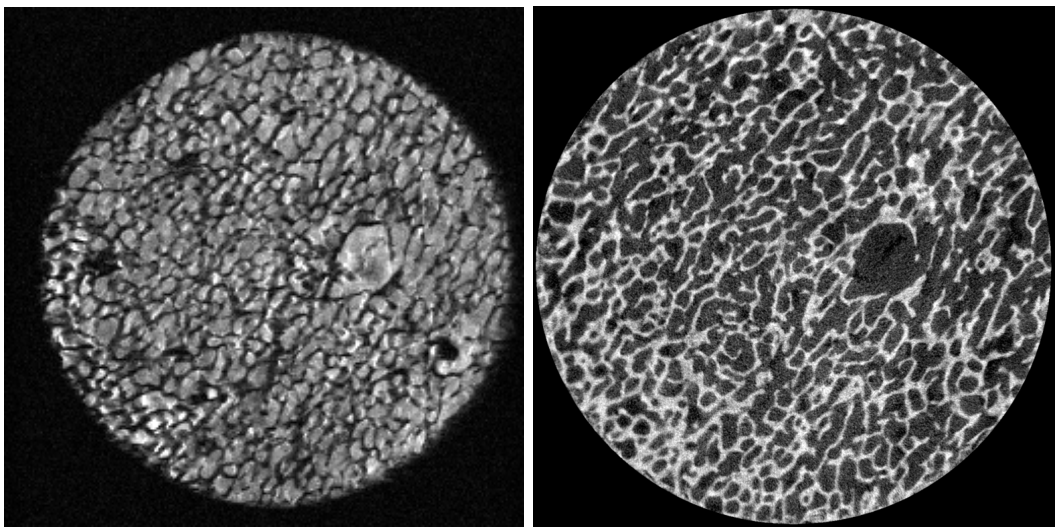

(a) MRI (b) micro-CT

Figure 8.12: MRI and micro-CT image of a slice of Bone III.

parameter in assessing the micro-structure of the trabecular bone, can be correctly evaluated by using low-field single-sided NMR. Different single-sided NMR devices have advantages and disadvantages, but definitively they are able to assess the BV/TV with the advantage of being portable and low-cost devices. By the characterization of the tissues surrounding the trabecular bone, performed through two-dimensional correlation experiments with the NMR-MOLE, it has been shown a way to suppress the signal coming from tissues different from marrow, making more realistic the scenario of *in-vivo* applications.

# Conclusions

The aim of this thesis was to set-up an original and new technique to investigate the trabecular structure of the bone through low field NMR measurement, using single-sided NMR scanners, with the final goal to propose a new low-cost, non-invasive procedure for the diagnosis of osteoporosis. The experiments have been performed at the NMR Lab of the Department of Physics and Astronomy or the University of Bologna and during a five months visit at the NMR Lab of the School of Chemical and Physical Sciences of the Victoria University of Wellington, New Zealand.

The World Health Organization (WHO) defines osteoporosis how *a systematic skeletal disease characterized by low bone mass and micro-architectural deterioration of bone tissue, with a consequent increase in bone fragility and susceptibility to fracture.* Currently, the established modality to diagnose and monitor osteoporosis in a clinical setting is the dual-energy X-ray absorptiometry (DXA), which provides areal bone mineral density (BMD), but it does not say anything about the micro-architectural structure of the trabecular bone. Studies have shown that BMD does not explain clearly the increasing in the fracture risk [3][4] and remark the importance to assess parameter related to the micro-architectural structure of the trabecular bone. One important parameter that can be used for extracting structural information about the micro-structure of the trabecular bone is the Bone Volume to Total Volume ratio (BV/TV). Magnetic Resonance Imaging can be used to analyse the structure of the bone, but it is a very expensive technique. Because of the cost of the system itself and the service related costs, its spreading in clinical environment is limited. Provided these consideration it appears really worthwhile to find new techniques based on NMR able to assess the micro-architectural structure of the trabecular bone decreasing the related costs.

The fundamental idea of this thesis was that a good way to reduce the cost was to switch from high-field NMR to low-field NMR, and to transfer techniques and knowledges from different NMR fields to solve this problem, in particular the field of NMR applied to the study of porous media. Trabecular bone is a porous media and seemed possible to evaluate the BV/TV ratio using the same technique utilized in the field of NMR applied to the study of the rocks, i.e. by a ratio of the signal of a saturated water rock sample and a water reference sample.
The instruments used int this work are the NMR-MOUSE, produced by Magritek, and the NMR-MOLE. Both devices are open NMR sensors equipped with a permanent magnet.
The advantage of these scanners, which belongs to the class of unilateral, single-sided scanners, is that the sample can be of any size. In the usual NMR scanners, the sample must fit the limited space available in the bore of the magnet. Another relevant advantage is their low cost if compared with the NMR total body scanner. Moreover, these scanners are portable, so allowing screening of population with easy and low cost procedures.
Besides these advantages, there are some disadvantages, such as the inhomogeneity of the polarizing field $B_0$ and the RF pulse $B_1$, that degrades the sensibility of the instrument.
The NMR-MOUSE and NMR-MOLE have a fundamental difference. The NMR-MOUSE has a constant field gradient in the sensitive volume ( around 14 T/m), whereas the NMR-MOLE has been design to have a sensitive volume in which the polarizing field $B_0$ is relatively homogeneous, resulting in a distribution of field gradients, whit the highest value of 2 T/m. The NMR-MOUSE is equipped with a lift that allows one to perform experiments at different depths inside the sample

In order to verify the feasibility of such a technique the BV/TV ratios of pig trabecular bone samples have been evaluated by this NMR technique. The micro-CT, performed at the Laboratorio di Tecnologia BioMmdica of the Istituto Ortopedico Rizzoli, Bologna, has been used as reference measurement. Many initial measurements have been performed by NMR-MOUSE PM10 in order to optimize the measurement conditions and protocols. On a set of six cylindrical pig's shoulder

trabecular bone samples, characterized by different trabecular matrices, the porosity in different sections inside the samples have been determined, and the BV/TV computed. Because the final aim of this research is a clinic application of the technique, the experiments preformed on these samples have been design in such a way to simulate a possible diagnostic test. For each sample NMR signal has been acquired with the sample placed with its principal axis parallel to the surface RF-coil. Then the sample has been rotated of $90^o$, $180^o$ and $270^o$ around its principal axis, in order to assess the signal in different slices inside the sample. The signal from a reference bulk marrow sample has been detected and the BV/TV has been evaluated.
The results of the NMR analysis have been compared whit those obtained by the micro-CT, and the comparison showed a general good agreement.

Once verified the feasibility of the technique, wanting for the extension of the measurements to an *in-vivo* scenario, a deeper study was needed in order to find the procedures useful to discriminate the signal coming from the marrow contained in the inter-trabecular space and the others tissues surrounding the bone, such as muscle and cartilage. Whit this aim the NMR-MOLE has been used to perform two dimensional correlation experiments, $T_1 - T_2$ maps and $D - T_2$ maps, on biological samples that contained not only the trabecular structure, but also different tissues surrounding the bone, like fat, muscle and cartilage.
From these experiments it was possible to determine the experimental way to suppress the signal of cartilage and muscle. In order to verify the method a pulse sequence, Diffusion Weighted $T_1 - T_2$ correlation map, has been created in such a way to allow one to weights the $T_1 - T_2$ with the diffusion. The result shows that when sufficient time to the molecules to diffuse is left, the $T_1 - T_2$ map does not shows anymore the signal components due to the cartilage and muscle, whereas the components of the marrow are still present. This means that in this way it is possible to suppress the signal coming from those tissues, making more realistic the scenario of *in-vivo* applications.
As final investigation, the BV/TV ratio of a pig's femur trabecular bone sample has been evaluated with three different single-sided NMR devices, the NMR-MOLE, NMR-MOUSE PM5 and NMR-MOUSE PM10 in order to assess the differences

of these device in assessing the BV/TV ratio. Also in this experiment the results of the NMR analysis have been compared with those obtained with the micro-CT analysis, giving very good agreement among NMR devices and micro-CT.

In summary, the BV/TV, a very important parameter to assess the micro-structure of thetrabecular bone, can be correctly evaluated using low-field, single-sided NMR. Different single-sided NMR devices have advantages and disadvantages. For example, the NMR-MOLE has the largest sensitive volume, and this assures the maximum Signal-to-Noise ratio (SNR), but makes the measure less sensitive to the changes in the BV/TV in different positions of the sample. The NMR-MOUSE, on the contrary, assures thepossibility to localize the depth inside the sample, and also the slice thickness, but the SNR can be much smaller. The whole of the experiments performed assure that single-sided NMR scanners can be used to assess the value of BV/TV in trabecular bone, with the advantage of being portable, low-cost and non-invasive devices, so allowing to perform in an easy way wide campaigns of screening of the population at risk of osteoporosis.

# Acknowledges

Almost nothing can be done all alone, and this thesis is an excellent example. I need to thank many people that in these months helped me to product this thesis. However, and I think it is the one of the most important thing, thanks to this project I had the pleasure to meet and work with wonderful persons, each of them showed me his professional skills, but his human side as well, and I really appreciated that. I do not take that for granted, and I was glad to cross the path with these people.

First of all I want to thank my supervisor prof. Paola Fantazzini. This project started thanks to her. I thank her for the fortitude she had during my first period here in the Lab, when I had to be trained to get started with NMR and for the constant attention she paid to me. I thank her also for the opportunities that gave me. When I expressed the will to make an overseas experience related with this project I found a person ready to hear me. I thank her for the economic support that allowed me to take part at the ANZMAG conference and to handle some costs related to the research activity I did in Wellington, at the NMR group of the University of Wellington. These money has been invested from her personal research assets, and in the Italian research public founding scenario it has not to be taken for granted. For the help in the write of this thesis, for all this just thank you.

I really want to thank my assistant supervisor, Dr. Leonardo Brizi (Leo for friends), he helped me a lot in the beginning, and actually continued to help me until the end of this thesis period, when I was new to most of the NMR techniques. He really had a good approach when he taught me the first times, which helped me to become more and more confident with the subject. Even of Leo I really appre-

ciated his human side, making more enjoyable going every day to the lab.

Thanks to this project I spent five months in New Zealand at the NMR group of the University of Wellington. I do want to thank Dr. Petrik Galvosas because he allowed me to be part of his group for that period. I really thank him for the welcome I received, I had good time in that Lab and I appreciated the way in which he supervises the group. I remember, with pleasure, lunches and dinners all together. I am glad to have been part of your group for a while.
I thank each member of that group. Huabing, but now I would better say Dr. Huabing, I really appreciated his help when, just arrived, he introduced me in the city. I thank you for the nice discussion around your desk, also I thank you to have shown me really good noodles shops. I thank Marcel, I really appreciated the help with the MOLE and precious discussions about NMR in general and related with my thesis project. I also enjoyed the fun we have together, having fun about my funny English, and even Italian. I thank Sergei, I learned a lot from him about the electronic underlying the NMR scanners and the RF coil. I also appreciated your suggestions for my trips around New Zealand, I think I can say "you are a good guy". I thank Tim and Bridget, when I had a question about English I knew where I had to go, how many discussion about English and food. I thank Fangrong for to have helped with the MRI, and for the nice discussions about the future. Finally, I thank all the people that populated that Lab in those months.

I thank my parents. This thesis is the ending of a path that would have not been possible without their economical and moral support. I do not need to much words, just I love you. Beside them, I also thank all my family

Finally, I thank all my friends. Alby, Dario, Alle, Gaia, Menni and Catti that together form the legendary *Los*. My team mates of the *Dress*: Cappe, Paul, Save, Manfre, Fillo, Ricky, Sumone, Simo and Lory.
My *old* university mates from Modena: Anna, Giulia, Bacca, Alle and Bibi. A particular thanks to Bibi and Alle for the good time spent even in Bologna. I also thank my *new* university mates I met in Bologna in particular Cecilia and Alice, thanks for all the good time spent together, and Fillo to the reciprocal support in

writing this thesis. A final thanks to my friend Marco, a really good friend.

# Bibliography


[1] M. Jergas H.K. Genant, G. Guglielmi. *Bone Densitometry and Osteoporosis*. Springer, 1998.

[2] Ministero della salute Italiano. Appropriatezza diagnostica e terapeutica nella prevenzione delle fratture da fragilità da osteoporosi. Quaderno n. 4 - Luglio-Agosto 2010 -.

[3] Wehrli F et al. Role of magnetic resonance for assessing structure and function of trabecular bone. *Top Magn Reson Imaging*, 13:335–355, 2002.

[4] S. Majumdar R.Krug, A.J. Burghardt. High-resolution imaging techniques for the assessment of osteoporosis. *Radiol Clin North Am.*, (48):601–621, May 2010.

[5] E.E. Sigmund, H. Cho, and Y.-Q. Song. High-resolution mri of internal field diffusion-weighting in trabecular bone. *NMR in Biomedicine*, 22(4):436–448, 2009.

[6] B. Manz, A. Coy, R. Dykstra, C.D. Eccles, M.W. Hunter, B.J. Parkinson, and P.T. Callaghan. A mobile one-sided {NMR} sensor with a homogeneous magnetic field: The nmr-mole. *Journal of Magnetic Resonance*, 183(1):25 – 31, 2006.

[7] G. Gnanasegran I. Fogelman. *Radionuclide and Hybrid Bone Imaging*, chapter 2, pages 29–57. Springer, 2012.

[8] Qingwen Ni et al. The characterization of human compact bone structure changes by low-field nuclear magnetic resonance. *Meas. Sci. Technol.*, (15):1–9, 2004.

[9] S. Majumdar R.Krug, A.J. Burghardt. T.m. link, high-resolution imaging techniques for the assessment of osteoporosis. *Radiol Clin North Am*, 48(3):601–621, May 2010.

[10] H. K. Genant S. Majumdar. *Bone Densitometry adn Osteoporosis*, chapter 20, pages 408–416. Springer, 1998.

[11] B. Blümich F.Casanova, J.Perlo. *Single-Sided NMR*. Springer, 2010.

[12] Marcel Nogueira d'Eurydice and Petrik Galvosas. Measuring diffusion–relaxation correlation maps using non-uniform field gradients of single-sided {NMR} devices. *Journal of Magnetic Resonance*, 248:137 – 145, 2014.

[13] M.D Hürlimann and L Venkataramanan. Quantitative measurement of two-dimensional distribution functions of diffusion and relaxation in grossly inhomogeneous fields. *Journal of Magnetic Resonance*, 157(1):31 – 42, 2002.

[14] Arthur C. Guyton. *Textbook of Medical Physiology (8th ed.)*. Philadelphia: W.B. Saunders., 1991.

[15] Leonardo Brizi. Studio nmr dell'atuo-diffusione molecolare: impeigo di un gradiente di campo magnetico costante in condizioni di diffuisione ristretta e non riestretta. Master's thesis, Università di Bologna, 2011.

[16] Mayo Clinic. *Materials Science and Tissue Engineering: Repairing the Heart.*, 2013.

[17] P. Fantazzini G. C. Borgia, R. J. S. Brown. Uniform-penalty inversion of multiexponential decay data. *J Magn Reson*, (132):65–77, 1998.

[18] Paola Fantazzini et al. The search for negative amplitude components in quasi-continuous distributions of relaxation times: the example of 1h magnetization exchange in articular cartilage and hydrated collagen. *New Journal of Physics*, 2011.